Imperial College of Science, Technology and Medicine
Department of Mathematics

Decoding quantum errors with the Gottesman-Kitaev-Preskill code

Kwok Ho Wan

Submitted in partial fulfilment of the requirements for the degree of
PhD in Mathematics of Imperial College London, August 2023

Abstract

Implementing quantum error correction has been difficult in practice. Techniques from engineering, computer science, coding theory, experimental and theoretical physics have been blended together to tackle this problem. Traditionally, quantum error correcting codes mostly focus on dealing with phenomenological Pauli errors primarily due to their theoretical convenience. But this approach neglects physical types of noise, which are more realistically modelled with physically motivated noise models.

This work focuses on a specific encoding in quantum computing called the Gottesman-Kitaev-Preskill (GKP) codes. Firstly we study the basic properties and quantum estimation capabilities of a closely related state that is symmetric in phase space called the grid sensor state, motivating the GKP code as a good candidate for physical qubit level error correction in quantum optics. The grid codes aim to correct for errors before they build up to become Pauli errors. Then, we propose a quantum error correction protocol for continuous-variable finite-energy, approximate GKP states undergoing small Gaussian random displacement errors, based on the scheme of Glancy and Knill [Phys. Rev. A **73**, 012325 (2006)]. We show that combining multiple rounds of error-syndrome extraction with Bayesian estimation offers enhanced protection of GKP-encoded qubits over comparible single-round approaches. Furthermore, we show that the expected total displacement error incurred in multiple rounds of error followed by syndrome extraction is bounded by $2\sqrt{\pi}$. Finally, we show that by recompiling the syndrome-extraction circuits, all the squeezing operations can be subsumed into auxiliary state preparation, reducing them to beamsplitter transformations and quadrature measurements.

Statement of Originality

To the best of my knowledge, the content of this thesis is my own work with the exception of other works that are referenced appropriately. The results of the research are obtained during my doctoral studies in collaboration with my supervisors. Parts of chapter 5 have already been published in:

Memory-assisted decoder for approximate gottesman-kitaev-preskill codes
K. H. WAN, A. NEVILLE, and S. KOLTHAMMER, *Phys. Rev. Research* vol. 2, p. 043280, Nov 2020.

Chapter 4 is based on works in preparation with my supervisor Steve Kolthammer, the functional minimisation problem in chapter 4, section 4.1 is loosely based on unpublished works done with summer student, Agathe Vianey-Liaud, co-supervised with Robert Adam Jonathan Gardner and Myungshik Kim.

Copyright Declaration

Acknowledgements

I would like to express thanks to my supervisors, Alex Neville and Steve Kolthammer for their academic and personal advice, my parents for their unwavering support, and finally my friends Luca Cocconi and Robert Gardner for their time and effort in keeping me motivated. A large part of this PhD thesis is based on the published work [1].

A part of the PhD was on providing theoretical support for the experimental realisation of the single photon error correcting scheme proposed by [2]. This is not presented in this thesis due to the experiment being partially completed. This PhD thesis .tex template is kindly provided by Frank Milthaler [3] on Github. The quantum circuits included in this thesis are created using the Quantikz LaTeX package [4].

Unfortunately, I have experienced life-altering medical issues during the completion of my PhD, coupled with the long COVID lockdown in the United Kingdom and losing family members in the process. These were the main reasons for extending the submission deadline of the PhD thesis by almost a year.

Dedication

To everyone who supported me.

Contents

List of Tables

List of Figures

Chapter 1

Introduction

1.1 Motivations

Understanding our physical reality has always been a difficult task. The invention of modern computers greatly aided our quest to understand the physics of our world. However the sheer number of variables and the lack of symmetries in real-world physical problems made it hard even for computer programs to solve these problems. This was one of the motivations to Richard P. Feynman's famous keynote in 1981 [7], where he wanted to know, "Can (quantum) physics be simulated by a universal computer?" using a locally interconnected machine with scalable resources relative to the size of of the system. He suggested using quantum computers to simulate quantum physics by designing approximate numerical algorithms that simulate said physical problem, and then using a quantum computer "to compute these algorithms". He believed that this would give researchers an approximate view of what types of physical theories should be studied theoretically. These ideas were influenced by concepts in cellular automation, a popular alternative theory of computation in the 1980s first suggested to study self-organised criticality in statistical mechanics [8].

In the decade before Feynman's keynote, many others had discovered important concepts exclusive to quantum computing, these include topics such as James Park's non-cloning theorem [9] in 1970, Alexander Holevo's bound [10] in 1973 or Roman Stanislaw Ingarden's foundations

of quantum information theory [11] in 1976 to name a few. These are all examples of mixing ideas of the booming information theory at that time into physics.

In 1985, David Deutsch laid down the foundations of what a universal quantum computer is through definitions of quantum Turing machines [12] and in 1995 Benjamin Schumacher coined the term qubit [13], a quantum bit consisting of a set of orthogonal logical quantum states of $|0_{\mathrm{L}}\rangle$ and $|1_{\mathrm{L}}\rangle$ [12]. A qubit can be a superposition $|0_{\mathrm{L}}\rangle$ and $|1_{\mathrm{L}}\rangle$ at the same time, $|Q\rangle = \alpha\,|0_{\mathrm{L}}\rangle + \beta\,|1_{\mathrm{L}}\rangle$. This is different to classical probabilistic mixtures of logical zero and one bits. The qubit's superposition in a different basis may give rise to different probability distributions after the application of the Born rule. This is a starkly different to just probabilistic mixtures of logical zeros and ones.

It was not until 1992, when David Deutsch and Richard Jozsa found an oracle-based boolean function problem, where quantum computers can efficiently solve in polynomial oracle evaluations [14], while no deterministic classical algorithms can solve in polynomial number of oracle queries. However one can devise an efficient stochastic algorithm to solve the Deutsch-Jozsa problem with high probability [15]. Despite the exponential speed up of the Deutsch-Jozsa algorithm, the problem does not provide any practical real world applications. Following this, Daniel R. Simon proposed another oracle-based boolean function problem (commonly known as Simon's problem) [16]. The structure of Simon's problem inspired the now famous period-finding Shor's algorithm [17]. Shor's algorithm promises the ability to factor large numbers into their prime factors exponentially faster than the best classical algorithm (the general number sieve) [18]. This is the first quantum exponential speed up that can be applied to real-world problems, as much of public-key cryptography security revolves around the perceived classical hardness of factoring large integers on a classical computer [19].

Other quantum algorithms of interest have also been discovered. Grover search [20]. This algorithm saturates the lower bound for quantum black-box structure-free searches, first proven by [21]. Another example is the Harrow-Hassidim-Lloyd quantum algorithm for solving linear equations, where the exponential speed-up depends strongly on the specific sparsity of the matrix to be solved [22]. There exist other approaches to quantum algorithms, for instance:

adiabatic quantum algorithms, quantum walk related algorithm and other analog and digital quantum simulations [23].

Most of the earlier quantum algorithms loosely achieve their advantage through large scale superpositions of states using clever quantum gates and measurement strategies. Numerical quantum algorithms are devised such that many terms in the quantum superposition cancel out. The state is sampled in polynomial complexity relative to the input size before feeding the data into a classical computer pipeline for post-processing, so it achieves the desired answer.

Due to the success of Shor's algorithm, a considerable amount of attention had been focused on building scalable quantum computing hardware. This is another difficult problem in its own right because of the prevalence of quantum noise [24] and the fragility of precisely prepared quantum states. To name a few issues, there exists the difficulty of controlled operations, readout measurements, and the ability to classically post-process measured results efficiently [25, 26].

The presence of errors motivates a need for some form of quantum error correction (QEC) at the logical qubit and hardware level. Asher Peres, first borrowed ideas from repetition classical error correcting codes and incorporated them in a quantum computing setting [27]. Classical bit flip errors from $0 \leftrightarrow 1$, are drastically simpler compared to the errors a quantum bit can experience. A logical qubit can experience bit flips (known as $\hat{X}$ errors), phase flips (known as $\hat{Z}$ errors), and a combined bit and phase flip (known as $\hat{Y}$ errors). Hence, quantum codes for protection of qubits tends to be more involved and complicated in their structure compared to their classical counterparts. In 1995, Shor proposed the first quantum error correcting code (QECC) that requires 9 physical qubits to implement a single logical qubit, commonly known as the Shor code [28]. Shortly after, Andrew Steane expanded upon similar concepts [29]. The idea behind repetition codes relies on spreading the logical information of the qubit over many physical qubits, hence any single corruption of a single physical qubit can be corrected. For example, in Shor's code, the logical states are entangled within qubits 1 to 3, 4 to 6 and 7 to 9, namely $|\mu_L\rangle \propto \big(|000\rangle + (-1)^{\mu}|111\rangle\big)^{\otimes 3}$, $\mu \in \{0, 1\}$. This is an example of an entangled state. Resources unavailable in the classical realm such as entanglement, magic, superposition,

non-classicality, often provide new methods of solving existing problems [30].

One of the most important and interesting aspects of quantum computing is the quantum threshold theorem [31, 32, 33]. In light of faulty preparation, evolution and readout measurements of quantum resource states, the threshold theorem states that with apt QECC, suitable error channels, and effective error rates represented as a probability of failure, there is a threshold probability of error that corresponds to if the errors are correctable. This ties in with the idea that a fault tolerant quantum computer (FTQC) is needed for large scale quantum computation. Much effort was put into the experimental feasibility study and theoretical development of QECC. One can fill up "a zoo" [34] with different error correcting codes, ranging from stabilizers or surface codes [25] for logical level protection, to even exotic bosonic code [35], that could be used as a physical layer of error correction for the qubit concatenated underneath a logical QECC.

Every quantum computing hardware systems suffers from varying degrees of theoretical, experimental and engineering developmental bottlenecks. There are drawbacks and advantages to each platform despite the different advantages the variety of different platforms brings. In photonics, the qubit can be encoded as a state in bosonic modes [36], hence a lot of techniques from quantum optics can be employed [37, 38, 39].

Encoding and manipulating quantum information in continuous variable (CV) systems [40, 41, 42] is a promising route to realising a useful quantum computing device. Large scale CV cluster states can be generated on demand [43, 44]. Fault tolerant, measurement-based quantum computation is possible using CV cluster states along with CV measurements and non-Gaussian state injection [45, 46], though the levels of optical squeezing required for fault tolerance are beyond the reach of current experiments [45, 47, 48, 49, 50]. Unfortunately, bosonic modes are very prone to loss/amplitude damping errors that constantly drive the state of interest into the ground state. Considerable effort had been allocated to deal with the issue of loss, ranging from quDit codes [51], cat codes [52, 37], binomial codes [53], Gottesman-Kitaev-Preskill (GKP) grid codes [35], and many more (see [54] for a detailed review of bosonic codes). Qualitatively, these codes acquire their error resilience by roughly spreading the quantum information over phase

space to counteract the loss of photons.

The aim of this thesis is to look at a very specific problem in bosonic QEC, namely at states with grid like structure in phase space [35, 55], and investigate their error correcting capabilities in optical quantum computing [56].

1.2 Thesis outline

This thesis is written in a way that assumes the reader to have a basic understanding of quantum physics and quantum information. Firstly, some basic concepts of quantum computing and bosonic quantum computing in chapter 2 are introduced before presenting the research performed during the PhD in chapters 4 and 5. Here are the detailed outline of the materials in each chapter:

In chapter 2, firstly, the mains ideas behind quantum computing such as qubits, gates, requirements of quantum computing and quantum transformations are introduced. Secondly, a simple example of a bitflip error channel and a QECC to counteract this are illustrated. Finally, basic definitions of bosonic quantum theory is laid out, which will be used throughout this thesis.

In chapter 4, properties of the grid sensor state are explored. This includes its Fourier transformation and displacement errors sensing capabilities. Furthermore, the grid sensor state's Fock state amplitudes are calculated explicitly. Additionally, resource theory will be employed to explain the difficulty of generating such states. Finally, the advantages and details of generating entangled GKP Bell states from the grid sensor states will be discussed. Theses ideas and conventions will act as a gentle introduction to chapter 5.

In chapter 5, an improved decoder for the GKP code is presented. Following the Glancy-Knill syndrome[1] extractions circuits, Bayesian optimisation techniques are employed with the aid of a classical memory to decode the quantum errors. This enhances the fidelity of recovery in the presence of the Gaussian random displacement channel. Furthermore, the error extraction and

[1]The word syndrome is inherited from coding theory, it provides ways to detect certain errors in a code [57].

recovery optical circuit is recompiled such that all the squeezing is done offline on auxiliary GKP qubits.

Finally, chapter 6 is the summary of the main theoretical result findings during the PhD and provide an outlook for future works.

Chapter 2

Background and theory

In this chapter, the theoretical and mathematical framework used throughout the thesis will be introduced. Firstly we will go through the basics of quantum computing, starting with the qubit, universal gate sets all the way to the basics of quantum error correcting syndrome extractions and decoding. Concepts of phase space representations and Gaussian quantum information specific to optical quantum information will be introduced next, including the dominant error channels such as amplitude damping. Leading this finally to the introduction of the Gottesman-Kitaev-Preskill code and the grid sensor state. These concepts will be crucial in the analysis and decoding of errors in the later chapters.

2.1 Quantum computation

One of the leading advantages of digital over analogy information processing/computing is the ability to digitise and isolate two distinct 0 and 1 states, called bits, from a continuous system, such as a current. Confusingly this is called "quantization" in classical information theory. The digitisation of information allows the user to systematically devise error correcting repetition codes to combat hardware failures when the bit is flipped from 0 to 1 and vice versa, or the loss of the bit entirely [58, 57].

2.1.1 The qubit

The fundamental unit of quantum information is the qubit, a quantum bit, that carries a bit of quantum information. An ideal qubit consists of two orthogonal quantum states $|0_{\mathrm{L}}\rangle, |1_{\mathrm{L}}\rangle$ that represents the logical 0 and 1 states respectively. A qubit $|Q\rangle$ can be represented as a superposition of the logical states/codewords $|0_{\mathrm{L}}\rangle, |1_{\mathrm{L}}\rangle$,

$$|Q\rangle = \alpha\,|0_{\mathrm{L}}\rangle + \beta\,|1_{\mathrm{L}}\rangle \ , \tag{2.1}$$

where $\alpha, \beta \in \mathbb{C}^2$ are known as the amplitudes, and their absolute squares sums up to 1 via the normalisation of the qubit state: $\langle Q|Q\rangle = 1 = |\alpha|^2 + |\beta|^2$. A representation of a qubit can be written as a vector in the $\{|0_{\mathrm{L}}\rangle, |1_{\mathrm{L}}\rangle\}$ basis.

$$|Q\rangle = \begin{pmatrix} \alpha \\ \beta \end{pmatrix} \ , \tag{2.2}$$

Qubits are vastly different from just a probabilistic mixtures of 0 and 1 bits. For simplicity and ease of comparisons to $|Q\rangle$, a classical probabilistic mixture of a bit can be represented using the probability vector $\vec{\mathbb{P}}$:

$$\vec{\mathbb{P}} = \begin{pmatrix} |\alpha|^2 \\ |\beta|^2 \end{pmatrix} \ , \tag{2.3}$$

where $\mathbb{P}(0) = |\alpha|^2$ and $\mathbb{P}(1) = |\beta|^2$. Suppose we have $\alpha = \frac{1}{\sqrt{2}} = \beta$ this implies $|Q\rangle = \left(1/\sqrt{2}, 1/\sqrt{2}\right)^{\mathrm{T}}$ and $\vec{\mathbb{P}} = \left(1/2, 1/2\right)^{\mathrm{T}}$. The only probability distribution that can be generated with the classical randomness is equal probability in 0 or 1. However in the qubit, if we re-write $|Q\rangle$ in the $|+_{\mathrm{L}}\rangle = \frac{1}{\sqrt{2}}(|0_{\mathrm{L}}\rangle + |1_{\mathrm{L}}\rangle)$ and $|-_{\mathrm{L}}\rangle = \frac{1}{\sqrt{2}}(|0_{\mathrm{L}}\rangle - |1_{\mathrm{L}}\rangle)$ basis, we have $|Q\rangle = |+_{\mathrm{L}}\rangle$, means the probability of being in the $\pm$ state given $|Q\rangle$ is exactly 1. So it's certain that we have $|Q\rangle$ in $|+_{\mathrm{L}}\rangle$, $\mathbb{P}(+|\,|Q\rangle) = 1$. The crux of the matter is that a quantum superposition can give rise to different probability distributions based on different basis. This is drasticaly different to it classical counterpart. There are many many difference one can dive into between what a quantum or classical state is, or even the classical to quantum transitions [59].

To store quantum information in multiple qubits, a tensor product between different systems is used. A n-qubit system will in general be written as:

$$|\Psi\rangle = \sum_{j \in \{0,1\}^{\otimes n}} \alpha_j |j\rangle \ , \tag{2.4}$$

which has $N = 2^n$ basis terms. In order to simulate such a general n-qubit state on a classical computer without any information or symmetries on the mathematical structure of the amplitudes, $\mathcal{O}(2^n)$ numbers needs to be stored. Hence, just the memory requirements is exponential in terms of the input system size n. This is one of the reasons why the simulation of quantum systems is hard.

2.1.2 DiVincenzo's criteria

What are the physical requirements for implementing a n-qubit quantum computer? DiVincenzo was the first to lay out the reqirements which could be broadly listed as these five key criteria [60].

1. Definition: defining a scalable physical systems to serve as the building block of a qubit.
2. Initialisation: ability to generate qubits to a initial state such as $|0000...000\rangle$.
3. Universal gate set: the ability to perform an universal set of quantum gates that could bring the initial state to any possible state required in the quantum computation.
4. Error resilience: decoherence times (time-frame for errors to occur) $\gg$ gate operation time or other schemes of error correction required.
5. Readout and post processing: the ability to measure the channels at the end of the quantum circuit and perform efficient classical computation with data acquired to achieve the desired answer.

In this thesis, we are most concerned with the Error resilience aspect. We aim to develop quantum error correcting codes to combat this.

2.1.3 General quantum maps

In general, quantum states under the presence of classical preparation uncertainty are represented by density matrices $\hat{\rho}$ that are probabilistic mixtures of pure states $|x_j\rangle$:

$$\hat{\rho} = \sum_j p_j \, |x_j\rangle\langle x_j| \ , \tag{2.5}$$

where p_j is a probability satisfying $\sum_j p_j = 1$ and it represents the uncertainty of being in the state $|x_j\rangle$. Alternatively for probability density $\mathcal{P}(x)$ we can write $\hat{\rho}$ as an integral for continuous states:

$$\hat{\rho} = \int_x dx \ \mathcal{P}(x) \, |x\rangle\langle x| \ , \tag{2.6}$$

where $\int_x dx \ \mathcal{P}(x) = 1$ and $\int_x dx \ \ |x\rangle\langle x| = \hat{\mathbb{1}}$, the identity operator. Unitary transformations ($\hat{U}\hat{U}^\dagger = \hat{\mathbb{1}} = \hat{U}^\dagger\hat{U}$) of $\hat{\rho}$ will be represented by $\hat{U}\hat{\rho}\hat{U}^\dagger$. Unitary transformations are not the most general quantum evolution. In the presence of errors and measurements the density matrix would under go a completely positive (CP) and trace preserving (CPTP) map [25], given by $\Lambda(\cdot)$:

$$\Lambda(\hat{\rho}) = \sum_j E_j \hat{\rho} E_j^\dagger \ , \tag{2.7}$$

where E_j are known as Kraus operators satisfying $\sum_j E_j^\dagger E_j = \hat{I}$. Unitary evolution is just a limiting case of a CPTP map with only one Kraus operator. Types of physical systems to define a qubit, the steps for resource and initial state generation readout measurements are physical platform dependent. However, there are well agreed upon universal gate sets and error correcting scheme between different physical platforms. These will be discussed in the next two sections.

2.1.4 Quantum gates

Once a physical system is defined, a quantum computation maps the initial n-qubit state $|000...000\rangle$ to a final state $\sum_{\vec{x}} c_{\vec{x}} |x_1 x_2 x_3 ... x_{n-2} x_{n-1} x_n\rangle$ via a n-qubit unitary transformation, $\hat{U}$.

$$|000...000\rangle \rightarrow \hat{U} |000...000\rangle = \sum_{\vec{x}} c_{\vec{x}} |x_1 x_2 x_3 ... x_{n-2} x_{n-1} x_n\rangle \tag{2.8}$$

A general n-qubit unitary $\hat{U}$ will have $\mathcal{O}(4^n)$ parameters, hence further demonstrating the exponential resources needed to represent a quantum state. A single qubit unitary can always be written in the preferred matrix basis of $\{\hat{I}, \hat{X}, \hat{Y}, \hat{Z}\}$, where $\hat{I}$ is the 2 by 2 identity matrix and $\hat{X}, \hat{Y}, \hat{Z}$ are the X-, Y- and Z-Pauli matrices given by (in the $|0_{\mathrm{L}}\rangle, |1_{\mathrm{L}}\rangle$ basis):

$$\hat{X} = \begin{pmatrix} 0 & 1 \\ 1 & 0 \end{pmatrix} \ , \ \hat{Y} = \begin{pmatrix} 0 & -i \\ i & 0 \end{pmatrix} \ , \ \hat{Z} = \begin{pmatrix} 1 & 0 \\ 0 & -1 \end{pmatrix} \ . \tag{2.9}$$

Note that the $\hat{X}$ is the classical analogue of bit flipping, whereas $\hat{Z}$ gives the $|1_{\mathrm{L}}\rangle$ a -1 phase and $\hat{Y} = -i\hat{X}\hat{Z}$ is a combination of $\hat{X}$ and $\hat{Z}$ up to a $-i$ phase. Due to the Solovay-Kitaev theorem [61], a n-qubit unitary can always be decomposed in to elementary 2-qubit and 1-qubit unitaries known as gates and the combination of these smaller elementary gates is known as a quantum circuit. An example of a quantum circuit shown in figure 2.1.

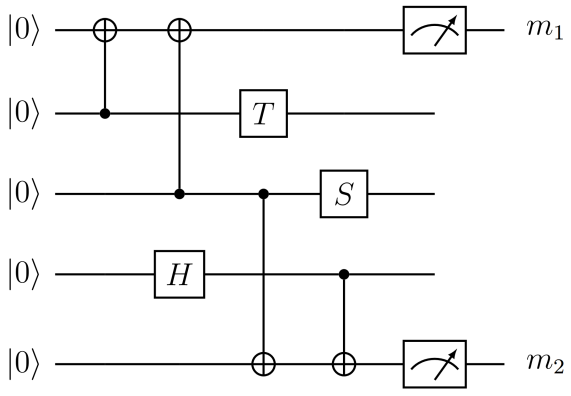

Figure 2.1: A 4 layers depth quantum circuit consisting of 2- and 1-qubits gates initialised with the state $|0\rangle^{\otimes 5}$ and measurements in the Pauli-Z basis in systems 1 and 5 at the end of the circuit.

There are many choices of a set of elementary single and two qubit gates to achieve universal quantum computing, but the most common gate set is the Clifford generator set with a non-Clifford gate such as a $\hat{T}$ gate [62]. The Clifford gates are often expressed by the generator set $\{\hat{H}, \hat{S}, \hat{C}_X\}$,

$$\hat{H} = \frac{1}{\sqrt{2}} \begin{pmatrix} 1 & 1 \\ 1 & -1 \end{pmatrix} = \quad -\boxed{H}-$$

$$\hat{S} = \begin{pmatrix} 1 & 0 \\ 0 & i \end{pmatrix} = \quad -\boxed{S}- \tag{2.10}$$

$$\hat{C}_X = \begin{pmatrix} 1 & 0 & 0 & 0 \\ 0 & 1 & 0 & 0 \\ 0 & 0 & 0 & 1 \\ 0 & 0 & 1 & 0 \end{pmatrix} =$$

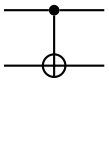

The non-Clifford gate T is,

$$\hat{T} = \begin{pmatrix} 1 & 0 \\ 0 & e^{-i\pi/4} \end{pmatrix} = \quad -\boxed{T}- \quad . \tag{2.11}$$

This is just one choice of a universal gate set. The most important reason why $\underbrace{\{\hat{H}, \hat{S}, \hat{C}_X\}}_{\text{Clifford set}} \cup \hat{T}$ is an important universal gate set is due to the Gottesman-Knill theorem [63]. The Gottesman-Knill theorem can be used to explain why certain quantum circuits can be classically simulated. Essentially logical zeros input states: $|0\rangle^{\otimes n}$ along with Clifford gate can be simulated in $\mathcal{O}(n^3)$ space-time computational cost because only a linear number of Group operators needed to be tracked to perform the Clifford circuit. Starting with a n-qubit initial state $|000...000\rangle$, a classical computer can efficiently simulate the quantum circuit if we only apply the Clifford gate set in any combination to the initial state and measure in the $|0\rangle, |1\rangle$ basis at the end. However

as soon as we include $\hat{T}$ gates, the problem becomes intractable for classical computers. This is one of the first examples pointing to what circuits are hard to simulate. Even highly entangled states can be efficiently simulated via a classical computer as long as they are generated via the Clifford gate set acting on the initial state. The formal reasoning behind this revolves around expressing qubit operators in the Heisenberg representation (stabilizer formalism) [63].

2.2 Continuous variables quantum computation

Continuous variables (CV) quantum computing is an alternative implementation of quantum computing based on the manipulation of quantum fields and encoding the qubit in a bosonic mode. This framework is well suited to quantum optics, where passive optical elements, homodyne detection and photonic resource states are used to carry out the quantum computation.

Optical quantum computing promises the ability to generate on-demand large scale entangled states (up to a million modes [64]), the two qubit gates are fast and have low errors, the ability to do most of the quantum computation in room temperature (except the superconducting photon counting detectors) and push the generation of resource states offline [56]. Hence, optical quantum computing systems are well suited to the new paradigm of measurement based quantum computing (MBQC), where the quantum operations/gates are replaced by measurement patterns of the preparation of a large scale highly entangled cluster state [65], where you use up the easily generated large scale cluster state as a resource for the quantum computation. However, the additional non-Gaussian resources states needed to perform universal fault tolerant quantum computation are often difficult to generate. Furthermore, fault tolerant quality photonic Gottesman-Kitaev-Preskill resource states have not been generated experimentally [66].

A short introduction to quantum optics will be presented here before discussing the notations in CV quantum information.

2.2.1 Bosonic mode definitions

Starting with a bosonic mode, it has an infinite dimensional Hilbert space $\mathcal{H}_{\text{boson}}$. Observables in this Hilbert space can have a continuous eigenspectrum[1]. These systems are also commonly known as continuous variables (CV) quantum systems. There are two crucial independent and complete basis in $\mathcal{H}_{\text{boson}}$, they are the q- and p-quadrature basis represented by $|x\rangle_q$ and $|r\rangle_p$ respectively, with $x, r \in \mathbb{R}$. Natural units $\hbar = 1$ will be used throughout the text. Note that $|x\rangle_q, |r\rangle_p$ are eigenstates to the q- and p-quadrature operators respectively:

$$\begin{aligned} \hat{q}\,|x\rangle_q &= x\,|x\rangle_q \\ \hat{p}\,|r\rangle_p &= r\,|r\rangle_p \end{aligned} \tag{2.12}$$

where the quadratures operators follow the canonical commutator relationship: $[\hat{q}, \hat{p}] = i\hat{\mathbb{I}}$, where $\hat{\mathbb{I}}$ is the identity on the infinite dimensional Hilbert space support. The q-quadrature wavefunction $\Psi(x)$ of any pure state $|\Psi\rangle \in \mathcal{H}_{\text{boson}}$ is define as:

$${}_q\langle x|\Psi\rangle = \Psi(x)\ , \tag{2.13}$$

while the p-quadrature wavefunction $\tilde{\Psi}(r)$ is related to $\Psi(x)$ via the Fourier transform $\mathcal{F}_{x\to r}$:

$$\mathcal{F}_{x\to r}\Big\{\Psi(x)\Big\} = \int_{x\in\mathbb{R}} dx\ \frac{e^{-ixr}}{\sqrt{2\pi}}\Psi(x) \tag{2.14}$$

The quadrature eigenstates follows the relation: ${}_p\langle r|x\rangle_q = \dfrac{e^{-irx}}{\sqrt{2\pi}}$. Conveniently, $\hat{q}, \hat{p}$ is related to the annihilation operator $\hat{a}$ through:

$$\hat{a} = \frac{\hat{q} + i\hat{p}}{\sqrt{2}}\ , \tag{2.15}$$

where we can re-write $\hat{q} = \frac{\hat{a}+\hat{a}^\dagger}{\sqrt{2}}$ and $\hat{p} = \frac{\hat{a}-\hat{a}^\dagger}{\sqrt{2}i}$. The annhilation operator is a eigen-operator to the set of over-complete wavefunctions called the coherent states, $\{|\alpha\rangle\}_{\alpha\in\mathbb{C}}$. The eigenvalue

[1]Not necessarily always continuous, for example you can still have discretely countable infinite number of energy eigenvalues in the quantum harmonic oscillator.

equation is $\hat{a}\,|\alpha\rangle = \alpha\,|\alpha\rangle$. The coherent state has a q-quadrature wavefunction of the form:

$$\alpha(x) = \frac{1}{\pi^{\frac{1}{4}}} e^{-\frac{1}{2}(x-\sqrt{2}\alpha)^2} e^{-\frac{1}{2}(|\alpha|^2-\alpha^2)} \ . \tag{2.16}$$

The conjugate transpose of the annihilation operator $\hat{a}^\dagger$ is known as the creation operation and they follow the commutation relation, $[\hat{a}, \hat{a}^\dagger] = \hat{\mathbb{I}}$. The number operator $\hat{n}$ is an eigen-operator to the Fock states $\{|m\rangle\}_{m=0}^{\infty}$ with $\hat{n} = \hat{a}^\dagger\hat{a}$.

$$\begin{aligned} \hat{n}\,|m\rangle &= m\,|m\rangle \\ \hat{a}\,|m\rangle &= \sqrt{m}\,|m-1\rangle \\ \hat{a}^\dagger\,|m\rangle &= \sqrt{m+1}\,|m+1\rangle \end{aligned} \tag{2.17}$$

These two quadrature bases can be transformed from one to another via the Fourier transform operator $\hat{F}$:

$$\hat{F} = e^{i\frac{\pi}{4}} e^{i\frac{\pi\hat{n}}{2}} \ . \tag{2.18}$$

The $(q, p) \in \mathbb{R}^2$ define a two dimensional plane called phase space. An alternative description of a quantum state is given by a Wigner function (quasi-probability distribution) [67] for a state $\hat{\rho}$:

$$W(q, p|\hat{\rho}) = \frac{1}{\pi} \int_{y\in\mathbb{R}} dy \ \ {}_q\langle q+y|\,\hat{\rho}\,|q-y\rangle_q\, e^{2ipy} \ , \tag{2.19}$$

additionally the density matrix function (which will be used frequently) is defined as:

$$\rho(x, y|\hat{\rho}) = \ {}_q\langle x|\,\hat{\rho}\,|y\rangle_q \ , \tag{2.20}$$

which is the matrix elements of the density matrix $\hat{\rho}$ in the q-quadrature basis. Another set of important operators are the displacement operators:

$$\begin{aligned} \hat{\sigma}_x(u) &= e^{-iu\hat{p}} \\ \hat{\sigma}_z(v) &= e^{iv\hat{q}} \ , \end{aligned} \tag{2.21}$$

these operators, $(\hat{\sigma}_x(u), \hat{\sigma}_z(v))$, shift the (q, p) axis of phase space by (u, v) respectively. Together these two operators $\hat{\sigma}_x(u)$ and $\hat{\sigma}_z(v)$ defines the total displacement operator in phase space:

$$\hat{d}(u, v) = e^{-iv\hat{q}} e^{-iu\hat{p}} = \hat{\sigma}_z(v)\hat{\sigma}_x(u) \ . \tag{2.22}$$

An important two mode entangling operator is the beamsplitter, defined as:

$$\hat{B}_\phi = \mathrm{e}^{-\frac{\phi}{2}(\hat{a}^\dagger \hat{b} - \hat{a}\hat{b}^\dagger)} \ , \tag{2.23}$$

this operator rotates a two mode q-quadrature wavefunction $\psi(x, y)$ by ϕ radians in the x-y plane. Another important single mode operator is the squeezing operator

$$\hat{S}_c = \mathrm{e}^{\frac{\ln(c)}{2}(\hat{a}^2 - (\hat{a}^\dagger)^2)} \ , \tag{2.24}$$

it transforms a q-quadrature wavefunction by, $\psi(x) \to \psi(cx)$, effectively shrinking or stretching the wavefunction by c. Operations such as the displacement, squeezing operators and beamsplitter in quantum optics are part of a larger class of bosonic operators called Gaussian operations, which are defined as unitary operations that has at most quadratic multiples of $\hat{a}$ and $\hat{a}^\dagger$ in its Hamiltonian [56, 44].

2.2.2 Dominant error models

The most dominant physical noise in a bosonic mode is the amplitude damping channel [68], we have written the completely positive map $\mathcal{N}$ for the amplitude damping channel and one choice of its Kraus operators in terms of the annihilation and creation operators [24]:

$$\begin{aligned} \mathcal{N}_\gamma(\hat{\rho}) &= \sum_{n=0}^{\infty} E_n \hat{\rho} E_n^\dagger \ , \\ E_n &= \Big(\frac{\gamma}{1-\gamma}\Big)^{n/2} \frac{\hat{a}^n}{\sqrt{n!}} (1-\gamma)^{\hat{n}/2} \ . \end{aligned} \tag{2.25}$$

The action of this error channel can be interpreted as loss of photons in the Fock basis, with $0 \leq \gamma \leq 1$ being a probability of loss. A Taylor expansion with $\gamma \ll 1$ demontrates this point.

Suppose $(1-\gamma)^{\hat{n}/2} = \hat{\mathbb{I}} - (\gamma/2)\hat{n} + \mathcal{O}(\gamma^2)$, dropping terms from order $\mathcal{O}(\gamma^2)$, then the Kraus operators are given by

$$E_n \approx \gamma^{n/2}(1+n\gamma/2)\frac{\hat{a}^n}{\sqrt{n!}}\Big(\mathbb{I} - \frac{\gamma}{2}\hat{n}\Big) \ . \tag{2.26}$$

If we drop all terms from $\mathcal{O}(\gamma)$, then only 2 possible Kraus operators exist, they are E_0 and E_1:

$$\begin{aligned} E_0 &\approx \hat{\mathbb{I}} \ , \\ E_1 &\approx \sqrt{\gamma}\hat{a} \ . \end{aligned} \tag{2.27}$$

The operator E_0 implies no loss while E_1 enacts an annihilation operation on the state, effectively causing single photon loss at rate γ. In a realistic setting, if it were possible to measure the loss rate γ offline and pre-amplify the state prior to the loss channel, we can transform the amplitude damping channel to the random Gaussian displacement channel given by $\mathcal{E}_{\sigma_0}$ [69]. This error channel has can be interpreted as a random displacement in phase space in both the q- and p-quadrature direction with the magnitude of the displacement following a Gaussian distribution:

$$\mathcal{E}_{\sigma_0}(\hat{\rho}) = \frac{1}{2\pi\sigma_0^2}\iint_{\alpha\in\mathbb{C}} \mathrm{d}u\mathrm{d}v \ e^{-\frac{u^2+v^2}{2\sigma_0^2}} \ \hat{d}(u,v)\,\hat{\rho}\,\hat{d}(u,v)^\dagger \ , \tag{2.28}$$

and the width $\gamma = \sigma_0^2$ quantifies the extent of the error. The random Gaussian displacement error channel describes amplitude damping that is preceded by an offsetting pre-amplification [70], and it is therefore highly relevant to many experimental platforms.

2.3 Bayesian estimators [5]

We wish to establish an overview of Bayesian estimators, which will be used extensively in chapter 5 to decode the syndrome. Suppose we have an error that follows a known error distribution $\mathbb{P}(U)$ and its error realisation $u \sim U$. In addition, we have a measurement result x_m that is correlated with u. The likelihood is the distribution of the measurement result given

a known u. The likelihood is represented by $\mathbb{P}(x_\mathrm{m}|u)$. Following Bayes' theorem, the posterior can be calculated as follows:

$$\underbrace{\mathbb{P}(u|x_\mathrm{m})}_{\text{posterior}} = \frac{\overbrace{\mathbb{P}(x_\mathrm{m}|u)}^{\text{likelihood}}\,\mathbb{P}(u)}{\underbrace{\int_u du\ \mathbb{P}(x_\mathrm{m}|u)\mathbb{P}(u)}_{\text{Normalisation factor}}}\ . \tag{2.29}$$

The posterior is the distribution of the error given the measurement result. The mean of the posterior distribution given by:

$$\tilde{u}(x_\mathrm{m}) = \int_u du\ u\mathbb{P}(u|x_\mathrm{m})\ , \tag{2.30}$$

this can be used as an estimator to infer the error parameter u given the measurement result. The estimator of u is written as $\tilde{u}(x_\mathrm{m})$, which is a function dependent on x_m. Finally, the mean square error of the estimator can be given by the standard deviation of the posterior:

$$\sigma(u|x_\mathrm{m}) = \sqrt{\int_u du\ u^2\mathbb{P}(u|x_\mathrm{m}) - \left(\int_u du\ u\mathbb{P}(u|x_\mathrm{m})\right)^2}\ . \tag{2.31}$$

With the above information given the likelihood and error distribution, we can calculate the posterior and use the 1st and 2nd order moments of the posterior to infer the error u with the estimators and bound its error of estimation: $\tilde{u}(x_\mathrm{m}) \pm \sigma(u|x_\mathrm{m})$.

Chapter 3

The grid states

This chapter introduces well-known aspects of the grid states, starting with the wavefunction definitions of the Gottesman-Kitaev-Preskill and grid sensor states, before a short description of the generalisation of these states via the stabiliser formalism. The definitions of these states will be used extensively throughout this thesis.

3.1 Definitions

3.1.1 The Gottesman-Kitaev-Preskill states

The approximate GKP codewords with width $\vec{\Delta} = (\Delta, \kappa)$ are defined as,

$$\psi_{\mu}^{\vec{\Delta}}(x) = \frac{\sqrt{2}}{\pi^{\frac{1}{4}}} \sum_{s \in \mathbb{Z}} G_{\frac{1}{\kappa}}[(2s+\mu)\sqrt{\pi}]\, G_{\Delta}[x - (2s+\mu)\sqrt{\pi}] \tag{3.1}$$

where $G_{\Sigma}(z) = \exp\left\{(-\frac{z^2}{2\Sigma^2})\right\}$ and $\mu \in \{0, 1\}$ defines the logical basis states. Informally, for the logical 0 (1) state we have a superposition of Gaussians of width Δ centered at even (odd) multiples of $\sqrt{\pi}$, with an overall Gaussian envelope of width $1/\kappa$. Better approximations to the ideal GKP state are achieved with smaller values of Δ and κ, although these also correspond to larger average energy and an apparent increase in experimental difficulty. The

normalisation before the summation can be expressed as elliptic theta functions, but it can often be approximated to be $\frac{\sqrt{2}}{\pi^{\frac{1}{4}}}$ in the case of high quality GKP states. A more mathematically rigorous definition of the normalisation constants in terms of Δ and how other definitions of GKP states coincide with each other is given in [71].

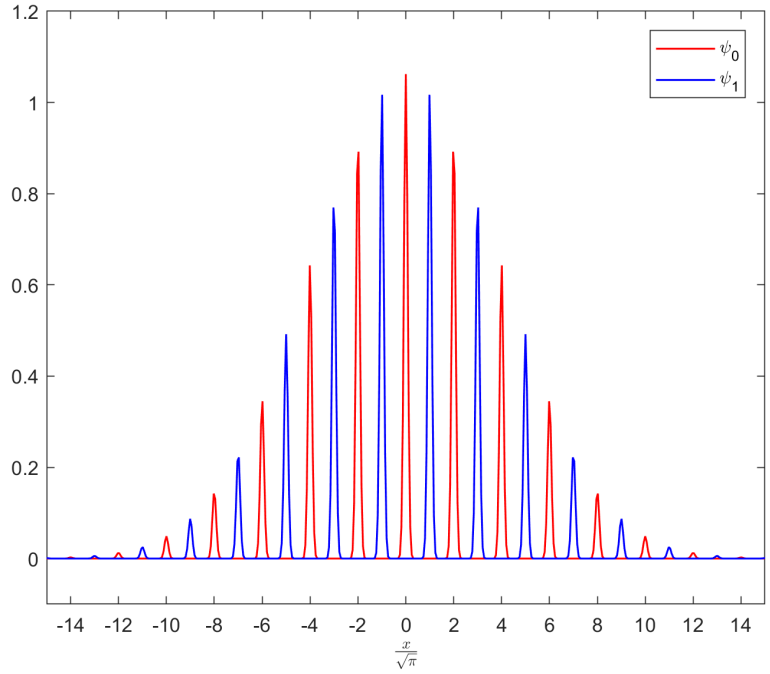

Figure 3.1: GKP logical states ψ_0 and ψ_1 in the q-quadrature using $\Delta = 0.1$ here.

3.1.2 The grid sensor state

The finite-energy grid sensor state (also known as the *qunaught state* in the literature) [55] is a bosonic state first introduced as a modified GKP state to tackle problems in quantum sensing. The width between each Gaussian peaks for the grid sensor state is $\sqrt{2\pi}$ compared to integers multiples of $\sqrt{\pi}$ in the GKP state. The grid sensor state, $|S_\Delta\rangle$, is parameterised by a width parameter Δ, and has a q-quadrature wavefunction of the form:

$$S_\Delta(x) = \lambda(\Delta) \sum_{n\in\mathbb{Z}} G_{\frac{1}{\Delta}}\left(n\sqrt{2\pi}\right) G_\Delta\left(x - n\sqrt{2\pi}\right) \ . \tag{3.2}$$

Where $\lambda(\Delta)$ is a normalisation constant with a limiting value of $\lim_{\Delta\to 0} \lambda(\Delta) = (2/\pi)^{1/4}$ for $\Delta \leq 1/\sqrt{2\pi}$. Also note that $\lim_{\Delta\to 0} S_\Delta(x) = \text{Ш}(x) = \sum_{n\in\mathbb{Z}} \delta(x - n\sqrt{2\pi})$, a Dirac comb of

width $\sqrt{2\pi}$, which is the tempered distribution eigenfunction of the Fourier transform operator with eigenvalue 1 [72]. Note that, $|S_\Delta\rangle$ has an average photon number of $\bar{n} \approx \frac{\Delta^2+\Delta^{-2}}{2} - \frac{1}{2}$ [73].

3.1.3 Generalisations of the GKP state

We wish to now lay down the theoretical definitions of the infinite energy grid states and generalisations of it. This is important because we can gain intuition as to where their periodicity comes from. We wish to give a short definition of stabiliser states before proceeding with the definitions of the GKP states via stabilisers.

Pure stabiliser states [74]

Pure stabiliser states are joint eigenstate to a set of operators s that forms the generators of a *group* $\mathcal{S}$. The group $\mathcal{S}$ is called the stabiliser group and $V_\mathcal{S}$ is the spanning set of states (stabiliser states) stabilised by $s \in \mathcal{S}$. The formal definition is as follows:

$$s\,|A\rangle = |A\rangle \;\; \forall s \in \mathcal{S} \Leftrightarrow \mathcal{S} \text{ stabilises } V_\mathcal{S} = \{|A\rangle\} \; . \tag{3.3}$$

Note that $\mathcal{S}$ must be Abelian because only commuting operators have simultaneous eigenstates. We can write $\mathcal{S}$ in terms of its generators:

$$\mathcal{S} = \langle s_1, s_2, ..., s_k \rangle \; , \tag{3.4}$$

where the group $\mathcal{S}$ is written in the standard notation of its generators inside the $\langle ... \rangle$ brackets.

Ideal square-lattice GKP states [75]

The ideal square-lattice GKP state(s) [75] are bosonic state defined by the stabiliser generators:

$$\mathcal{S}_{\text{GKP}}(\alpha, \beta) = \langle \hat{\sigma}_x(2\alpha), \hat{\sigma}_z(2\beta) \rangle \; , \tag{3.5}$$

where $\hat{\sigma}_x(u) = e^{-iu\hat{p}}, \hat{\sigma}_z(v) = e^{iv\hat{q}}$ as defined in equation 2.21. The Abelian constraint of the group $\mathcal{S}_{\text{GKP}}(\alpha, \beta)$ means that $\alpha\beta = 2D\pi$ where $n \in \mathbb{Z}$. The parameter $D = \dim(V_{\mathcal{S}_{\text{GKP}}})$, denotes the dimension of the spanning set of states stabilised by $\mathcal{S}_{\text{GKP}}$. An *unbiased* [76] square-lattice GKP state means $\alpha = \beta$. For the rest of the section we shall focus on the unbiased case and will drop the second parameter in $\mathcal{S}_{\text{GKP}}(\alpha, \alpha) = \mathcal{S}_{\text{GKP}}(\alpha)$.

For example, when $D = 1 \Rightarrow \alpha = \sqrt{2\pi}$, the group $\mathcal{S}_{\text{GKP}}(\sqrt{2\pi})$:

$$\mathcal{S}_{\text{GKP}}(\sqrt{2\pi}) = \left\langle \hat{\sigma}_x(\sqrt{2\pi}), \hat{\sigma}_z(\sqrt{2\pi}) \right\rangle \tag{3.6}$$

The corresponding set to $\mathcal{S}_{\text{GKP}}(\sqrt{2\pi})$, $V_{\mathcal{S}_{\text{GKP}}(\sqrt{2\pi})}$, comprises of one state:

$$\sum_{j\in\mathbb{Z}} \left| j\sqrt{2\pi} \right\rangle_q \ , \tag{3.7}$$

This is the state $|S_{\Delta\to 0}\rangle$ grid sensor state [73].

The set of states stabilised by $\mathcal{S}_{\text{GKP}}$ when $D = 2$ are the conventional GKP states as defined by the original authors [77], the set is spanned by:

$$V_{\mathcal{S}_{\text{GKP}}(2\sqrt{\pi})} = \text{span}\left\{ \underbrace{\sum_{j\in\mathbb{Z}} \left|(2j)\sqrt{\pi}\right\rangle_q}_{\left|\psi_0^{(\Delta=0,\kappa=0)}\right\rangle}, \overbrace{\sum_{j\in\mathbb{Z}} \left|(2j+1)\sqrt{\pi}\right\rangle_q}^{\left|\psi_1^{(\Delta=0,\kappa=0)}\right\rangle} \right\} , \tag{3.8}$$

and

$$\mathcal{S}_{\text{GKP}}(2\sqrt{\pi}) = \left\langle \hat{\sigma}_x(2\sqrt{\pi}), \hat{\sigma}_z(2\sqrt{\pi}) \right\rangle . \tag{3.9}$$

These states are the infinite energy versions of the logical zero and one GKP states.

Notice the ideal square-lattice GKP states are generalisations of the grid states such as GKP or grid sensor states. The stabilisers in $\mathcal{S}_{\text{GKP}}(2\sqrt{\pi})$ implies that any integer multiple of $2\sqrt{\pi}$ shift in either the q- or p-quadrature direction leaves the infinite energy GKP state unchanged, this defines the GKP state's periodicity. Similarly, the infinite energy sensor state is invariant under any integer multiple of $\sqrt{2\pi}$ in either the q- or p-quadrature direction.

Chapter 4

Properties of the grid states

A leading approach to CV quantum computation, proposed by Gottesman, Kitaev and Preskill (GKP) [35], is based on the idea of encoding a qubit within an (infinite dimensional) oscillator. Ideal codeword wavefunctions within this paradigm correspond to infinite-energy Dirac combs, and are commonly referred to as GKP states. In practice, this ideal wavefunction is replaced by a finite-energy approximation, such as a comb of narrow Gaussian peaks modulated by a broad Gaussian envelope. A close relative to the GKP state is the grid sensor state, proposed in [55] as a quantum state used to infer small displacements in phase space for quantum metrology. The GKP states and grid sensor state differ only by the spacing of neighbouring Gaussian peaks in the q-quadrature wavefunction, with spacings of $\sqrt{\pi}$ and $\sqrt{2\pi}$ respectively.

Some promising results from [78] show that the grid sensor state can double the scan-rate of detecting a small displacement in the electromagnetic field (related to squeezed vacuum states) in searches for axion particles, a potential candidate for dark matter. They are also used as resource in quantum teleportation schemes involving GKP states in a larger CV quantum computation architecture [79]. Additionally, the state are used for adaptive phase estimation [55] and improving distributed sensing [80]. The appeal of GKP-encoded qubits or grid sensors states are their intrinsic robustness to physically motivated error channels, the existence of natural schemes for error syndrome extraction and correction using the GKP-encoded qubits [66] and the ability to simultaneously estimate displacement/error in phase space in two per-

pendicular directions [81]. Firstly the GKP states and grid sensor states are defined, before exploring the many different aspects of the grid sensor state in this chapter. The properties of the grid sensor state motivates the logical GKP qubits as a promising candidate for bosonic error correction.

This chapter explores several different aspects of the grid sensor state including its error resilience to Gaussian random displacement channel, Fourier transform properties, its Fock state amplitudes, the resource cost of generation, the quantum parameter estimation capabilities and finally on its transformation to the GKP Bell states briefly.

Displacement sensing

In section 4.1, we wish to layout some motivations for the the displacement sensing problem in CV quantum systems via functional minimisation. This will be a good introduction to section 4.2 and 4.3 where the sensing properties of quantum states are laid out through the quantum Fisher information.

4.1 Motivations for the displacement sensing problem

Section 4.1 consists of my own work.

Quantum information in a bosonic mode [82] can be quickly destroyed by noise. This noise can be largely represented as an unwanted shift in the q- and p-quadrature basis of the wavefunction. For example, the vacuum state to the quantum harmonic oscillator is:

$$\phi_0(x) = \frac{e^{-\frac{x^2}{2}}}{\pi^{\frac{1}{4}}} \ . \tag{4.1}$$

A small shift in the q-quadrature can be represented in figure 4.1. The shift is the error and is

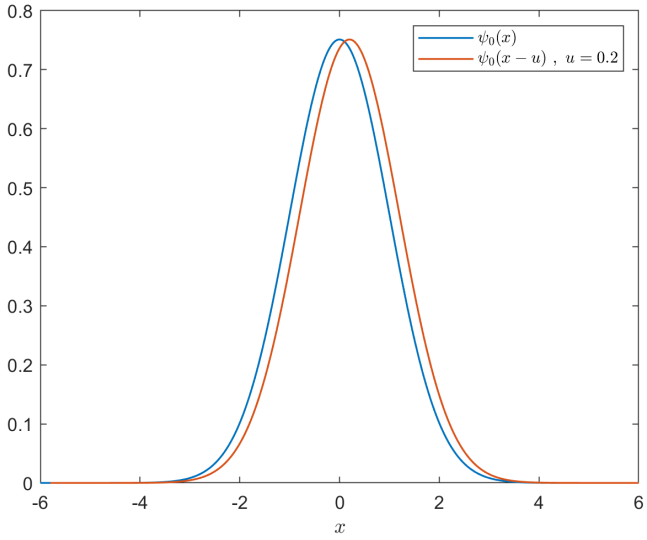

Figure 4.1: A vacuum state and its shifted counterpart (by 0.2).

undesirable. Sensor states are useful in detecting such shifts. To illustrate this point, consider

measuring the wavefunction $\phi_0(x)$ in the q-quadrature basis, which has results distributed according to the probability density:

$$\mathbb{P}(y) = |\phi_0(y)|^2 \ , \tag{4.2}$$

given the measurement result y, the wavefunction collapse into $\delta(x-y)$.

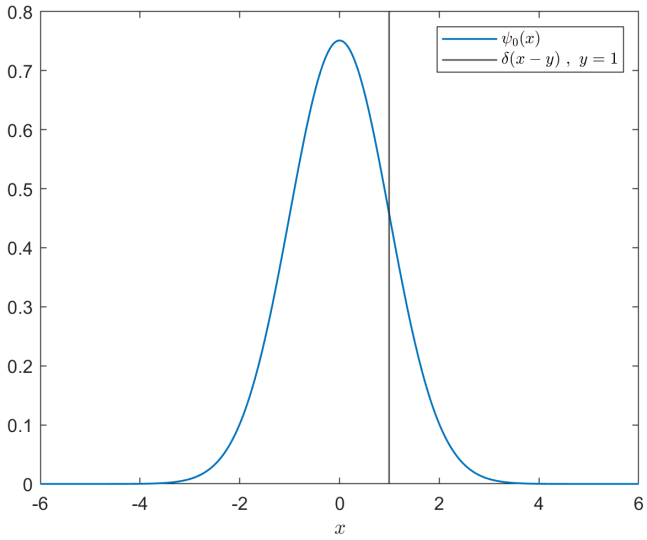

Figure 4.2: A vacuum state measured in the q-quadrature basis will collapse to a delta wavefunction into $\Delta(x-y)$. In this example above, $y=1$.

Given the input state $|\Psi\rangle$, the protocol is as follows:

$$\Psi(x) \xrightarrow[\text{error}]{x\to x-u} \Psi(x-u) \xrightarrow[\text{measurement result } y]{\text{q basis}} \delta(x-y) \ , \tag{4.3}$$

The state first acquires an unknown error u and then undergoes a q-quadrature measurement with measurement result y, the probability of getting this measurement results is $|\Psi(y-u)|^2 dx$. The measurement result y should be a functional in terms of Ψ and a function in terms of the error u, $y\{[\Psi],(u)\}$. What wavefunction Ψ gives the best estimate of the error u on average given the random measurement result y? The goal is to devise a decoding function $\tilde{u} = f(y)$ such that $\tilde{u}$ is an estimation for u. Displacement errors are physically relevant as any general quantum error on a bosonic mode can be decomposed into a statistical ensemble of displacement errors [24].

4.1.1 Toy problems

Understanding sensing in the q-quadrature

To motivate the general problems sensor states are used to solve, this section will introduce a series of toy models. Starting with a toy model, fix the decoding function to be linear $f(y) = y$, using the measurement result gives as an estimator for the shift u. The measurement result y is sampled from the probability distribution $|\Psi(y-u)|^2$. Then $\Psi(x) = \delta(x)$ gives the optimal wavefunction for this decoding function. Starting with a trial function of (a squeezed vacuum state here):

$$\Psi(x) = \frac{1}{\sqrt{\lambda}}\psi_0(x/\lambda) = \frac{e^{-\frac{x^2}{2\lambda^2}}}{(\lambda^2\pi)^{\frac{1}{4}}} \ . \tag{4.4}$$

The delta function is the optimal (albeit unrealistic) wavefunction in this case. The conditional probability density of measuring in the q-quadrature given the error u is $\mathbb{P}(x|u) = |\Psi(x-u)|^2 = \frac{e^{-\frac{(x-u)^2}{\lambda^2}}}{\sqrt{\lambda^2\pi}}$. Sampling $X \sim \mathbb{P}(X|u)$, the expectation value is $\langle X\rangle_{\mathbb{P}(X|u)} = u$. This implies the mean of the samples gives you an unbiased estimator for u.

The mean square error is $\langle X^2\rangle_{\mathbb{P}(X|u)} - \langle X\rangle^2_{\mathbb{P}(X|u)} = \lambda^2/2$. Minimising the mean square error in this case, $\lambda^2/2 \to 0$, gives the optimal estimator. Note that the limit $\lim_{\lambda\to 0} \frac{e^{-\frac{x^2}{2\lambda^2}}}{(\lambda^2\pi)^{\frac{1}{4}}} = \delta(x)$, hence the delta function is recovered. This shows the optimal wavefunction is $\delta(x)$ for the decoding function $f(y) = y$. Localised states are most susceptible to shifts errors and thus more informative when probed by a measurement. Unfortunately, a highly localised state in the q-quadrature is delocalised in the p-quadrature. Hence there is a trade-off between the performance in conjugate quadratures.

Ideally, this problem could be solved by functional minimisation with Lagrange multipliers and introduce a normalisation constraint, so that the wavefunctions are square integrable. Also, the delta function is an infinite energy state that is unphysical. Typically, in physical situations when a finite energy constraint is required, squeezed states are introduced with infinite squeezing corresponding to infinite energy.

Understanding sensing in the q- and p-quadrature

The most relevant quantum errors to bosonic stabiliser codes are displacement errors [83]. Hence, error channels that can be decomposed as a weighted linear combination of shift over both quadratures are error channels of interest. It is then required that error shifts in either quadrature are sensed equally well. Suppose the function $\Psi(x)$ is the variable function to be functionally minimised. Note that, the Fourier transform of $\Psi(x)$ to its conjugate is $\mathcal{F}[\Psi(x)] = \tilde{\Psi}(p) = \frac{1}{\sqrt{2\pi}} \int_{-\infty}^{\infty} \Psi(x) e^{-ixp} dx$, the set up is as follows:

$$\Psi(x) \xrightarrow[\text{error}]{x \to x-u \ , \ p \to p-v} e^{ixv} \Psi(x-u) \xrightarrow[\text{measurement result } y]{\text{q or p basis}} , \tag{4.5}$$

The q-quadrature representation after error is $e^{ixv}\Psi(x-u)$ and the measurement result is sampled from $Y \sim |\Psi(Y-u)|^2$. On the other hand, the p-quadrature representation is $e^{-ipu}\tilde{\Psi}(p-v)$ after errors and the measurement result is sampled from $\Omega \sim |e^{-ipu}\tilde{\Psi}(\Omega - v)|^2 = |\tilde{\Psi}(\Omega - v)|^2$. Now a symmetric constraint is introduced, $\mathcal{F}[\Psi(x)] = e^{i\theta}\Psi(x)$, which is motivated from the fact that neither quadrature should be favoured. Then, it implies $X \sim |\Psi(X-u)|^2$ should be sampled from for the q-quadrature and $\Omega \sim |\Psi(\Omega - v)|^2$ for the p-quadrature. The goal is to have a minimum variance unbiased estimator. One such set of functions $\Psi(x)$ that satisfies this requirement are the Hermite-Gaussian functions which are the Fock state wavefunctions: $\phi_n(x) = (2^n n! \sqrt{\pi})^{-\frac{1}{2}} e^{-\frac{x^2}{2}} H_n(x)$, $n \in \mathbb{N} = \{0, 1, 2, 3, ...\}$ [55]. A functional minimisation is needed to find the state Ψ that minimises the mean square error. The following requirements apply:

1. Unbiased in the q-quadrature:
   $\int_{x=-\infty}^{\infty} dx \ x|\Psi(x-u)|^2 = u$ for all $u \in \mathbb{R} \Rightarrow \int_{x=-\infty}^{\infty} dx \ x|\Psi(x)|^2 = 0$
2. Unbiased in p-quadrature:
   $\int_{p=-\infty}^{\infty} dp \ p|\tilde{\Psi}(p-v)|^2 = v$ for all $v \in \mathbb{R}$. $\Rightarrow \int_{p=-\infty}^{\infty} dp \ p|\tilde{\Psi}(p)|^2 = 0$
3. Minimum variance in both quadratures simultaneously:
   $\min_{\Psi} \Big\{ \int_{x=-\infty}^{\infty} dx \ x^2|\Psi(x-u)|^2 + \int_{p=-\infty}^{\infty} dp \ p^2|\tilde{\Psi}(p-v)|^2 \Big\}$

4. Normalisation constraint:
$$\int_{x=-\infty}^{\infty} dx\ |\Psi(x)|^2 = 1$$

A function Ψ that minimises the variance can be found via by setting the functional derivative of $D[\Psi]$ to be zero and solving for $\Psi(x')$. Considering functional D,

$$D = \langle \hat{q}^2 \rangle_{\Psi(x-u)} + \langle \hat{p}^2 \rangle_{\tilde{\Psi}(p-v)} =$$
$$\int_{x=-\infty}^{\infty} dx\ x^2 |\Psi(x-u)|^2 + \int_{p=-\infty}^{\infty} dp\ p^2 \frac{1}{\sqrt{2\pi}} \int_{-\infty}^{\infty} \Psi(x_1) e^{-ix_1(p-v)} dx_1 \frac{1}{\sqrt{2\pi}} \int_{-\infty}^{\infty} \Psi^*(x_2) e^{ix_2(p-v)} dx_2 \tag{4.6}$$

Re-writing all the wavefunctions in $p \to x$.
$$\Rightarrow D = \int_{x=-\infty}^{\infty} dx\ x^2 \Big[|\Psi(x-u)|^2 + \frac{1}{2\pi} \Big(\int_{x_1=-\infty}^{\infty} \Psi(x_1) e^{-ix_1(x-v)} dx_1 \Big) \Big(\int_{x_2=-\infty}^{\infty} \Psi^*(x_2) e^{ix_2(x-v)} dx_2 \Big) \Big]$$

Recall one definition of the functional derivative is,

$$\frac{\delta}{\delta Q} \Big(\int_{x\in\mathbb{R}} dx\ f(x) Q(x) \Big) = \int_{x\in\mathbb{R}} dx\ f(x) \underbrace{\frac{\delta Q(x)}{\delta Q(x')}}_{\delta(x-x')} = f(x').$$

Using the definition of the functional derivative, assuming $\Psi \in \mathbb{R}$ for simplicity, and with further simplifications.

$$\Rightarrow \frac{\delta D}{\delta \Psi} = 2(x'+u)^2 \Psi(x') + \int_x dx\ \Big\{ \frac{x^2}{2\pi} \Big[\Big(e^{-ix'(x-v)} \Big) \Big(\int_{x_2} \Psi(x_2) e^{ix_2(x-v)} dx_2 \Big) + \Big(\int_{x_1} \Psi(x_1) e^{-ix_1(x-v)} dx_1 \Big) \Big(e^{ix'(x-v)} \Big) \Big] \Big\}\ .$$

For the normalisation constraint, we add a Lagrange multiplier ϵ, transforming the functional minimisation to $\frac{\delta}{\delta \Psi(x')} \Big(D - \epsilon \int_{x=-\infty}^{\infty} dx\ |\Psi(x)|^2 \Big) = 0$ solving for $\Psi(x')$ to obtain the optimal $\Psi(x')$.

$$\begin{aligned} \Rightarrow \frac{\delta}{\delta \Psi} \Big(D - \epsilon \int_{x=-\infty}^{\infty} dx\ |\Psi(x)|^2 \Big) &= \frac{\delta D}{\delta \Psi(x')} - \epsilon \int_{x=-\infty}^{\infty} dx\ \frac{\delta \Psi^2(x)}{\delta \Psi(x')} \\ &= \frac{\delta D}{\delta \Psi(x')} - \epsilon \int_{x=-\infty}^{\infty} dx\ 2\Psi(x) \delta(x-x') \\ &= \frac{\delta D}{\delta \Psi(x')} - \epsilon 2 \Psi(x') \end{aligned} \tag{4.7}$$

$$\Rightarrow \frac{\delta}{\delta\Psi(x')}\Big(D - \epsilon\int_{x=-\infty}^{\infty} dx\ |\Psi(x)|^2\Big) =$$
$$2\Psi(x')(-\epsilon + (x'+u)^2)$$
$$+\int_x dx\ \Big\{\frac{x^2}{2\pi}\Big[\Big(e^{-ix'(x-v)}\Big)\Big(\int_{x_2}\Psi(x_2)e^{ix_2(x-v)}dx_2\Big) + \Big(\int_{x_1}\Psi(x_1)e^{-ix_1(x-v)}dx_1\Big)\Big(e^{ix'(x-v)}\Big)\Big]\Big\} \tag{4.8}$$

Setting equation 4.8 to zero, and solving for $\Psi(x')$,

$$\Rightarrow -2\Psi(x')(-\epsilon + (x'+u)^2) = \int_x dx\ \Big\{\frac{x^2}{\sqrt{2\pi}}\Big[\Big(e^{-ix'(x-v)}\Big)\tilde{\Psi}(v-x) + \tilde{\Psi}(x-v)\Big(e^{ix'(x-v)}\Big)\Big]\Big\} \tag{4.9}$$

Using two further simplifications, firstly Ψ is invariant up to a phase after a Fourier transform: $\tilde{\Psi} = \mathcal{F}\Psi = e^{i\theta}\Psi$. This is also a physical constraint because this further ensures that there is no bias between the two quadratures. Secondly, Ψ is even, $\Psi(x) = \Psi(-x)$, as there is should be no difference between sensing in the positive and negative x direction.

$$\begin{aligned}\Rightarrow -2\Psi(x')(-\epsilon + (x'+u)^2) =& e^{i\theta}\int_x dx\ \frac{x^2}{\sqrt{2\pi}}\Big(e^{-ix'(x-v)}\Big)\Psi(v-x) + \\ & e^{i\theta}\int_x dx\ \frac{x^2}{\sqrt{2\pi}}\Psi(x-v)\Big(e^{ix'(x-v)}\Big)\end{aligned} \tag{4.10}$$

Make a change of variable in both the integrals $x = y + v$:

$$\Rightarrow -2\Psi(x')(-\epsilon + (x'+u)^2) = e^{i\theta}\Big(\underbrace{\int_y dy\ (y+v)^2\Psi(y)\frac{e^{-ix'y}}{\sqrt{2\pi}}}_{\mathcal{F}_{y\to x'}\Big\{(y+v)^2\Psi(y)\Big\}} + \int_y dy\ (y+v)^2\Psi(y)\frac{e^{ix'y}}{\sqrt{2\pi}}\Big) \tag{4.11}$$

Make another change of variable in the integral to the right, $y \to -y$:

$$\Rightarrow -2\Psi(x')(-\epsilon + (x'+u)^2) = e^{i\theta}\mathcal{F}_{y\to x'}\Big\{2(y^2+v^2)\Psi(y)\Big\} \tag{4.12}$$

Re-naming $x' \to z$

$$\Rightarrow \mathcal{F}_{y\to z}\Big\{ \underbrace{(v^2+y^2)}_{\text{quadratic in } y}\ \Psi(y)\Big\} = (-e^{-i\theta})\underbrace{(-\epsilon+u^2+2uz+z^2)}_{\text{quadratic in } z}\Psi(z) \tag{4.13}$$

The following identity can be used to simplify this,

$$\mathcal{F}_{y\to z}\{y^2\Psi(y)\} = -\frac{\partial^2}{\partial z^2}\mathcal{F}_{y\to z}\{\Psi(y)\} = -e^{i\theta}\frac{\partial^2}{\partial z^2}\Psi(z) \tag{4.14}$$

$$\Rightarrow \frac{\partial^2}{\partial z^2}\Psi(z) = (e^{-i2\theta})\Big[v^2e^{i2\theta}-\epsilon+u^2+2uz+z^2\Big]\Psi(z) \tag{4.15}$$

Since Ψ is real and even this implies $\theta = 0, \pi$

$$\Rightarrow \frac{\partial^2}{\partial z^2}\Psi(z) = \Big[(v^2+u^2-\epsilon)+2uz+z^2\Big]\Psi(z) \tag{4.16}$$

This second-order ordinary linear differential equation is called the Weber's differential equation. In the standard form it is given by:

$$\Rightarrow \frac{\partial^2}{\partial z^2}\Psi(z) = \Big[c+bz+az^2\Big]\Psi(z)\ , \tag{4.17}$$

where a, b, c are constants in z. There are two independent solutions to this ODE, y_1 and y_2:

$$\begin{aligned} y_1(z|u,v,\epsilon) &= \mathbb{D}_{\frac{-1+\epsilon-v^2}{2}}\left(\sqrt{2}(z+u)\right) \\ y_2(z|u,v,\epsilon) &= \mathbb{D}_{\frac{-1-\epsilon+v^2}{2}}\left(i\sqrt{2}(z+u)\right) \end{aligned} \tag{4.18}$$

the solutions $\mathbb{D}_g(x)$ are the parabolic cylinder function [84]. The solutions y_2 diverges as $z \to \infty$, so it's not a valid wavefunction, hence they will be discard as valid solutions. As a wavefunction, y_1 needs to be square integrable and so the Lagrange mutltiplier ϵ can be introduced to enforce this constraint. In order for $y_1(z|u,v,\epsilon) = \mathbb{D}_{\frac{-1+\epsilon-v^2}{2}}\left(\sqrt{2}(z+u)\right)$ to be square integrable, $\frac{-1+\epsilon-v^2}{2}$ needs to be a non-negative integer. Further restriction of Ψ being an even function means $u \to 0$ and $\frac{-1+\epsilon-v^2}{2}$ needs to be an even integer [84]. A choice of $\epsilon = v^2+1+4m,\ m \in \mathbb{N}$.

$$\Rightarrow \Psi(x) \propto \mathbb{D}_{2m}\big(\sqrt{2}x\big), \tag{4.19}$$

Using the identity $\mathbb{D}_n(x) = 2^{-n/2}e^{-x^2/4}H_n(x/\sqrt{2})$, where n is a non-negative integer, finally arriving at,

$$\Rightarrow \Psi(x) \propto e^{-x^2/2}H_{2m}(x)\ , \tag{4.20}$$

where $H_n(x)$ is the Hermite polynomial. This means $|\Psi\rangle = |2m\rangle$, a Fock state with even photon number. Under constricting conditions, the model above functionally searches for a quantum state that minimises the phase space variance when inferring a shift in phase space with a linear decoding function and simple measurement in the two quadrature basis. Additional constraints such as Ψ is an even real function and it needs to be invariant up to a phase under the Fourier transform have been added to ensure no bias between q- and p- quadratures. The model has shown that a Fock state is a good starting point when choosing what states to use for this particular quantum metrology problem. Unfortunately, the dominant errors in quantum optics are often photon loss, which is a separate errors to phase space shifts. While in the toy model Fock states are shown to be resourceful, in reality they are not a feasible choice due to their lack of resistance to loss. We need to search for states with more error resistance to loss. This is a good motivation to study the grid sensor state under realistic errors.

Furthermore, we will provide a short introduction to quantum parameter estimation theory and formalise the quantum displacement sensing problem in both q- and p-quadrature simultaneously in section 4.2. And then applying those results to the grid sensor state in section 4.3.

4.2 Quantum parameter estimation

This section (section 4.2) consists of a short introduction to quantum parameter estimation theory from [85].

Quantum parameter estimation aims to estimate (usually real) parameters in a quantum system by providing a probe/sensor state and then performing a POVM, using the measurement statistics afterwards to infer these unknown parameters. One good figure of merit for the choice of a particular probe state is the quantum Fisher information or the quantum Fisher information matrix if multiple parameters needs to be estimated. The quantum Cramér Rao bound or the Helstrom bound aims to lower bound the errors of the estimation. There also exists a necessary and sufficient condition for the attainability of this lower bound. We shall discuss these two different aspects after some preliminary definitions.

Suppose we have unknown parameters $\vec{u}$ and a probe state given by density matrix $\hat{\rho}$. We shall denote $\hat{\rho}_{\vec{u}}$ as the transformed probe state encoding these unknown parameters, this is a positive map of $\hat{\rho}$ and the Kraus operators are functions of $\vec{u}$. The quantum Fisher information matrix is defined as:

$$\mathbb{F}_{k,l} = \frac{\mathrm{Tr}(\hat{\rho}_{\vec{u}}\{L_k, L_l\})}{2} \tag{4.21}$$

where $\{\cdot,\cdot\}$ is the anti-commutator and L_k is a hermitian operator called the symmetric logrithmic derivative corresponding to the k^{th} entry of $\vec{u}$ to be estimated (u_k), it is defined by:

$$\frac{\partial}{\partial u_k}\hat{\rho}_{\vec{u}} = \frac{\{\hat{\rho}_{\vec{u}}, L_k\}}{2} \ . \tag{4.22}$$

Given a POVM E_y with measurement result y. The Helstrom/quantum Cramér Rao bound gives the the minimum combined variances of the any possible estimator and measurement results:

$$\sum_j \mathrm{Var}(\tilde{u}_j(y)|E_y) \geq \mathrm{Tr}\big(\mathbb{F}^{-1}\big) \geq \sum_n \frac{1}{\mathbb{F}_{n,n}} \ , \tag{4.23}$$

where $\tilde{u}_j(y)$ is the estimator of the j^{th} element of $\vec{u}$. In other words the trace of the inverse

quantum Fisher information matrix gives the lowest possible mean square error of estimation of parameters $\vec{u}$. This lowest bound may not be always attainable, at least in the multiparameter estimation case, because the POVM might not exists. Luckily, [86] provided the necessary and sufficient conditions for the attainability of this bound if the probe state is pure $\hat{\rho} = |\psi\rangle\langle\psi|$ and the hidden parameters are induced by a unitary transformation i.e. $|\psi(\vec{u})\rangle\langle\psi(\vec{u})| = \hat{U}(\vec{u})\,|\psi\rangle$. The Helstrom bound is attainable if

$$\sum_j \mathrm{Var}(\tilde{u}_j(y)|E_y) = \mathrm{Tr}\big(\mathbb{F}^{-1}\big) \Leftrightarrow \langle\psi|\,[\mathcal{H}_k, \mathcal{H}_l]\,|\psi\rangle = 0 \;\forall\; k, l\;, \tag{4.24}$$

where $\mathcal{H}_k = -i\hat{U}^\dagger(\vec{u})\big(\frac{\partial}{\partial u_k}\hat{U}(\vec{u})\big)$.

4.3 The Helstrom bound for the displacement problem using the grid sensor state

Section 4.3 consists of my own work.

The GKP type grid sensor state was first suggested to be a an exotic quantum state used to perform multi-parameter quantum estimation in [55]. We will describe how the grid sensor state explicitly saturates the Helstrom bound exactly for the displacement estimation problem in phase space and why this is a good motivation for the GKP state as a quantum error correcting code.

The grid sensor state without any approximations in its normalisation constant is:

$$S_\Delta(x) = \lambda(\Delta) \sum_{n\in\mathbb{Z}} e^{-\frac{(n\sqrt{2\pi})^2\Delta^2}{2}} e^{-\frac{(x-n\sqrt{2\pi})^2}{2\Delta^2}} \ , \tag{4.25}$$

and its Fourier transform is:

$$\mathcal{F}_{y\to x}\{S_\Delta(y)\} = \tilde{S}_\Delta(x) = \lambda(\Delta) e^{-\frac{x^2\Delta^2}{2}} \sum_{n\in\mathbb{Z}} e^{-\frac{(x-n\sqrt{2\pi})^2}{2\Delta^2}} \ , \tag{4.26}$$

The normalisation constant $\lambda(\Delta)$ is the same in both $S_\Delta(x)$ or $\tilde{S}_\Delta(x)$, this is due to the Parseval's theorem in Fourier analysis [87]. We shall calculate this normalisation constant explicitly now. This will be useful in our following calculations. Starting with the normalisation of $\tilde{S}_\Delta(x)$:

$$\begin{aligned} 1 = \int_x dx \ |\tilde{S}_\Delta(x)|^2 &= \lambda^2(\Delta) \int_x dx \ \Big| \sum_{n\in\mathbb{Z}} e^{-\frac{x^2\Delta^2}{2}} e^{-\frac{(x-n\sqrt{2\pi})^2}{2\Delta^2}} \Big|^2 \\ &= \lambda^2(\Delta) \sum_{n\in\mathbb{Z}} \sum_{m\in\mathbb{Z}} \int_x dx \ e^{-x^2\Delta^2} e^{-\frac{(x-n\sqrt{2\pi})^2}{2\Delta^2}} e^{-\frac{(x-m\sqrt{2\pi})^2}{2\Delta^2}} \ , \end{aligned} \tag{4.27}$$

the integral inside the double sums simplifies to:

$$\int_x dx \ e^{-x^2\Delta^2} e^{-\frac{(x-n\sqrt{2\pi})^2}{2\Delta^2}} e^{-\frac{(x-m\sqrt{2\pi})^2}{2\Delta^2}} = \frac{\sqrt{\pi}}{\sqrt{\Delta^2+\Delta^{-2}}} e^{-\frac{\pi(m-n)^2}{2\Delta^2}} e^{-\frac{\pi(m+n)^2}{2(\Delta^2+\Delta^{-2})}} \tag{4.28}$$

Now we re-write the double sums $\sum_{n\in\mathbb{Z}}\sum_{m\in\mathbb{Z}} \to \frac{1}{2}\sum_{a\in\mathbb{Z}}\sum_{b\in\mathbb{Z}}$ where $a = m+n$ and $b = m-n$, this implies:

$$1 = \int_x dx\ |\tilde{S}_\Delta(x)|^2 = \lambda^2(\Delta)\frac{1}{2}\sum_{a\in\mathbb{Z}}\sum_{b\in\mathbb{Z}}\frac{\sqrt{\pi}}{\sqrt{\Delta^2+\Delta^{-2}}}e^{-\frac{\pi b^2}{2\Delta^2}}e^{-\frac{\pi a^2}{2(\Delta^2+\Delta^{-2})}}$$

$$1 = \lambda^2(\Delta)\frac{1}{2}\frac{\sqrt{\pi}}{\sqrt{\Delta^2+\Delta^{-2}}}\underbrace{\sum_{b\in\mathbb{Z}}e^{-\frac{\pi b^2}{2\Delta^2}}}_{\theta_3\left(0,e^{-\frac{\pi}{2\Delta^2}}\right)}\underbrace{\sum_{a\in\mathbb{Z}}e^{-\frac{\pi a^2}{2(\Delta^2+\Delta^{-2})}}}_{\theta_3\left(0,e^{-\frac{\pi}{2(\Delta^2+\Delta^{-2})}}\right)} \tag{4.29}$$

$$\Rightarrow \lambda^2(\Delta) = \left(\frac{1}{2}\sqrt{\frac{\pi}{\Delta^2+\Delta^{-2}}}\theta_3\left(0,e^{-\frac{\pi}{2\Delta^2}}\right)\theta_3\left(0,e^{-\frac{\pi}{2(\Delta^2+\Delta^{-2})}}\right)\right)^{-1}. \tag{4.30}$$

As illustrated in [55], if we have a quantum state $|\psi\rangle$ and we have a displacement $\hat{U}(\vec{u}) = e^{iv\hat{q}}e^{iu\hat{p}}$ on the quantum state $|\psi\rangle$ such that $|\psi(\vec{u})\rangle = e^{iv\hat{q}}e^{iu\hat{p}}|\psi\rangle$. We wish to estimate the hidden parameters $\vec{u} = (u,v)^{\mathrm{T}}$ via a POVM E_y, such that $\mathrm{Tr}_{\mathrm{system}}\Big(E_y|\psi(\vec{u})\rangle\langle\psi(\vec{u})|\Big) = \mathbb{P}(y|u,v)$, the conditional probability of the POVM measurement result y given the unknown shifts u, v. Suppose we have unbiased estimators for u, v that depends of y given by $\tilde{u}, \tilde{v}$. The Helstrom bound, gives the minimum combined variances of the estimators for this 2 parameter estimation problem.

$$\mathrm{Var}(\tilde{u}(y)|E_y) + \mathrm{Var}(\tilde{v}(y)|E_y) \geq \mathrm{Tr}\big(\mathbb{F}^{-1}\big) \geq \sum_n \frac{1}{\mathbb{F}_{n,n}}\ , \tag{4.31}$$

where $\mathrm{Var}(\tilde{u}(y)|E_y) = \sum_y \mathbb{P}(y|u,v)(\tilde{u}(y)-u)^2$, the unbiased estimator condition is given by $\sum_y \mathbb{P}(y|u,v)(\tilde{u}(y)-u) = 0$ and $\mathbb{F}$ is the 2 by 2 quantum Fisher information matrix. The maxtrix $\mathbb{F}$ is a function in terms of u, v and a functional in $|\psi\rangle$. The equality on the right in equation 4.31 is satisfied if and only if $\mathbb{F}$ is diagonal. Using calculations from [55], the individual matrix

elements of $\mathbb{F}$ for the displacement estimation problem is given by:

$$\begin{aligned}
\frac{\mathbb{F}_{u,u}}{4} &= \langle\psi(\vec{u})| \left(\hat{q} - \langle\psi(\vec{u})|\,\hat{q}\,|\psi(\vec{u})\rangle\right)^2 |\psi(\vec{u})\rangle \\
\frac{\mathbb{F}_{v,v}}{4} &= \langle\psi(\vec{u})| \left(\hat{p} - \langle\psi(\vec{u})|\,\hat{p}\,|\psi(\vec{u})\rangle\right)^2 |\psi(\vec{u})\rangle \\
\frac{\mathbb{F}_{u,v}}{4} &= \langle\psi(\vec{u})|\,\hat{q}\,|\psi(\vec{u})\rangle\,\langle\psi(\vec{u})|\,\hat{p}\,|\psi(\vec{u})\rangle - \frac{1}{2}\,\langle\psi(\vec{u})|\,\{\hat{p},\hat{q}\}\,|\psi(\vec{u})\rangle = \frac{\mathbb{F}_{v,u}}{4}\ .
\end{aligned} \tag{4.32}$$

Using transformation of the displacement operators on $\hat{q},\hat{p}$, $e^{iu\hat{p}}\hat{q}e^{-iu\hat{p}} = \hat{q}+u$ and $e^{-iv\hat{q}}\hat{p}e^{iv\hat{q}} = \hat{p}+v$ and also $\left\langle \tilde{S}_\Delta \right| \hat{q} \left| \tilde{S}_\Delta \right\rangle = 0 \left\langle \tilde{S}_\Delta \right| \hat{p} \left| \tilde{S}_\Delta \right\rangle$, when we substitute in $\psi = \tilde{S}_\Delta$.

$$\mathbb{F}/4 = \begin{pmatrix} \left\langle \tilde{S}_\Delta \right| \hat{q}^2 \left| \tilde{S}_\Delta \right\rangle & \frac{\mathbb{F}_{u,v}}{4} \\ \frac{\mathbb{F}_{u,v}}{4} & \left\langle \tilde{S}_\Delta \right| \hat{p}^2 \left| \tilde{S}_\Delta \right\rangle \end{pmatrix} \tag{4.33}$$

The anti-commutator of $\hat{p},\hat{q}$ is an hermitian operator so the expectation values must be real. Re-writing $\{\hat{p},\hat{q}\} = \hat{p}\hat{q}+\hat{q}\hat{p}-\hat{p}\hat{q}+\hat{p}\hat{q} = 2\hat{p}\hat{q}+[\hat{p},\hat{q}] = 2\hat{p}\hat{q}+i\hat{\mathbb{I}}$. Using this and the transformation of the displacement of the quadrature operators on $\mathbb{F}_{u,v}/4$, we get:

$$\frac{\mathbb{F}_{u,v}}{4} = \left\langle \tilde{S}_\Delta \right| \hat{q}+u \left| \tilde{S}_\Delta \right\rangle \left\langle \tilde{S}_\Delta \right| \hat{p}+v \left| \tilde{S}_\Delta \right\rangle - \left\langle \tilde{S}_\Delta \right| (\hat{p}+v)(\hat{q}+u) + \frac{i}{2}\hat{\mathbb{I}} \left| \tilde{S}_\Delta \right\rangle\ . \tag{4.34}$$

Since $\left\langle \tilde{S}_\Delta \right| \hat{q} \left| \tilde{S}_\Delta \right\rangle = 0 = \left\langle \tilde{S}_\Delta \right| \hat{p} \left| \tilde{S}_\Delta \right\rangle$, this implies:

$$\frac{\mathbb{F}_{u,v}}{4} = -\frac{i}{2} - \left\langle \tilde{S}_\Delta \right| \hat{p}\hat{q} \left| \tilde{S}_\Delta \right\rangle\ . \tag{4.35}$$

Now the aim is to compute $\left\langle \tilde{S}_\Delta \right| \hat{p}\hat{q} \left| \tilde{S}_\Delta \right\rangle$, which we will abbreviate by $\langle\hat{p}\hat{q}\rangle_{\tilde{S}_\Delta}$:

$$
\begin{aligned}
\langle \hat{p}\hat{q} \rangle_{\tilde{S}_\Delta} &= \int_x dx(-i\partial_x \tilde{S}_\Delta(x))^* x \tilde{S}_\Delta(x) \\
&= i \int_x dx(\partial_x \tilde{S}_\Delta(x)) x \tilde{S}_\Delta(x) \\
&= i \int_x dx\ \lambda(\Delta)\ \partial_x \Big(\sum_{n\in\mathbb{Z}} e^{-\frac{x^2\Delta^2}{2}} e^{-\frac{(x-n\sqrt{2\pi})^2}{2\Delta^2}} \Big)\ x\ \lambda(\Delta) \sum_{m\in\mathbb{Z}} e^{-\frac{x^2\Delta^2}{2}} e^{-\frac{(x-m\sqrt{2\pi})^2}{2\Delta^2}} \\
&= i\lambda^2(\Delta) \int_x dx\ \partial_x \Big(\sum_{n\in\mathbb{Z}} e^{-\frac{x^2\Delta^2}{2}} e^{-\frac{(x-n\sqrt{2\pi})^2}{2\Delta^2}} \Big)\ x \sum_{m\in\mathbb{Z}} e^{-\frac{x^2\Delta^2}{2}} e^{-\frac{(x-m\sqrt{2\pi})^2}{2\Delta^2}} \\
&= i\lambda^2(\Delta) \sum_{n\in\mathbb{Z}} \sum_{m\in\mathbb{Z}} \underbrace{\int_x dx\ e^{-\frac{x^2\Delta^2}{2}} e^{-\frac{(x-n\sqrt{2\pi})^2}{2\Delta^2}} \Big(\frac{n\sqrt{2\pi}}{\Delta^2} - x(\Delta^2+\Delta^{-2}) \Big)\ x e^{-\frac{x^2\Delta^2}{2}} e^{-\frac{(x-m\sqrt{2\pi})^2}{2\Delta^2}}}_{e^{-\frac{\pi\left((m-n)^2+\frac{\Delta^4}{1+\Delta^4}(m+n)^2\right)}{2\Delta^2}} ((m-n)(m+n)\pi+\Delta^2+\Delta^6) \frac{\sqrt{\pi}}{(-2\Delta(1+\Delta)^{\frac{3}{2}})}} \\
&= i\lambda^2(\Delta) \sum_{n\in\mathbb{Z}} \sum_{m\in\mathbb{Z}} e^{-\frac{\pi\left((m-n)^2+\frac{\Delta^4}{1+\Delta^4}(m+n)^2\right)}{2\Delta^2}} ((m-n)(m+n)\pi+\Delta^2+\Delta^6) \frac{\sqrt{\pi}}{(-2\Delta(1+\Delta)^{\frac{3}{2}})}
\end{aligned}
\tag{4.36}
$$

Using the trick, $\sum_{n\in\mathbb{Z}} \sum_{m\in\mathbb{Z}} \to \frac{1}{2} \sum_{a\in\mathbb{Z}} \sum_{b\in\mathbb{Z}}$ where $a = m+n$ and $b = m-n$, again implies:

$$
\begin{aligned}
\langle \hat{p}\hat{q} \rangle_{\tilde{S}_\Delta} &= i\lambda^2(\Delta) \frac{1}{2} \sum_{a\in\mathbb{Z}} \sum_{b\in\mathbb{Z}} e^{-\frac{\pi b^2}{2\Delta^2}} e^{-\frac{\pi a^2}{2(\Delta^2+\Delta^{-2})}} (ab\pi + \Delta^2 + \Delta^6) \frac{\sqrt{\pi}}{(-2\Delta(1+\Delta)^{\frac{3}{2}})} \\
&= i\lambda^2(\Delta) \frac{1}{2} \sum_{a\in\mathbb{Z}} \sum_{b\in\mathbb{Z}} e^{-\frac{\pi b^2}{2\Delta^2}} e^{-\frac{\pi a^2}{2(\Delta^2+\Delta^{-2})}} (ab\pi + \Delta^2 + \Delta^6) \frac{\sqrt{\pi}}{(-2\Delta(1+\Delta)^{\frac{3}{2}})} \\
&= i\lambda^2(\Delta) \frac{1}{2} \frac{\sqrt{\pi}}{(-2\Delta(1+\Delta)^{\frac{3}{2}})} \Bigg[\underbrace{\sum_{a\in\mathbb{Z}} \sum_{b\in\mathbb{Z}} e^{-\frac{\pi b^2}{2\Delta^2}} e^{-\frac{\pi a^2}{2(\Delta^2+\Delta^{-2})}} (ab\pi)}_{=0 \text{ as positive and negative terms cancel}} + \sum_{a\in\mathbb{Z}} \sum_{b\in\mathbb{Z}} e^{-\frac{\pi b^2}{2\Delta^2}} e^{-\frac{\pi a^2}{2(\Delta^2+\Delta^{-2})}} (\Delta^2 + \Delta^6) \Bigg] \\
&= i\lambda^2(\Delta) \frac{1}{2} \frac{\sqrt{\pi}\Delta^2(1+\Delta^4)}{(-2\Delta(1+\Delta)^{\frac{3}{2}})} \underbrace{\Bigg[\sum_{a\in\mathbb{Z}} \sum_{b\in\mathbb{Z}} e^{-\frac{\pi b^2}{2\Delta^2}} e^{-\frac{\pi a^2}{2(\Delta^2+\Delta^{-2})}} \Bigg]}_{\theta_3\left(0, e^{-\frac{\pi}{2\Delta^2}}\right) \theta_3\left(0, e^{-\frac{\pi}{2(\Delta^2+\Delta^{-2})}}\right)} .
\end{aligned}
\tag{4.37}
$$

$$
\Rightarrow \langle \hat{p}\hat{q} \rangle_{\tilde{S}_\Delta} = -\frac{i}{2} \lambda^2(\Delta) \underbrace{\frac{\sqrt{\pi}}{2\sqrt{\Delta^{-2}+\Delta^2}} \theta_3\left(0, e^{-\frac{\pi}{2\Delta^2}}\right) \theta_3\left(0, e^{-\frac{\pi}{2(\Delta^2+\Delta^{-2})}}\right)}_{\frac{1}{\lambda^2(\Delta)}} = -\frac{i}{2}
\tag{4.38}
$$

$$
\Rightarrow \mathbb{F}_{u,v} = 0 .
$$

Plugging this back into $\mathbb{F}$, gives us a diagonal $\mathbb{F}$:

$$\mathbb{F}/4 = \begin{pmatrix} \left\langle \tilde{S}_\Delta \right| \hat{q}^2 \left| \tilde{S}_\Delta \right\rangle & 0 \\ 0 & \left\langle \tilde{S}_\Delta \right| \hat{p}^2 \left| \tilde{S}_\Delta \right\rangle \end{pmatrix} . \tag{4.39}$$

This implies, the state $\psi = \tilde{S}_\Delta$ gives a minimum trace of $\mathbb{F}^{-1}$ for the displacement problem. Another way to see that $\mathbb{F}_{u,v} = 0$ is by observing the anti-commutator of $\hat{p}, \hat{q}$ is a Hermitian operator, so its expectation must be real. This implies $\mathbb{F}_{u,v}$ must be real [1]. Notice that $\langle \hat{p}\hat{q} \rangle_{\tilde{S}_\Delta}$ is the imaginary unit i multiplied by an integral concerning real functions $\partial_x S_\Delta(x), S_\Delta(x), x$, hence $\langle \hat{p}\hat{q} \rangle_{\tilde{S}_\Delta}$ is purely imaginary. Since $\underbrace{\mathbb{F}_{u,v}/4}_{\in \mathbb{R}} = -i/2 - i$ (real integral), which means $\mathbb{F}_{u,v}$ must be zero. Choosing $\left| \tilde{S}_\Delta \right\rangle$ as the state for sensing ensures that the lowest possible $\mathrm{Tr}\big(\mathbb{F}^{-1}\big)$ is obtained. However, this does not guarantee anything regarding the attainability of whether $\mathrm{Var}(\tilde{u}(y)|E_y) + \mathrm{Var}(\tilde{v}(y)|E_y) = \min_\psi(\big(\mathbb{F}^{-1}\big))$, as the variance of the estimators depends on the actual estimator functions and also the POVM used. In general there may not be a POVM that could attain the quantum Fisher information in the multi-parameter case [85].

4.3.1 Attainability of the Helstrom bound

We now wish to compute $\left\langle \tilde{S}_\Delta \right| [\mathcal{H}_k, \mathcal{H}_l] \left| \tilde{S}_\Delta \right\rangle \ \forall \ k, l$ to gauge whether the Helstrom bound is attainable. For the 2 parameter case, when $k = l$, the commutator is trivially zero. Only the off diagonal $\left\langle \tilde{S}_\Delta \right| [\mathcal{H}_u, \mathcal{H}_v] \left| \tilde{S}_\Delta \right\rangle$ needs to be computed. Using the symmetric logarithmic derivative for the displacement problem from [55]:

$$\begin{aligned} L_u &= -2i[\hat{p}, \left| \tilde{S}_\Delta(\vec{u}) \right\rangle \left\langle \tilde{S}_\Delta(\vec{u}) \right|] \\ L_v &= 2i[\hat{q}, \left| \tilde{S}_\Delta(\vec{u}) \right\rangle \left\langle \tilde{S}_\Delta(\vec{u}) \right|] \ , \end{aligned} \tag{4.40}$$

this implies:

$$\mathcal{H}_u = -i\hat{U}^\dagger(\vec{u}) \frac{1}{2} \Big(\hat{U}(\vec{u} L_u + L_u \hat{U}(\vec{u})) \Big) = -\frac{i}{2} \Big(L_u + \hat{U}^\dagger(\vec{u}) L_u \hat{U}(\vec{u}) \Big) \tag{4.41}$$

[1] The matrix $\mathbb{F}$ is in general a semi-definite positive matrix [85].

$$
\begin{aligned}
\Rightarrow \mathcal{H}_u &= -i\hat{U}^\dagger(\vec{u})\frac{1}{2}\Big(\hat{U}(\vec{u}L_u + L_u\hat{U}(\vec{u}))\Big) = -\frac{i}{2}\Big(L_a + \hat{U}^\dagger(\vec{u})L_a\hat{U}(\vec{u})\Big) \\
&= -\frac{i}{2}\Big(L_a + (-2i)\Big((\hat{p}+v)\left|\tilde{S}_\Delta\right\rangle\!\left\langle\tilde{S}_\Delta\right| - \left|\tilde{S}_\Delta\right\rangle\!\left\langle\tilde{S}_\Delta\right|(\hat{p}+v)\Big)\Big) \\
&= -\frac{i}{2}\Big(L_a + (-2i)\Big((\hat{p}+v)\left|\tilde{S}_\Delta\right\rangle\!\left\langle\tilde{S}_\Delta\right| - \left|\tilde{S}_\Delta\right\rangle\!\left\langle\tilde{S}_\Delta\right|(\hat{p}+v)\Big)\Big) \\
&= -\Big[\hat{p}, \left|\tilde{S}_\Delta(\vec{u})\right\rangle\!\left\langle\tilde{S}_\Delta(\vec{u})\right| + \left|\tilde{S}_\Delta\right\rangle\!\left\langle\tilde{S}_\Delta\right|\Big]
\end{aligned}
\tag{4.42}
$$

by symmetry,

$$
\mathcal{H}_v = \Big[\hat{q}, \left|\tilde{S}_\Delta(\vec{u})\right\rangle\!\left\langle\tilde{S}_\Delta(\vec{u})\right| + \left|\tilde{S}_\Delta\right\rangle\!\left\langle\tilde{S}_\Delta\right|\Big] \ .
$$

Now we shall calculate $\left\langle\tilde{S}_\Delta\right|[\mathcal{H}_u, \mathcal{H}_v]\left|\tilde{S}_\Delta\right\rangle$:

$$
\begin{aligned}
&\left\langle\tilde{S}_\Delta\right|[\mathcal{H}_u, \mathcal{H}_v]\left|\tilde{S}_\Delta\right\rangle \\
&= -\left\langle\tilde{S}_\Delta\right|\left[\Big[\hat{p}, \left|\tilde{S}_\Delta(\vec{u})\right\rangle\!\left\langle\tilde{S}_\Delta(\vec{u})\right| + \left|\tilde{S}_\Delta\right\rangle\!\left\langle\tilde{S}_\Delta\right|\Big], \Big[\hat{q}, \left|\tilde{S}_\Delta(\vec{u})\right\rangle\!\left\langle\tilde{S}_\Delta(\vec{u})\right| + \left|\tilde{S}_\Delta\right\rangle\!\left\langle\tilde{S}_\Delta\right|\Big]\right]\left|\tilde{S}_\Delta\right\rangle \ ,
\end{aligned}
\tag{4.43}
$$

expanding and collecting terms of the commutator and using the fact that $\left\langle\tilde{S}_\Delta\right|\hat{q}\left|\tilde{S}_\Delta\right\rangle = 0 = \left\langle\tilde{S}_\Delta\right|\hat{p}\left|\tilde{S}_\Delta\right\rangle$ and $\left\langle\tilde{S}_\Delta\right|\hat{p}\hat{q}\left|\tilde{S}_\Delta\right\rangle = -i/2$ calculated earlier in equation 4.38, we get:

$$
\begin{aligned}
\left\langle\tilde{S}_\Delta\right|[\mathcal{H}_u, \mathcal{H}_v]\left|\tilde{S}_\Delta\right\rangle = &+ u\left\langle\tilde{S}_\Delta\right|\hat{U}(\vec{u})\left|\tilde{S}_\Delta\right\rangle\left\langle\tilde{S}_\Delta\right|\hat{U}^\dagger(\vec{u})\hat{p} - \hat{p}\hat{U}(\vec{u})\left|\tilde{S}_\Delta\right\rangle \\
&- v\left\langle\tilde{S}_\Delta\right|\hat{U}(\vec{u})\left|\tilde{S}_\Delta\right\rangle\left\langle\tilde{S}_\Delta\right|\hat{U}^\dagger(\vec{u})\hat{q} - \hat{q}\hat{U}(\vec{u})\left|\tilde{S}_\Delta\right\rangle \\
&- \left\langle\tilde{S}_\Delta\right|\hat{U}(\vec{u})\left|\tilde{S}_\Delta\right\rangle\left\langle\tilde{S}_\Delta\right|\hat{U}^\dagger(\vec{u})\hat{q}\hat{p} - \hat{p}\hat{q}\hat{U}(\vec{u})\left|\tilde{S}_\Delta\right\rangle \\
&+ \left\langle\tilde{S}_\Delta\right|\hat{q}\hat{U}(\vec{u})\left|\tilde{S}_\Delta\right\rangle\left\langle\tilde{S}_\Delta\right|\hat{U}^\dagger(\vec{u})\hat{p}\left|\tilde{S}_\Delta\right\rangle \\
&- \left\langle\tilde{S}_\Delta\right|\hat{p}\hat{U}(\vec{u})\left|\tilde{S}_\Delta\right\rangle\left\langle\tilde{S}_\Delta\right|\hat{U}^\dagger(\vec{u})\hat{q}\left|\tilde{S}_\Delta\right\rangle \\
&- i \ .
\end{aligned}
\tag{4.44}
$$

To look at how this expression behaves, we look at the high energy and small error limit, we restrict $u, v < \sqrt{2\pi}$, one period of the grid sensor state and take $\Delta \to 0$. This implies $\left\langle\tilde{S}_\Delta\right|\hat{U}(\vec{u})\left|\tilde{S}_\Delta\right\rangle \to 0$, $\left\langle\tilde{S}_\Delta\right|\hat{U}^\dagger(\vec{u})\hat{q}\left|\tilde{S}_\Delta\right\rangle \to 0$, $\left\langle\tilde{S}_\Delta\right|\hat{U}^\dagger(\vec{u})\hat{p}\left|\tilde{S}_\Delta\right\rangle \to 0$ as the overlap of these integral are zero, the two delta comb function inside the integral will always multiply to zero. This implies $\left\langle\tilde{S}_\Delta\right|[\mathcal{H}_u, \mathcal{H}_v]\left|\tilde{S}_\Delta\right\rangle \to -i$ as $\Delta \to 0$ and with u, v smaller than a period of the grid

sensor state. Hence the Helstrom bound is not attainable with the grid sensor state even with increasing energies and small errors. The grid sensor state gives a diagonal quantum Fisher information matrix, i.e. the state is optimal for the lowest possible $\mathrm{Tr}(\mathbb{F}^{-1})$ but this bound is not attainable.

Error resilience and Fourier transform properties of the grid states

In sections 4.4, we wish to discuss the grid state's intrinsic resilience to displacement error due to their grid like structure, before discussing Fourier transform properties of the grid sensor state in section 4.5.

4.4 Random Gaussian displacement channel on the grid sensor state

Section 4.4 consists of my own work.

We wish to now explicitly calculate the intrinsic error resilience property of the sensor state by applying the Gaussian random displacement channel onto a pure copy of $|S_\Delta\rangle$ and calculate how this error channel reduces the fidelity of the errored state with a clean copy of $|S_\Delta\rangle$.

In chapter 2, a short introduction to the dominant sources of noise in optical quantum computing is identified to be amplitude damping. We choose to pre-amplify this channel, to cast the composite channel into a Gaussian random displacement for convenient mathematical analysis. We wish to compute how the grid sensor state ($|S_\Delta\rangle$) corrupt under the this channel, $\mathcal{E}_t(|S_\Delta\rangle\langle S_\Delta|)$, to quantify the state's error resilience. Starting with

$$\begin{aligned}\mathcal{E}_t(|S_\Delta\rangle\langle S_\Delta|) &= \int_{u,v} du\ dv\ \frac{e^{-\frac{u^2+v^2}{2t^2}}}{2\pi t^2}\ \hat{d}(u+iv)\,|S_\Delta\rangle\langle S_\Delta|\,\hat{d}(u+iv)^\dagger \\ &= \int_{u,v} du\ dv\ \frac{e^{-\frac{u^2+v^2}{2t^2}}}{2\pi t^2}\ e^{-iu\hat{p}}e^{iv\hat{q}}\,|S_\Delta\rangle\langle S_\Delta|\,e^{iu\hat{p}}e^{-iv\hat{q}}\end{aligned} \tag{4.45}$$

Let's look at $e^{-iu\hat{p}}e^{iv\hat{q}}\,|S_\Delta\rangle$:

$$e^{-iu\hat{p}}e^{iv\hat{q}}\,|S_\Delta\rangle = \int_x dx\ S_\Delta(x-u)e^{ivx}\,|x\rangle_q \tag{4.46}$$

$$
\begin{aligned}
\Rightarrow \mathcal{E}_t(|S_\Delta\rangle\langle S_\Delta|) &= \int_{u,v} du\ dv\ \frac{e^{-\frac{u^2+v^2}{2t^2}}}{2\pi t^2} \int_{x,y} dx\ dy\ S_\Delta(x-u)e^{iv(x-y)}S_\Delta(y-u)\,|x\rangle\langle y|_q \\
&= \int_{x,y} dx\ dy\ \underbrace{\overbrace{\left(\int_v dv\ \frac{e^{-\frac{v^2}{2t^2}}e^{iv(x-y)}}{\sqrt{2\pi t^2}}\right)}^{e^{-\frac{t^2(x-y)^2}{2}}}\left(\int_u du\ \frac{e^{-\frac{u^2}{2t^2}}}{\sqrt{2\pi t^2}}S_\Delta(x-u)S_\Delta(y-u)\right)}_{\rho(x,y;|S_\Delta\rangle)}|x\rangle\langle y|_q \\
&= \int_{x,y} dx\ dy\ \left(e^{-\frac{t^2(x-y)^2}{2}}\int_u du\ \frac{e^{-\frac{u^2}{2t^2}}}{\sqrt{2\pi t^2}}S_\Delta(x-u)S_\Delta(y-u)\right)|x\rangle\langle y|_q
\end{aligned}
\tag{4.47}
$$

We now look at $\rho(x,y;\mathcal{E}_t(|S_\Delta\rangle\langle S_\Delta|)$, the density matrix function of $|S_\Delta\rangle\langle S_\Delta|$ after the Gaussian random displacement channel,

$$
\begin{aligned}
\rho(x,y;\mathcal{E}_t(|S_\Delta\rangle\langle S_\Delta|) &= e^{-\frac{t^2(x-y)^2}{2}}\int_u du\ \frac{e^{-\frac{u^2}{2t^2}}}{\sqrt{2\pi t^2}}\sqrt{\frac{2}{\pi}}\sum_{n,m\in\mathbb{Z}^2} e^{-\frac{(n\sqrt{2\pi})^2\Delta^2}{2}}e^{-\frac{(x-u-n\sqrt{2\pi})^2}{2\Delta^2}}e^{-\frac{(m\sqrt{2\pi})^2\Delta^2}{2}}e^{-\frac{(y-u-m\sqrt{2\pi})^2}{2\Delta^2}} \\
&= \sqrt{\frac{2}{\pi}}\sum_{n,m\in\mathbb{Z}^2} e^{-\frac{(n\sqrt{2\pi})^2\Delta^2}{2}}e^{-\frac{(m\sqrt{2\pi})^2\Delta^2}{2}}\left(e^{-\frac{t^2(x-y)^2}{2}}\int_u du\ \frac{e^{-\frac{u^2}{2t^2}}}{\sqrt{2\pi t^2}}e^{-\frac{(x-u-n\sqrt{2\pi})^2}{2\Delta^2}}e^{-\frac{(y-u-m\sqrt{2\pi})^2}{2\Delta^2}}\right) \\
&= \sqrt{\frac{2}{\pi}}\sum_{n,m\in\mathbb{Z}^2} e^{-\frac{(n\sqrt{2\pi})^2\Delta^2}{2}}e^{-\frac{(m\sqrt{2\pi})^2\Delta^2}{2}}\left(e^{-\frac{t^2(x-y)^2}{2}}\underbrace{\int_u du\ \frac{e^{-\frac{u^2}{2t^2}}}{\sqrt{2\pi t^2}}e^{-\frac{(x-u-n\sqrt{2\pi})^2}{2\Delta^2}}e^{-\frac{(y-u-m\sqrt{2\pi})^2}{2\Delta^2}}}_{e^{-\frac{(x-n\sqrt{2\pi})^2+(y-m\sqrt{2\pi})^2}{2\Delta^2}}e^{\frac{t^2(x+y-(m+n)\sqrt{2\pi})}{2\Delta^2(2t^2+\Delta^2)^2}}\Big/\sqrt{1+2\left(\frac{t}{\Delta}\right)^2}}\right),
\end{aligned}
$$

we can re-write,

$$
\rho(x,y;\mathcal{E}_t(|S_\Delta\rangle\langle S_\Delta|)) = \sqrt{\frac{2}{\pi}}\frac{1}{\sqrt{1+2\left(\frac{t}{\Delta}\right)^2}}\sum_{n,m\in\mathbb{Z}^2} e^{-\frac{1}{2}\vec{r}^{\,\mathrm{T}}\underline{\underline{A}}\vec{r}}\ ,
\tag{4.48}
$$

where $\vec{r}^{\,\mathrm{T}}\underline{\underline{A}}\vec{r}$ is know as a quadratic form and $\underline{\underline{A}}$ is called the matrix of the quadratic equation

[88].. If we set $\vec{r}^{\,\mathrm{T}}\underline{\underline{A}}\vec{r}=0$, we get a 2-dimensional conic section and $\vec{r}=(x,y,1)^{\mathrm{T}}$.

$$\underline{\underline{A}}=\frac{1}{2t^2+\Delta^2}\begin{pmatrix}1+2t^4+t^2\Delta^2+\frac{t^2}{\Delta^2} & -\left(2t^4+t^2\Delta^2+\frac{t^2}{\Delta^2}\right) & \frac{(m-n)\sqrt{2\pi}t^2-n\sqrt{2\pi}\Delta^2}{\Delta^2}\\ -\left(2t^4+t^2\Delta^2+\frac{t^2}{\Delta^2}\right) & 1+2t^4+t^2\Delta^2+\frac{t^2}{\Delta^2} & \frac{(n-m)\sqrt{2\pi}t^2-m\sqrt{2\pi}\Delta^2}{\Delta^2}\\ \frac{(m-n)\sqrt{2\pi}t^2-n\sqrt{2\pi}\Delta^2}{\Delta^2} & \frac{(n-m)\sqrt{2\pi}t^2-m\sqrt{2\pi}\Delta^2}{\Delta^2} & 2\pi\left((m-n)^2\frac{t^2}{\Delta^2}+(m^2+n^2)\Delta^2(2t^2+\Delta^2+\Delta^{-2})\right)\end{pmatrix} \tag{4.49}$$

The determinant of this matrix is:

$$\det\left(\underline{\underline{A}}\right)=\frac{2\pi\left[(m-n)^2t^2+(m^2+n^2)\Delta^2(1+2t^2+\Delta^2)\right]}{\Delta^2(\Delta^2+2t^2)}\,, \tag{4.50}$$

The determinant $\det\left(\underline{\underline{A}}\right)>0$ when $m,n\neq 0$, This condition combined with $A_{3,3}>0$ means that this conic section is an ellipse [88]. Also, we can find the center location of this ellipse, which is determined via Gaussian elimination on the upper 2 rows of the matrix $\underline{\underline{A}}$. We will denote the co-ordinate of the center of the ellipse by $(x_c,y_c)^{\mathrm{T}}$:

$$\frac{1}{2t^2+\Delta^2}\begin{pmatrix}1+2t^4+t^2\Delta^2+\frac{t^2}{\Delta^2} & -\left(2t^4+t^2\Delta^2+\frac{t^2}{\Delta^2}\right)\\ -\left(2t^4+t^2\Delta^2+\frac{t^2}{\Delta^2}\right) & 1+2t^4+t^2\Delta^2+\frac{t^2}{\Delta^2}\end{pmatrix}\begin{pmatrix}x_c\\ y_c\end{pmatrix}=\begin{pmatrix}\frac{(m-n)\sqrt{2\pi}t^2-n\sqrt{2\pi}\Delta^2}{\Delta^2(2t^2+\Delta^2)}\\ \frac{(n-m)\sqrt{2\pi}t^2-m\sqrt{2\pi}\Delta^2}{\Delta^2(2t^2+\Delta^2)}\end{pmatrix} \tag{4.51}$$

Solving this system of equations gives the result:

$$\begin{pmatrix}x_c\\ y_c\end{pmatrix}=-\frac{\sqrt{2\pi}}{1+2t^2\Delta^2}\begin{pmatrix}n+(n+m)t^2\Delta^2\\ m+(n+m)t^2\Delta^2\end{pmatrix} \tag{4.52}$$

Furthermore, eigenvectors of the 2 by 2 sub-matrix are found by eliminating the final row and column of $\underline{\underline{A}}$ and these give the major and minor axis direction of this ellipses. If we diagonalise this sub-matrix and solve for the eigenvectors $\vec{g}_1,\vec{g}_2$ with corresponding eigenvalues g_1,g_2, we

get:

$$g_1 = \frac{1}{2t^2 + \Delta^2} \ , \ \vec{g}_1 = \begin{pmatrix} 1 \\ 1 \end{pmatrix}$$
$$g_2 = 2t^2 + \Delta^{-2} \ , \ \vec{g}_2 = \begin{pmatrix} -1 \\ 1 \end{pmatrix} \tag{4.53}$$

This implies $\rho(x, y; \mathcal{E}_t(|S_\Delta\rangle\langle S_\Delta|))$ can be re-written as a double sum of $e^{-\frac{1}{2}(\text{ellipse})}$, where the ellipse's major and minor axes are at 45 degrees with respect to the origin. This means the individual Gaussian peaks are sheared in the $(1, 1)^{\mathrm{T}}$ and $(-1, 1)^{\mathrm{T}}$ directions.

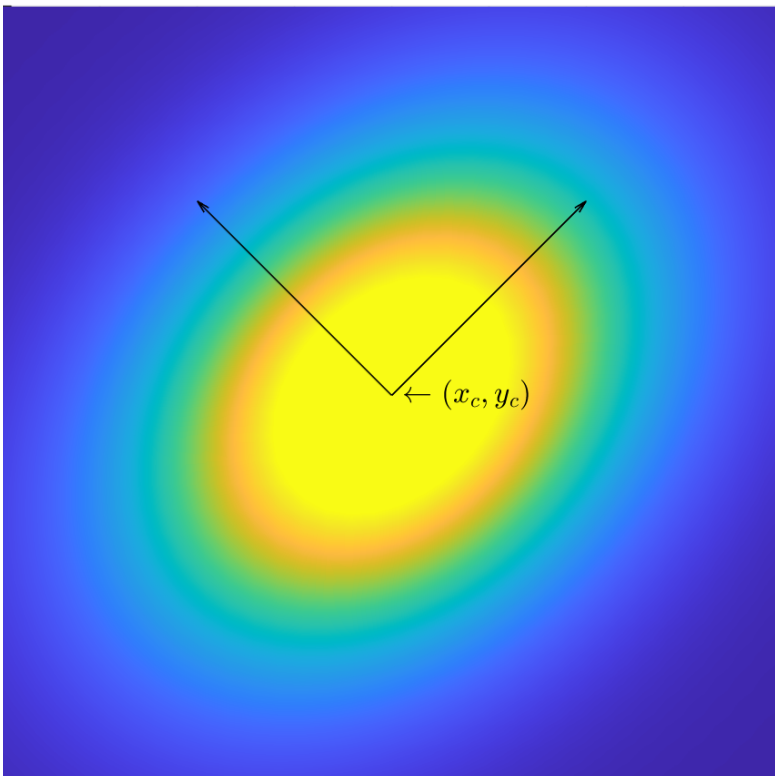

Figure 4.3: Contour plot of one of the Gaussian peaks after of the density matrix function of $|S_\Delta\rangle$ after the Gaussian random displacement channel. The squeezing parameter was arbitrarily chosen to be $\Delta = 0.3$ here and $t = 0.1$.

To understand the small error limit, let's make the approximation, it is useful to drop the $\mathcal{O}(t^4)$

and $\mathcal{O}(t^2\Delta^2)$ terms and assume $t \ll \Delta \ll 1$:

$$\underline{\underline{A}} \approx \frac{\Delta^{-2}}{1+2t^2/\Delta^2} \begin{pmatrix} 1+\frac{t^2}{\Delta^2} & -\frac{t^2}{\Delta^2} & (m-n)\sqrt{2\pi}\frac{t^2}{\Delta^2} - n\sqrt{2\pi} \\ -\frac{t^2}{\Delta^2} & 1+\frac{t^2}{\Delta^2} & (n-m)\sqrt{2\pi}\frac{t^2}{\Delta^2} - m\sqrt{2\pi} \\ (m-n)\sqrt{2\pi}\frac{t^2}{\Delta^2} - n\sqrt{2\pi} & (n-m)\sqrt{2\pi}\frac{t^2}{\Delta^2} - m\sqrt{2\pi} & 2\pi\Big((m-n)^2\frac{t^2}{\Delta^2} + (m^2+n^2)\Big) \end{pmatrix} \tag{4.54}$$

If we expand $(1+2t^2/\Delta^2)^{-1} \approx 1 - 2\frac{t^2}{\Delta^2} + \mathcal{O}(t^4/\Delta^4)$, we shall drop all the t^2/Δ^2 terms inside the matrix:

$$\underline{\underline{A}} \approx \Delta^{-2}\Big(1-2\frac{t^2}{\Delta^2}\Big) \begin{pmatrix} 1 & 0 & -n\sqrt{2\pi} \\ 0 & 1 & -m\sqrt{2\pi} \\ -n\sqrt{2\pi} & -m\sqrt{2\pi} & 2\pi(m^2+n^2)(1+\Delta^4) \end{pmatrix} + \mathcal{O}\Big(\frac{t^4}{\Delta^4}\Big) \tag{4.55}$$

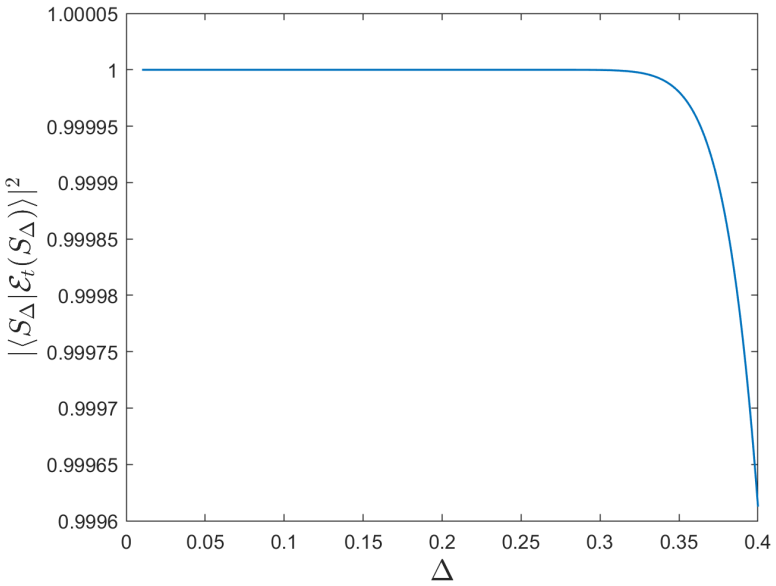

Figure 4.4: The approximate fidelity between $|S_\Delta\rangle$ and $\mathcal{O}(|S_\Delta\rangle\langle S_\Delta|)$, for $t = 0.0001$.

$$\Rightarrow \rho(x,y;\mathcal{E}_t(|S_\Delta\rangle\langle S_\Delta|)) \underset{\sim}{\propto} \left(\sum_{n\in\mathbb{Z}^2} e^{-\frac{(x-n\sqrt{2\pi})^2}{2\Delta^2\left(1+2\frac{t^2}{\Delta^2}\right)}} e^{-\frac{\Delta^2(n\sqrt{2\pi})^2}{2\left(1+2\frac{t^2}{\Delta^2}\right)}}\right)\left(\sum_{m\in\mathbb{Z}^2} e^{-\frac{(y-m\sqrt{2\pi})^2}{2\Delta^2\left(1+2\frac{t^2}{\Delta^2}\right)}} e^{\frac{\Delta^2(m\sqrt{2\pi})^2}{2\left(1+2\frac{t^2}{\Delta^2}\right)}}\right), \tag{4.56}$$

this means the density matrix function is approximately a pure state $|S_\Delta\rangle$ in the low error limit, but with modified widths. From the first order effects in (t^2/Δ^2), the grid sensor state's individual peaks will have a widening from $\Delta \to \Delta\sqrt{1+2\frac{t^2}{\Delta^2}}$, and the overall Gaussian envelope's width will get contracted from $\frac{1}{\Delta} \to \frac{\sqrt{1+2\frac{t^2}{\Delta^2}}}{\Delta}$. It is possible to qualitatively understand how, in the large error limit $t \to 1$, the Gaussian random displacement channel will drive any state to the vacuum state. We have computed numerically the fidelity between an error free grid sensor state and a grid sensor state with error for small t in figure 4.4.

4.5 Fourier transform eigenstate

Section 4.5 consists of my own work.

We wish to explicitly show that $|S_\Delta\rangle$ is an approximate eigenstate to the Fourier transform operator $\hat{F}$.

The infinite energy limit of the grid sensor state has a q-quadrature wavefunction of $\text{Ш}_{\sqrt{2\pi}}(x)$, a Dirac comb of width $\sqrt{2\pi}$ and it's an exact eigenstate of the Fourier transform operator $\hat{F}$, so that the p-quadrautre wavefunction is identical to the q-quadrautre wavefunction. The state $|S_\Delta\rangle$ is an approximate eigenstate to the Fourier transform operator $\hat{F} = e^{i\pi/4}e^{i\pi\hat{n}/2}$. One way to see it is to look at an alternative form of $|S_\Delta\rangle$,

$$|S_\Delta\rangle = \sqrt{2\pi}\Delta^2\Big(\frac{2}{\pi}\Big)^{\frac{1}{4}} e^{-\frac{\Delta^2\hat{p}^2}{2}} e^{-\frac{\Delta^2\hat{q}^2}{2}} |\text{Ш}\rangle \ . \tag{4.57}$$

We can see that $\hat{F} = e^{i\pi/4}e^{i\pi\hat{n}/2}$ almost commutes with $e^{-\frac{\Delta^2\hat{p}^2}{2}}e^{-\frac{\Delta^2\hat{q}^2}{2}}$, the operators to the left of $|\text{Ш}\rangle$ in equation 4.57. Some authors decide to define the approximate sensor states by $e^{-\beta(\hat{n}+1/2)}|\text{Ш}\rangle$, so that $\hat{F}$ commutes with the $e^{-\beta(n+\hat{1}/2)}$, hence making it an exact eigenstate of the Fourier transform, see approximation 3 in [71]. With our defintion of the grid sensor states, we want to quantify how does a finite energy ($\Delta \neq 0$) grid sensor state transform under the Fourier transform.

We wish to quantitatively understand how much does the Fourier transformed version of the sensor state, $\hat{F}|S_\Delta\rangle$, overlaps with itself. If this overlap is equivalent to 1 or close to 1 then $|S_\Delta\rangle$ is close to being a Fourier transform eigenstate. Starting with the expectation value

$\left|\left\langle S_\Delta\right|\hat{F}\left|S_\Delta\right\rangle\right|^2$, which is the Fidelity between the states $|S_\Delta\rangle$ and $\left|\tilde{S}_\Delta\right\rangle$,

$$\begin{aligned}\left|\left\langle S_\Delta\right|\hat{F}\left|S_\Delta\right\rangle\right|^2 &= \left|\int_x dx\ \tilde{S}_\Delta(x)S_\Delta\right|^2 \\ &= \lambda^4\left|\int_x dx\ \Big(\sum_{n\in\mathbb{Z}} e^{-\frac{x^2\Delta^2}{2}}e^{-\frac{(x-n\sqrt{2\pi})^2}{2\Delta^2}}\Big)\Big(\sum_{m\in\mathbb{Z}} e^{-\frac{(m\sqrt{2\pi})^2\Delta^2}{2}}e^{-\frac{(x-m\sqrt{2\pi})^2}{2\Delta^2}}\Big)\right|^2 \\ &= \lambda^4\left|\sum_{n\in\mathbb{Z}}\sum_{m\in\mathbb{Z}}\int_x dx\ e^{-\frac{x^2\Delta^2}{2}}e^{-\frac{(x-n\sqrt{2\pi})^2}{2\Delta^2}}e^{-\frac{(m\sqrt{2\pi})^2\Delta^2}{2}}e^{-\frac{(x-m\sqrt{2\pi})^2}{2\Delta^2}}\right|^2\end{aligned} \tag{4.58}$$

separating the double sum into $n=m$ terms and $n\neq m$ terms:

$$\begin{aligned}&\left|\left\langle S_\Delta\right|\hat{F}\left|S_\Delta\right\rangle\right|^2 \\ &\quad= \lambda^4\Bigg|\sum_{n\in\mathbb{Z}}\int_x dx\ e^{-\frac{x^2\Delta^2}{2}}e^{-\frac{(x-n\sqrt{2\pi})^2}{\Delta^2}}e^{-\frac{(n\sqrt{2\pi})^2\Delta^2}{2}} \\ &\quad+\sum_{n\in\mathbb{Z}}\sum_{m\in\mathbb{Z}}(1-\delta_{n,m})e^{-\frac{(m\sqrt{2\pi})^2\Delta^2}{2}}\int_x dx\ e^{-\frac{x^2\Delta^2}{2}}e^{-\frac{(x-n\sqrt{2\pi})^2}{2\Delta^2}}e^{-\frac{(x-m\sqrt{2\pi})^2}{2\Delta^2}}\Bigg|^2,\end{aligned} \tag{4.59}$$

The $n\neq m$ sum is very small because the overlap integral of Gaussians centered at different locations is very small if $\Delta \ll \sqrt{2\pi}$, dropping this term and using the integral identity $\int_x dx\ e^{-\frac{x^2\Delta^2}{2}}e^{-\frac{(x-n\sqrt{2\pi})^2}{\Delta^2}}e^{-\frac{(n\sqrt{2\pi})^2\Delta^2}{2}} = \sqrt{2\pi\Delta^2/(2+\Delta^4)}e^{-\frac{n^2\pi\Delta^2(4+\Delta^4)}{2+\Delta^4}}$,

$$\Rightarrow\left|\left\langle S_\Delta\right|\hat{F}\left|S_\Delta\right\rangle\right|^2 \geq \lambda^4\frac{2\pi\Delta^2}{(2+\Delta^4)}\Bigg|\underbrace{\sum_{n\in\mathbb{Z}} e^{-\frac{n^2\pi\Delta^2(4+\Delta^4)}{2+\Delta^4}}}_{\theta_3\left(0,e^{-\pi\frac{\Delta^2(4+\Delta^4)}{(2+\Delta^4)}}\right)}\Bigg|^2, \tag{4.60}$$

Using $\theta_3\Big(0,e^{-\pi\frac{\Delta^2(4+\Delta^4)}{(2+\Delta^4)}}\Big)\approx\sqrt{\frac{2+\Delta^4}{\Delta^2(4+\Delta^4)}}$ when $\Delta\ll\sqrt{2\pi}$ and taking $\lambda^4\approx 2/\pi$:

$$\Rightarrow\left|\left\langle S_\Delta\right|\hat{F}\left|S_\Delta\right\rangle\right|^2 \approx \Big(1+\frac{\Delta^4}{4}\Big)^{-1}, \tag{4.61}$$

The quantity $\left|\left\langle S_\Delta\right|\hat{F}\left|S_\Delta\right\rangle\right|^2$, is very close to one. Expanding this quantity as a Taylor series in terms of small Δ, $\Big(1+\frac{\Delta^4}{4}\Big)^{-1}\approx 1-\frac{\Delta^4}{4}+\mathcal{O}(\Delta^8)$. Finite energy grid sensor state wavefunction are good approximate Fourier transform eigenfunction.

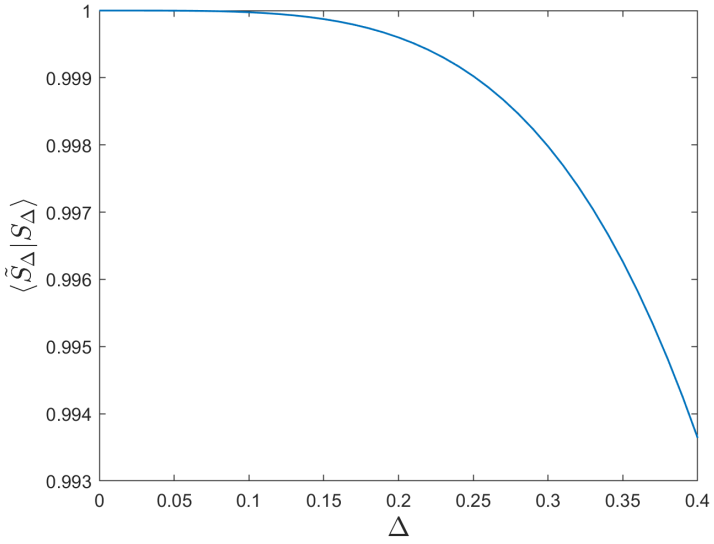

Figure 4.5: The expectation of the $\hat{F}$ with respect to the grid sensor state $|S_\Delta\rangle$.

Interestingly the grid sensor state could be written as a Gaussian $e^{-x^2\Delta^2/2}$ multiplied by a Jacobi theta function $\Delta\theta_3(\sqrt{\pi/2}x, e^{-\pi\Delta^2})$ up to normalisation constants, i.e. $\tilde{S}_\Delta(x) \propto \Delta e^{-x^2\Delta^2/2}\theta_3(x\sqrt{\pi/2}, e^{-\pi\Delta^2})$. The theta function is the Fourier transform of a Gaussian multiplied by a Dirac comb [89]:

$$\mathcal{F}_{x\to y}\Big\{\theta_3\Big(\frac{\pi}{2}x, e^{-\pi\Delta^2}\Big)\Big\} = \sqrt{2\pi}e^{-\Delta^2y^2/2}\text{Ш}_{\sqrt{2\pi}}(y)\ . \tag{4.62}$$

Equation equation 4.62 can be derived as follows:

$$\begin{aligned}
\mathcal{F}_{x\to y}\Big\{\theta_3\Big(\frac{\pi}{2}x, e^{-\pi\Delta^2}\Big)\Big\} &= \mathcal{F}_{x\to y}\Big\{\frac{1}{\Delta}\sum_{n\in\mathbb{Z}} e^{-\frac{(x-n\sqrt{2\pi})^2}{2\Delta^2}}\Big\} \\
&= \frac{1}{\Delta}\sum_{n\in\mathbb{Z}} \mathcal{F}_{x\to y}\Big\{e^{-\frac{(x-n\sqrt{2\pi})^2}{2\Delta^2}}\Big\} \\
&= \frac{1}{\Delta}\underbrace{\sum_{n\in\mathbb{Z}} e^{in\sqrt{2\pi}y}}_{\sqrt{2\pi}\text{Ш}_{\sqrt{2\pi}}(y)} e^{-\frac{\Delta^2y^2}{2}}\Delta \\
&= \sqrt{2\pi}e^{-\frac{\Delta^2y^2}{2}}\text{Ш}_{\sqrt{2\pi}}(y)\ .
\end{aligned} \tag{4.63}$$

According to the convolution theorem [87],

$$\mathcal{F}_{x\to y}\Big\{f(x)\Big\} \star \mathcal{F}_{x\to y}\Big\{g(x)\Big\} = \int_\tau \frac{d\tau}{\sqrt{2\pi}} f(y-\tau)g(\tau) = \mathcal{F}_{x\to y}\Big\{f(x)g(x)\Big\}\ , \tag{4.64}$$

We can now write the grid sensor state as a convolution of a Gaussian with a Dirac comb:

$$\begin{aligned} S_\Delta(x) = \mathcal{F}_{x\to y}\Big\{\tilde{S}_\Delta(x)\Big\} &= \lambda(\Delta)\mathcal{F}_{x\to y}\Big\{\sum_{n\in\mathbb{Z}} e^{-\frac{(x-n\sqrt{2\pi})^2}{2\Delta^2}}\Big\} \star \mathcal{F}_{x\to y}\Big\{e^{-\frac{x^2\Delta^2}{2}}\Big\} \\ &= \lambda(\Delta)\sqrt{2\pi}\Big(e^{-\frac{\Delta^2 y^2}{2}}\,\text{Ш}_{\sqrt{2\pi}}(y)\Big) \star \Big(e^{-\frac{y^2}{2\Delta^2}}\Big)\ . \end{aligned} \tag{4.65}$$

Another way to interpret the grid sensor state is to treat it as a convolution of a Gaussian function and a Dirac comb with finite width $1/\Delta$ in the individual peaks.

Fock state amplitudes and its approximations

In section 4.6, we wish to layout a way to explicitly calculate the Fock state amplitude of a grid sensor state. Then we proceed to show why the Fock state representation is not a favourable basis to study these grid states. This is due to the need to retain high number of Fock basis to minimise the fidelity loss after truncation of the Fock basis.

4.6 Fock state amplitides of $|S_\Delta\rangle$

Section 4.6 consists of my own work.

The Fock basis $(\{|n\rangle\}_{n=0}^{\infty})$ [2] is a preferred basis in optical quantum information. Many physical operations such as loss error operators, photon counting measurements are relatively easy to compute in this basis [90, 82, 91]. Hence we wish to compute the finite-energy grid sensor state amplitudes in this basis.

We sketch out the method of re-expressing $|S_\Delta\rangle$ in the Fock basis as follows. Firstly we noticed that the generating function of the shifted Gaussian can be expressed as a superposition of Hermite-Gauss functions, which are the q-quadrature wavefunction of the Fock states. This will allow us to express $|S_\Delta\rangle$ in the squeezed Fock basis. Then, use the summation formula of the squeezed Fock states to rewrite $|S_\Delta\rangle$ back into the Fock basis. Finally, we will simplify the expression and write it in an approximate form that makes the amplitudes more readily calculated.

4.6.1 $|S_\Delta\rangle$ in the squeezed Fock basis

Using the generating function of the shifted Gaussians [92]:

$$e^{-\frac{x^2}{2}+2xt-t^2} = \sum_{n=0}^{\infty} \frac{t^n\sqrt{2^n}}{\sqrt{n!}}\pi^{\frac{1}{4}}\phi_n(x) \ , \tag{4.66}$$

[2] We use the term Fock state and number state interchangeably.

where $\phi_n(x)$ is the Fock state wavefunction. With some algebra, one can derive:

$$\pi^{-\frac{1}{4}} e^{-\frac{(x-t)^2}{2}} = \sum_{n=0}^{\infty} \frac{t^n e^{-\frac{t^2}{4}}}{\sqrt{2^n n!}} \phi_n(x) \ , \tag{4.67}$$

where the left hand side is the q-quadrature wavefunction of $\hat{d}(t,0)\,|0\rangle$, $t \in \mathbb{R}$, with $\hat{d}(t,0)$ being the displacement operator that transform the vacuum wavefuntion from $\phi_0(x) \to \phi_0(x-t)$. Hence, we have derived the Fock basis amplitude of the displaced vacuum state as, $\frac{t^n e^{-\frac{t^2}{4}}}{\sqrt{2^n n!}}$,

$$\hat{d}(t,0)\,|0\rangle = \sum_{n=0}^{\infty} \frac{t^n e^{-\frac{t^2}{4}}}{\sqrt{2^n n!}} \,|n\rangle \ . \tag{4.68}$$

Using equation 4.67, we can re-write the shifted Gaussian inside the sum of the grid sensor state in terms of the squeezed Fock states:

$$\begin{aligned} S_\Delta(x) &= \lambda(\Delta) \sum_{m\in\mathbb{Z}} e^{-\frac{(x-m\sqrt{2\pi})^2}{2\Delta^2}} e^{-\frac{(m\sqrt{2\pi})^2}{2\Delta^{-2}}} \\ &= \lambda(\Delta) \sum_{m\in\mathbb{Z}} \sum_{n=0}^{\infty} \pi^{\frac{1}{4}} \sqrt{\Delta} e^{-\frac{(m\sqrt{2\pi})^2}{2\Delta^{-2}}} \frac{(m\sqrt{2\pi}/\Delta)^n e^{-\frac{(m\sqrt{2\pi}/\Delta)^2}{4}}}{\sqrt{2^n n!}} \frac{\phi_n(x/\Delta)}{\sqrt{\Delta}} \end{aligned} \tag{4.69}$$

Since the grid sensor state wavefunction is an even function in the q-quadrature, this means only the even integer n terms remain. As $|S_\Delta\rangle$ has an even wavefunction in the q-quadrature basis, this means that only the even Fock state amplitudes are non-zero, hence we can use the substitution $n = 2k,\ k \in \mathbb{Z}$,

$$\Rightarrow |S_\Delta\rangle = \lambda(\Delta) \sum_{k=0}^{\infty} \frac{\pi^{\frac{1}{4}} \sqrt{\Delta} \pi^k}{\Delta^{2k} \sqrt{(2k)!}} \left[\sum_{m\in\mathbb{Z}} m^{2k} e^{-\pi\left(\Delta^2 + \frac{1}{2\Delta^2}\right) m^2} \right] \hat{S}_\Delta^\dagger \,|2k\rangle \ . \tag{4.70}$$

Let $g(\Delta) = \pi\left(\Delta^2 + \frac{1}{2\Delta^2}\right)$, this implies:

$$|S_\Delta\rangle = \lambda(\Delta) \sum_{k=0}^{\infty} \frac{\pi^{\frac{1}{4}} \sqrt{\Delta} \pi^k}{\Delta^{2k} \sqrt{(2k)!}} \left[\sum_{m\in\mathbb{Z}} m^{2k} e^{-g(\Delta) m^2} \right] \hat{S}_\Delta^\dagger \,|2k\rangle \ , \tag{4.71}$$

or alternatively,

$$|S_\Delta\rangle = \lambda(\Delta)\sum_{k=0}^{\infty}\frac{\pi^{\frac{1}{4}}\sqrt{\Delta}\pi^k}{\Delta^{2k}\sqrt{(2k)!}}(-1)^k\frac{\partial^k}{\partial^k g}\Big(\theta_3(0,e^{-g})\Big)\hat{S}_\Delta^\dagger\,|2k\rangle\ , \tag{4.72}$$

where $\theta_3(z,q)$ is the Jacobi Theta function of the third kind in the standard form [93].

4.6.2 Squeezed number state in the Fock basis

We now need to re-express our squeezed even number states in the Fock basis, this was first worked out in [94, 95]. Our definition of the squeezing operator $\hat{S}_\Delta^\dagger = e^{\frac{\ln(\Delta)}{2}((\hat{a}^\dagger)^2-\hat{a}^2)}$ transform wavefunction from $\psi(x)\to\psi(x/\Delta)$. The squeezing operator is $\hat{S}_r^\dagger = e^{-\frac{r}{2}((\hat{a}^\dagger)^2-\hat{a}^2)}$ in [96]. Hence we plug $r=-\ln(\Delta)$ into equation 20 of [96] to obtain:

$$\hat{S}_\Delta^\dagger\,|2k\rangle = \sum_{j=0}^{\infty}|2j\rangle\,\frac{\sqrt{(2k)!(2j)!}}{\big(\cosh(-\ln(\Delta))\big)^{j+k+\frac{1}{2}}}\sum_{l=0}^{\min(j,k)}\Big(\frac{\sinh(-\ln(\Delta))}{2}\Big)^{k+j-2l}\frac{(-1)^{j-l}}{(2l)!(k-l)!(j-l)!} \tag{4.73}$$

Plugging equation 4.73 back into equation 4.71 to obtain:

$$\begin{aligned}\Rightarrow |S_\Delta\rangle = \lambda(\Delta)\sum_{j=0}^{\infty}|2j\rangle\,\pi^{\frac{1}{4}}\sqrt{\Delta}\frac{\sqrt{(2j)!}\,\tanh^j(\ln(\Delta))}{2^j\sqrt{\cosh(\ln(\Delta))}}\\ \left\{\sum_{k=0}^{\infty}\frac{\pi^k}{2^k\Delta^{2k}}\frac{\partial_g^k\big(\theta_3(0,e^{-g})\big)}{\big(\cosh(\ln(\Delta))\big)^k}\sum_{l=0}^{\min(j,k)}\big(\sinh(\ln(\Delta))\big)^{k-2l}\frac{2^{2l}(-1)^l}{(2l)!(k-l)!(j-l)!}\right\}\end{aligned} \tag{4.74}$$

In order to generate the amplitudes, we need to evaluate 2 infinite (sum over k and the derivatives of the θ_3 function) and 1 finite sum (sum over l). We shall name the coefficients C_{2j}, where the grid sensor state can be re-expressed as $|S_\Delta\rangle = \sum_{j=0}^{\infty}C_{2j}\,|2j\rangle$. With more simplifications,

the amplitudes can be written as:

$$C_{2j} = \lambda(\Delta)\frac{\pi^{\frac{1}{4}}\sqrt{\Delta}\sqrt{(2j)!}\,\tanh^j(\ln(\Delta))}{(j!)2^j\sqrt{\cosh(\ln(\Delta))}} \left\{\sum_{k=0}^{\infty}\frac{\left(\frac{-\pi\,\tanh(\ln(\Delta))}{2\Delta^2}\right)^k}{k!}\left(\delta_{k,0}+2\sum_{m=1}^{\infty}m^{2k}e^{-m^2\pi\left(\Delta^2+\frac{1}{2\Delta^2}\right)}\right){}_2F_1\left(-j,-k,\frac{1}{2},\frac{-4\Delta^2}{(1-\Delta^2)^2}\right)\right\}, \tag{4.75}$$

where ${}_2F_1\left(\{a,b\};\{c\};z\right)$ is the 2-1 hypergeometric function in the standard form [93]. Let the expression in the curly braces of equation 4.75 be:

$$H=\sum_{k=0}^{\infty}\frac{\left(-\frac{\pi(\Delta^2-1)}{2\Delta^2(\Delta^2+1)}\right)^k}{k!}\left(\delta_{k,0}+2\sum_{m=1}^{\infty}m^{2k}e^{-m^2\pi\left(\Delta^2+\frac{1}{2\Delta^2}\right)}\right){}_2F_1\left(-j,-k,\frac{1}{2},\frac{-4\Delta^2}{(1-\Delta^2)^2}\right). \tag{4.76}$$

Simplifying the kronecker delta and then rearrange the order of the m and k sum implies,

$$H=\theta_3\left(0,e^{-\pi\left(\Delta^2+\frac{1}{2\Delta^2}\right)}\right)+2\sum_{m=1}^{\infty}e^{-m^2\pi\left(\Delta^2+\frac{1}{2\Delta^2}\right)}\sum_{k=1}^{\infty}\frac{\left(-\frac{\pi m^2(\Delta^2-1)}{2\Delta^2(\Delta^2+1)}\right)^k}{k!}\,{}_2F_1\left(-j,-k,\frac{1}{2},\frac{-4\Delta^2}{(1-\Delta^2)^2}\right). \tag{4.77}$$

Note that, one can derive[3],

$$\sum_{k=1}^{\infty}\frac{x^k}{k!}\,{}_2F_1\left(-j,-k,\frac{1}{2},y\right)=-1+e^x\sum_{b=0}^{j}\binom{j}{b}\frac{(xy)^b}{\left(\frac{1}{2}\right)_b}=-1+e^x\,{}_1F_1\left(-j,\frac{1}{2},-xy\right) \tag{4.78}$$

with $(z)_b$ being the Pochhammer symbol and ${}_1F_1\left(a,b,z\right)$ is the Kummer confluent hypergeometric function (a.k.a the 1-1 hypergeometric function) in their standard forms [93]. Let $x=-\frac{\pi m^2(\Delta^2-1)}{2\Delta^2(\Delta^2+1)}$ and $y=\frac{-4\Delta^2}{(1-\Delta^2)^2}\Rightarrow xy=\frac{2\pi}{\Delta^4-1}m^2$. Using the identity in equation 4.78:

$$\Rightarrow H=1+2\sum_{m=1}^{\infty}e^{-m^2\pi\left(1+\frac{\Delta^4}{\Delta^2+1}\right)}\,{}_1F_1\left(-j,\frac{1}{2},\frac{2\pi m^2}{1-\Delta^4}\right). \tag{4.79}$$

[3] **The reduction formula, equation 4.78, is not known in any literature.**

Plugging equation 4.79 back into equation 4.75. Hence, removing the k infinite sum,

$$\Rightarrow C_{2j} = \lambda(\Delta)\frac{\pi^{\frac{1}{4}}\sqrt{\Delta}\sqrt{(2j)!}\,\tanh^{j}(\ln(\Delta))}{(j!)2^{j}\sqrt{\cosh(\ln(\Delta))}}\left\{1+2\sum_{m=1}^{\infty}e^{-m^{2}\pi\left(1+\frac{\Delta^{4}}{\Delta^{2}+1}\right)}{}_{1}F_{1}\left(-j,\frac{1}{2},\frac{2\pi m^{2}}{1-\Delta^{4}}\right)\right\}. \tag{4.80}$$

Note that ${}_{1}F_{1}\left(-j,\frac{1}{2},\frac{2\pi m^{2}}{1-\Delta^{4}}\right)=\frac{j!}{(1/2)_{j}}L_{j}^{-\frac{1}{2}}\left(\frac{2\pi m^{2}}{1-\Delta^{4}}\right)$ where $L_{n}^{\alpha}(x)$ is the generalized Laguerre polynomial in its standard form.

$$\Rightarrow C_{2j} = \lambda(\Delta)\frac{\pi^{\frac{1}{4}}\sqrt{\Delta}\sqrt{(2j)!}\,\tanh^{j}(\ln(\Delta))}{(1/2)_{j}2^{j}\sqrt{\cosh(\ln(\Delta))}}\left\{\sum_{m\in\mathbb{Z}}e^{-m^{2}\pi\left(1+\frac{\Delta^{4}}{\Delta^{2}+1}\right)}L_{j}^{-\frac{1}{2}}\left(\frac{2\pi m^{2}}{1-\Delta^{4}}\right)\right\}. \tag{4.81}$$

Using $(1/2)_{j}=(2j-1)!!/2^{j}$, where !! is the double factorial:

$$\Rightarrow C_{2j} = \lambda(\Delta)\frac{\pi^{\frac{1}{4}}\sqrt{\Delta}\sqrt{(2j)!}\,\tanh^{j}(\ln(\Delta))}{(2j-1)!!\sqrt{\cosh(\ln(\Delta))}}\left\{\sum_{m\in\mathbb{Z}}e^{-m^{2}\pi\left(1+\frac{\Delta^{4}}{\Delta^{2}+1}\right)}L_{j}^{-\frac{1}{2}}\left(\frac{2\pi m^{2}}{1-\Delta^{4}}\right)\right\}. \tag{4.82}$$

Using the approximate form of the normalisation constant $\lambda=(2/\pi)^{1/4}$,

$$\Rightarrow C_{2j} = 2^{\frac{3}{4}}\sqrt{\frac{\Delta^{2}}{\Delta^{2}+1}}\left(\frac{\Delta^{2}-1}{\Delta^{2}+1}\right)^{j}\frac{\sqrt{(2j)!}}{(2j-1)!!}\left\{\sum_{m\in\mathbb{Z}}e^{-m^{2}\pi\left(1+\frac{\Delta^{4}}{\Delta^{2}+1}\right)}L_{j}^{-\frac{1}{2}}\left(\frac{2\pi m^{2}}{1-\Delta^{4}}\right)\right\}. \tag{4.83}$$

Since $L_{n}^{-\frac{1}{2}}(x^{2})$ is related to the number wavefunctions via $L_{n}^{-\frac{1}{2}}(x^{2})e^{-x^{2}/2}(2^{2n}n!)(2^{2n}(2n)!\sqrt{\pi})^{-1/2}=\phi_{2n}(x)$. We can use the following expression to derive equation A.23 in [97]. Or similarly, we can use $\phi_{2n}(x)=(2^{2n}(2n)!\sqrt{\pi})^{-1/2}2^{2n}e^{-x^{2}/2}{}_{1}F_{1}\left(-n,1/2,x^{2}\right)$ to get to A.23 in [97]. We have laid out an entirely different method of obtaining the Fock state amplitudes of $|S_{\Delta}\rangle$ compared to [97]. In our approach, we started from the generating function of a shifted Gaussian function, where as [97] started from the Mehler's Hermite Polynomial formula and used properties of the generalised Jacobi Theta functions to achieve their results. As we can observe in figure 4.6, the photon number amplitudes decreases in absolute amplitude as Fock state number increases.

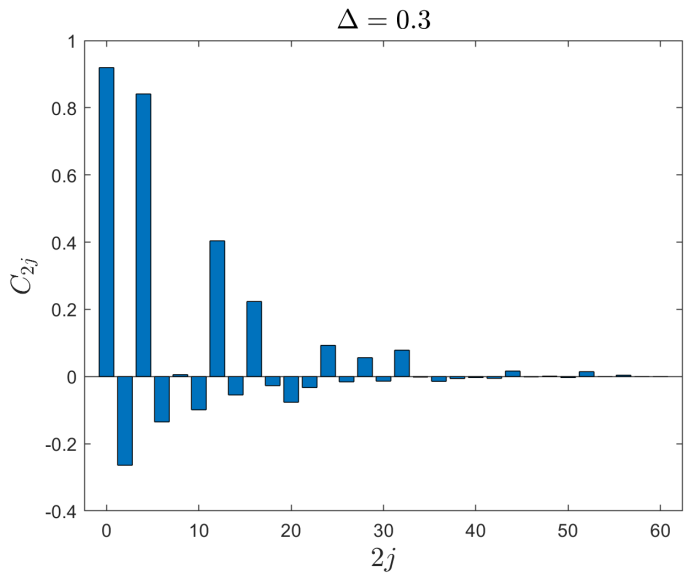

Figure 4.6: The photon number amplitude of $|S_\Delta\rangle$ with $\Delta = 0.3$ [4].

4.6.3 Approximations of C_{2j}

Let's look at four different types of approximations. We apply only one approximation at a time and keep the rest of it exact. In this case we can see if the amplitudes C_{2j} can have a better approximate form.

4.6.4 Truncating the m sum

Our goal is to truncate the m sum at a finite number, such that the majority of the contribution to the sum is retained. The function ${}_1F_1\left(-j, \frac{1}{2}, \frac{2\pi m^2}{1-\Delta^4}\right)$ is a polynomial of order j in $\frac{2\pi m^2}{1-\Delta^4}$. This imples,

$$e^{-m^2\pi\left(1+\frac{\Delta^4}{\Delta^2+1}\right)}\text{poly}\left[\left(\frac{2\pi}{1-\Delta^4}\right)^j m^{2j}\right]\Bigg|_{m\leq\mathcal{O}(j)} \gg e^{-m^2\pi\left(1+\frac{\Delta^4}{\Delta^2+1}\right)}\text{poly}\left[\left(\frac{2\pi}{1-\Delta^4}\right)^j m^{2j}\right]\Bigg|_{m>\mathcal{O}(j)}, \tag{4.84}$$

as the exponential dominates the polynomial on the right hand side. Hence we can truncate the m sum at around $\mathcal{O}(j)$ to get a reasonable approximation to the amplitudes. In order to

accommodate the $j=0$ term, we can terminate the m sum at $\chi_{\max}=j+1$. This imples:

$$C_{2j} \approx \lambda(\Delta)^{\frac{1}{4}} \frac{\pi^{\frac{1}{4}}\sqrt{\Delta}\sqrt{(2j)!}\,\tanh^j(\ln(\Delta))}{(j!)2^j\sqrt{\cosh(\ln(\Delta))}} \left\{ 1+2\sum_{m=1}^{j+1} e^{-m^2\pi\left(1+\frac{\Delta^4}{\Delta^2+1}\right)}\,{}_1F_1\left(-j,\frac{1}{2},\frac{2\pi m^2}{1-\Delta^4}\right)\right\} \tag{4.85}$$

This works really well numerically and can be computed quickly as we have only $\mathcal{O}(N^2)$ terms to compute if we terminate the j sum at N, (photon number cut off of $2N$).

Let's look at the truncation limit in more detail. Taking only the leading order dominant term (highest power in j) in the polynomial.

$$m^{2j} e^{-m^2\pi\left(1+\frac{\Delta^4}{\Delta^2+1}\right)} \left(\frac{2\pi}{1-\Delta^4}\right)^j \tag{4.86}$$

Let's look at the function (set $m=x$):

$$h_j(x;\Delta) = x^{2j} e^{-x^2\pi\left(1+\frac{\Delta^4}{\Delta^2+1}\right)} \left(\frac{2\pi}{1-\Delta^4}\right)^j,\ x\geq 0 \tag{4.87}$$

$h_j(x;\Delta)$ is a single peaked function with a maximum at $x=\sqrt{\frac{j}{\pi}\frac{1+\Delta^2}{1+\Delta^2+\Delta^4}}$. The peak has a width of roughly $\sqrt{\frac{1/2}{\pi}\frac{1+\Delta^2}{1+\Delta^2+\Delta^4}}$. Hence, by summing the m sum up to $\chi_{\max} > \sqrt{\frac{j}{\pi}\frac{1+\Delta^2}{1+\Delta^2+\Delta^4}} + \sqrt{\frac{1/2}{\pi}\frac{1+\Delta^2}{1+\Delta^2+\Delta^4}}$, you're expected to get the majority of the contribution to the infinite sum.

$$\chi_{\max} > \left(\sqrt{j}+1\right)\sqrt{\frac{1}{\pi}\frac{1+\Delta^2}{1+\Delta^2+\Delta^4}} \tag{4.88}$$

Suppose we take the worst $\Delta=\frac{1}{\sqrt{2\pi}}$ possible, $\chi_{\max} > \left(\sqrt{j}+1\right)\underbrace{\sqrt{\frac{1}{\pi}\frac{1+\Delta^2}{1+\Delta^2+\Delta^4}}}_{\approx 0.5581 \text{ if } \Delta=\frac{1}{\sqrt{2\pi}}}$. Hence we can set $\chi_{\max}=1+\lceil\sqrt{j}\rceil$:

$$\Rightarrow C_{2j} \approx \lambda(\Delta) \frac{\pi^{\frac{1}{4}}\sqrt{\Delta}\sqrt{(2j)!}\,\tanh^j(\ln(\Delta))}{(j!)2^j\sqrt{\cosh(\ln(\Delta))}} \left\{ 1+2\sum_{m=1}^{1+\lceil\sqrt{j}\rceil} e^{-m^2\pi\left(1+\frac{\Delta^4}{\Delta^2+1}\right)}\,{}_1F_1\left(-j,\frac{1}{2},\frac{2\pi m^2}{1-\Delta^4}\right)\right\}. \tag{4.89}$$

In order to compute the amplitudes at a photon number cutoff of $2N$, we have to compute

$\sum_{j=0}^{N}(1+\sqrt{j}) = N+\mathcal{H}_N(-1/2)$ terms ($\mathcal{H}_n(r)$ are the harmonic numbers). Since $N+\mathcal{H}_N(-1/2) < N + N^{1.5}$, hence we need to compute $\mathcal{O}(N^{\frac{3}{2}})$ terms.

4.6.5 Small $\Delta \ll 1$ limit

Suppose we ignore all $\mathcal{O}(\Delta^4)$ terms for $\Delta \ll 1$, then the hyperbolic trigonometric functions can be approximated by $\tanh^j(\ln(\Delta)) \approx (-1)^j(1-2j\Delta^2+\mathcal{O}(\Delta^4))$ and $\sqrt{\cosh(\ln(\Delta))} \approx (1+\Delta^2/2+\mathcal{O}(\Delta^4))/\sqrt{2\Delta}$:

$$\Rightarrow C_{2j} \approx \lambda(\Delta)\pi^{\frac{1}{4}}\frac{\sqrt{(2j)!}}{j!}\frac{(-1)^j}{2^{j-\frac{1}{2}}}\Delta\Big(1-\Big(2j+\frac{1}{2}\Big)\Delta^2\Big)\left\{1+2\sum_{m=1}^{\infty}e^{-m^2\pi}{}_1F_1\Big(-j,\frac{1}{2},2\pi m^2\Big)\right\} \tag{4.90}$$

4.6.6 Truncating the j sum at photon number cutoff $2N$

We can see from numerics in figure 4.7, the infidelity is approximately 10^{-3} for states with $\Delta = 0.2$ if we truncate at Fock state $|n=100\rangle$. This illustrates the difficulty in simulating finite energy GKP states in the Fock basis, because in order to keep an effective error of at least 10^{-3}, we need to keep a a 100 by 1 vector just to simulate a one mode grid sensor state.

Suppose we wish to have a maximum photon number cutoff at N, hence $\left|S_\Delta^{(N)}\right\rangle \approx \sum_{n=0}^{N} C_{2n}$. How close is the inner product $\left\langle S_\Delta^{(N)}\middle|S_\Delta^{(N)}\right\rangle$ to 1? The standard deviation of $|S_\Delta\rangle$'s photon number distribution is approximately: $\sigma_{\hat{n}} = \sqrt{\langle S_\Delta|\,\hat{n}^2\,|S_\Delta\rangle - \langle S_\Delta|\,\hat{n}\,|S_\Delta\rangle^2} \approx \frac{1}{2\Delta^2}$, and the mean is $\langle S_\Delta|\,\hat{n}\,|S_\Delta\rangle \approx (\Delta^2+\Delta^{-2}-1)/2$. The m^{th} standard deviation away from the mean is: $\langle S_\Delta|\,\hat{n}\,|S_\Delta\rangle + m\sigma \approx \frac{\Delta^2-1}{2} + \frac{m+1}{2}\frac{1}{\Delta^2} \approx \frac{m+1}{2}\frac{1}{\Delta^2} - \frac{1}{2}$. If we set the photon cutoff N to be at least m standard deviation away from the mean, we are sure to capture most of the probability distribution while cutting off higher photon numbers. Let's set $N \approx \frac{m+1}{2}\frac{1}{\Delta^2}$. One choice to truncate N would be to set $N = \mathcal{O}(m\Delta^{-2})$.

A photon number cut off at $N = 100$ is already exceptionally high. For example, if we have merely 10 subsystems of GKP states we wish to simulate, then we need to store in memory a

$100^{10} = 10^{20}$ length vector and $100^{10} \times 100^{10}$ matrices when applying unitary operators. Even just storing the state vector is multiple orders of magnitude beyond the memory requirements needed to store the full state-vector of Google's quantum advantage experiment which requires a $2^{53} \approx 10^{16}$ length vectors to be stored and manipulated [98].

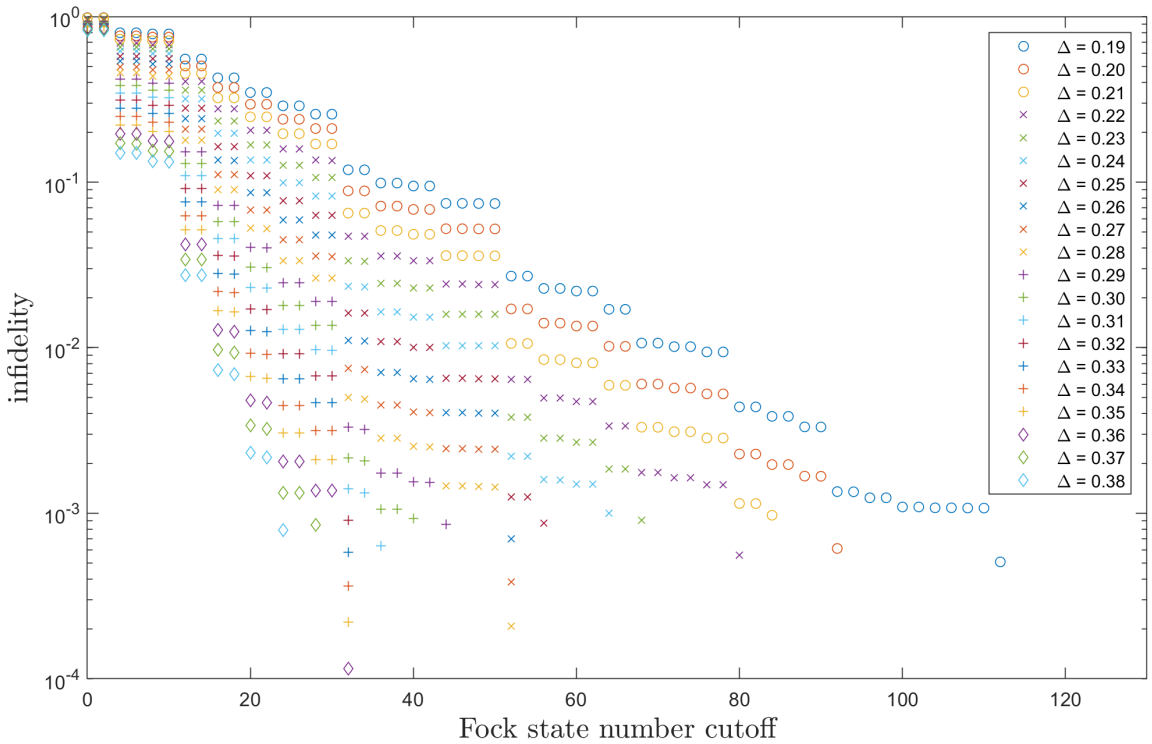

Figure 4.7: The infidelity of the grid sensor state vs. maximum photon cut off number. Different scatter plots indicates different values of Δ.

Grid state generation properties

In section 4.7, basic resource theory for quantum systems is introduced, especially the resource theory of non-Gaussianity in CV systems. This is then applied to the grid sensor state to explain the difficulty in generating them in a photonic platform. Then, in section 4.8, a method to generate the GKP Bell state is explored given that we have perfect copies of grid sensor state available on demand.

4.7 Resource theories and measures of non-Gaussianity

Resource theories provides a solid mathematical formalism to study possible quantum state transformations if we restrict the set of admissible state transformation. A resource theory assigns a measure to a set of quantum states. Given a set of allowed operations called free operations, and freely available, free states, we can now quantify how many free states is required to create a particular resource state.

Non-Gaussian states are invaluable resource in the study of continuous variable quantum information. In particular, there exists no-go theorems in the conversion of states with different levels of non-Gaussianity. If we set our free operations to be Gaussian operations, One can study these state inter-conversion laws using resource theory. In order to quantify the feasibility of specific conversions, we need to look at monotones. Monotones are functional measures that maps a set of quantum states to a non-negative real number [99].

4.7.1 Wigner negativity as a monotone

The volume of the negative sections of the Wigner function can be used to quantify how non-Gaussian a state is. Wigner negativity can be used as a monotone to give bounds on the inter-conversion between states. The Wigner logarithmic negativity (WLN) can be defined as:

$$\mathcal{W}[\hat{\rho}] = \log\left(\int_{q,p} dq\ dp\ \left|W(q,p|\hat{\rho})\right| \right) , \tag{4.91}$$

where $\mathcal{W} > 0$ and W is the wigner function. Furthermore, Wigner negativity had been known to be a necessary but not sufficient resource for CV systems quantum computational speed-ups [100, 101], looking at it from its hardness of classical simulation.

The results in [99] allowed feed-forward stochastic Gaussian process and measurements. In addition, they admit WLN as a measure and have positive Wigner function states as free state in their resource theory. Is the conversion of k copies of $\hat{\rho}_A$ to m copies of $\hat{\rho}_B$ possible with probability p? Using equation 5 of [99] we can compute the minimum number of copies of $\hat{\rho}_A$ (on average) required to do so. Let the minimum copies of $\hat{\rho}_A$ be n, then the expectation of n follows this inequality:

$$\mathbb{E}(n) = \frac{k}{p} \geq m \frac{\mathcal{W}[\hat{\rho}_B]}{\mathcal{W}[\hat{\rho}_A]} . \tag{4.92}$$

If only one copy of $\hat{\rho}_B$ is needed to be distilled, with unit probability then,

$$n \geq \frac{\mathcal{W}[\hat{\rho}_B]}{\mathcal{W}[\hat{\rho}_A]} . \tag{4.93}$$

This implies if state $\hat{\rho}_A$ has zero WLN (Gaussian states [99] have zero WLN), then it's impossible to use Gaussian operations and Gaussian measurements to distill out even a single copy of a state with any Wigner negativity. In optical quantum computing, the number of single photon $|1\rangle$ states required to engineer a particular resource state is a realistic figure of merit. We wish to quantify the number of single photons needed along with Gaussian operations and measurements to form a particular finite energy GKP or sensor Grid state using the bound from equation 4.93. The Wigner function of a Fock state $|n\rangle$ is well known and is given by [102]:

$$W(q,p|\,|n\rangle\langle n|) = \frac{(-1)^n}{\pi} e^{-(q^2+p^2)} L_n(2(p^2+q^2)) , \tag{4.94}$$

where L_n are the Laguerre polynomials of the n^{th} order [103]. With single photon states, $n = 1$. The WLN of a single photon can be computed explicitly using $L_1(x) = 1 - x$:

$$\begin{aligned}
\mathcal{W}[|1\rangle\langle 1|] &= \log\Big(\int_{p,q} dp\ dq\ \Big| \frac{(-1)^n}{\pi} e^{-(q^2+p^2)} \big(1 - 2(q^2+p^2)\big) \Big| \Big) \\
&= \log\Big(\int_{p,q} dp\ dq\ \Big| \frac{(-1)^n}{\pi} e^{-(q^2+p^2)} \big(1 - 2(q^2+p^2)\big) \Big| \Big) \\
&= \log\Big(2 \int_{r=0}^{\infty} dr\ r e^{-r^2} (1 - 2r^2) \Big) \\
&= \log\Big(2 \int_{r=0}^{1/\sqrt{2}} dr\ r e^{-r^2} (1 - 2r^2) - \int_{r=1/\sqrt{2}}^{\infty} dr\ r e^{-r^2} (1 - 2r^2) \Big) \\
&= \log(2) + \log\Big(e^{-r^2} \big(r^2 + \frac{1}{2}\big) \Big|_0^{1/\sqrt{2}} - e^{-r^2} \big(r^2 + \frac{1}{2}\big) \Big|_{1/\sqrt{2}}^{\infty} \Big) \\
&= \log(2) + \log\Big(2e^{-\frac{1}{2}} - \frac{1}{2} \Big) \\
&= \log\Big(\frac{4}{\sqrt{e}} - 1 \Big) \approx 0.5\ .
\end{aligned} \tag{4.95}$$

Along with the inter-conversion inequality from equation 4.93, $\mathcal{W}[|1\rangle\langle 1|]$ can be used to obtain the minimum number of photons needed to generate a particular state.

4.7.2 Wigner function of the grid states

Subsection 4.7.2 consists of my own work.

We aim to derive the Wigner functions of the finite energy logical GKP states and grid sensor states in order to compute their WLN. An even wavefunctions have a Wigner functions of the form:

$$W(q, p|\hat{\rho}) = \frac{1}{\sqrt{\pi}} \mathcal{F}_{y \to \sqrt{2}p} \Big\{ R[\rho(\sqrt{2}q, y)] \Big\}\ , \tag{4.96}$$

where $\rho(x, y)$ is the density matrix function of the state, $\mathcal{F}_{a \to b}$ is the Fourier transform from variable $a \to b$ and $R[f(x, y)] = f\Big(\frac{x-y}{\sqrt{2}}, \frac{x+y}{\sqrt{2}}\Big)$ is the rotation of a two-dimensional function $f(x, y)$ by $\frac{\pi}{4}$ radians anticlockwise. We will use equation 4.96 to compute the following Wigner functions.

Wigner function of $|S_\Delta\rangle$

We shall compute the Wigner function of the grid sensor state now, starting with equation 4.96:

$$\begin{aligned} W(q,p|\,|S_\Delta\rangle) =& \frac{1}{\sqrt{\pi}}\mathcal{F}_{z\to\sqrt{2}p}\Big\{S_\Delta\Big(q-\frac{z}{\sqrt{2}}\Big)S_\Delta\Big(q+\frac{z}{\sqrt{2}}\Big)\Big\} \\ &= \frac{\sqrt{2}}{\pi}\mathcal{F}_{z\to\sqrt{2}p}\left\{\sum_{n\in\mathbb{Z}} e^{-\frac{(n\sqrt{2\pi})^2\Delta^2}{2}} e^{-\frac{(q-z/\sqrt{2}-n\sqrt{2\pi})^2}{2\Delta^2}} \sum_{m\in\mathbb{Z}} e^{-\frac{(m\sqrt{2\pi})^2\Delta^2}{2}} e^{-\frac{(q+z/\sqrt{2}-m\sqrt{2\pi})^2}{2\Delta^2}}\right\} \\ &= \frac{\sqrt{2}}{\pi}\mathcal{F}_{z\to\sqrt{2}p}\left\{\sum_{n,m} e^{-\frac{((m-n)\sqrt{\pi})^2\Delta^2}{2}} e^{-\frac{(z-(m-n)\sqrt{\pi})^2}{2\Delta^2}} e^{-\frac{((m+n)\sqrt{\pi})^2\Delta^2}{2}} e^{-\frac{(\sqrt{2}q-(m+n)\sqrt{\pi})^2}{2\Delta^2}}\right\} \end{aligned} \tag{4.97}$$

Using the sum re-indexing technique of $\sum_{n,m\in\mathbb{Z}^2} = \sum_{j=0}^{1}\sum_{a,b\in\mathbb{Z}^2}$ with $m+n=2a+j, m-n=2b+j$:

$$\begin{aligned} W(q,p|\,|S_\Delta\rangle) &= \frac{1}{\sqrt{2\pi}}\sum_{j=0}^{1}\mathcal{F}_{z\to\sqrt{2}p}\left\{\frac{\sqrt{2}}{\pi^{1/4}}\sum_m e^{-\frac{((2m+j)\sqrt{\pi})^2\Delta^2}{2}} e^{-\frac{(z-(2m+j)\sqrt{\pi})^2}{2\Delta^2}}\right\}\psi_j^\Delta(\sqrt{2}q) \\ &= \frac{1}{\sqrt{\pi}}\frac{\Big(\psi_0^\Delta(\sqrt{2}q)\psi_+^\Delta(\sqrt{2}p)+\psi_1^\Delta(\sqrt{2}q)\psi_-^\Delta(\sqrt{2}p)\Big)}{\sqrt{2}}\,, \end{aligned} \tag{4.98}$$

the Wigner function of the grid sensor state can be expressed back as sum of scaled wavefunctions of the GKP state.

WLN of the grid sensor state

Using the expression in equation 4.99 for the Wigner function of the grid sensor state, the only negative region of the Wigner function resides on the term containing ψ_-^Δ, therefore the absolute value of this Wigner can be obtained by turning $\psi_-^\Delta(\sqrt{2}p) \to \psi_+^\Delta(\sqrt{2}p)$ in the second term of 4.99,

$$\big|W(q,p|\,|S_\Delta\rangle)\big| = \frac{1}{\sqrt{\pi}}\psi_+^\Delta(\sqrt{2}q)\psi_+^\Delta(\sqrt{2}p)\,, \tag{4.99}$$

Computing the following integral in order to compute the WLN:

$$\int_{q,p} dq\ dp\ \big|W(q,p|\,|S_\Delta\rangle)\big| = \Delta^2\left(\sum_{n\in\mathbb{Z}} e^{-\pi\Delta^2 n^2/2}\right)^2 = \Delta^2\theta_3\big(0, e^{-\pi\Delta^2/2}\big)\ , \tag{4.100}$$

the theta function is approximately $\sqrt{2}/\Delta$ for small Δ, hence the integral $\int_{q,p} dq\ dp\ \big|W(q,p|\,|S_\Delta\rangle)\big| \approx 2$. This implies the WLN is approximately $\log(2)$, with a full expression being:

$$\mathcal{W}(|S_\Delta\rangle) = \log\Big(\Delta^2\theta_3\big(0, e^{-\pi\Delta^2/2}\big)\Big) \approx \log(2) \approx 0.69\ , \tag{4.101}$$

Wigner function of the logical GKP state

We shall compute the Wigner function of the logical GKP states now: Starting with equation 4.96 with $\hat{\rho} = \Big|\psi_\mu^{\vec{\Delta}}\Big\rangle\Big\langle\psi_\mu^{\vec{\Delta}}\Big|$:

$$W\Big(q,p\Big|\Big|\psi_\mu^{\vec{\Delta}}\Big\rangle\Big) = \frac{1}{\sqrt{\pi}}\mathcal{F}_{z\to\sqrt{2}p}\Big\{\psi_\mu^{\vec{\Delta}}\Big(q-\frac{z}{\sqrt{2}}\Big)\psi_\mu^{\vec{\Delta}}\Big(q+\frac{z}{\sqrt{2}}\Big)\Big\} \tag{4.102}$$

$$\begin{aligned} &W\Big(q,p\Big|\Big|\psi_\mu^{\vec{\Delta}}\Big\rangle\Big) \\ &= \frac{2}{\pi}\frac{\kappa}{\Delta}\mathcal{F}_{z\to\sqrt{2}p}\Big\{\sum_{n\in\mathbb{Z}} e^{-\frac{((2n+\mu)\sqrt{\pi})^2\kappa^2}{2}} e^{-\frac{(q-z/\sqrt{2}-(2n+\mu)\sqrt{\pi})^2}{2\Delta^2}} \sum_{m\in\mathbb{Z}} e^{-\frac{((2m+\mu)\sqrt{\pi})^2\kappa^2}{2}} e^{-\frac{(q+z/\sqrt{2}-(2m+\mu)\sqrt{\pi})^2}{2\Delta^2}}\Big\} \end{aligned} \tag{4.103}$$

Expanding and completing the square in the exponential with q, z, this implies,

$e^{-\frac{(q-z/\sqrt{2}-(2n+\mu)\sqrt{\pi})^2}{2\Delta^2}} e^{-\frac{(q+z/\sqrt{2}-(2m+\mu)\sqrt{\pi})^2}{2\Delta^2}} = e^{-\frac{2(q-(n+m+\mu)\sqrt{\pi})^2}{2\Delta^2}} e^{-\frac{(z+(n-m)\sqrt{2\pi})^2}{2\Delta^2}}$, substituting this back into equation 4.103:

$$\begin{aligned} &\Rightarrow W\Big(q,p\Big|\Big|\psi_\mu^{\vec{\Delta}}\Big\rangle\Big) \\ &= \frac{2}{\pi}\frac{\kappa}{\Delta}\mathcal{F}_{z\to\sqrt{2}p}\sum_{n,m\in\mathbb{Z}^2}\Big\{e^{-\frac{2(q-(n+m+\mu)\sqrt{\pi})^2}{2\Delta^2}} e^{-\frac{(z+(n-m)\sqrt{2\pi})^2}{2\Delta^2}} e^{-\frac{((2n+\mu)\sqrt{\pi})^2\kappa^2}{2}} e^{-\frac{((2m+\mu)\sqrt{\pi})^2\kappa^2}{2}}\Big\} \end{aligned} \tag{4.104}$$

Using the sum re-indexing technique of $\sum_{n,m\in\mathbb{Z}^2} = \sum_{\nu=0}^{1}\sum_{a,b\in\mathbb{Z}^2}$ with $m+n = 2a+\nu, m-n = 2b+\nu$:

$$\Rightarrow W\left(q,p\middle|\left|\psi_\mu^{\vec{\Delta}}\right\rangle\right) = \frac{2}{\pi}\frac{\kappa}{\Delta}\sum_{\nu=0}^{1}\sum_{a,b\in\mathbb{Z}^2}\mathcal{F}_{z\to\sqrt{2}p}\left\{e^{-\frac{2(q-(2a+\nu+\mu)\sqrt{\pi})^2}{2\Delta^2}}e^{-\frac{(z+(2b+\nu)\sqrt{2\pi})^2}{2\Delta^2}}e^{-\frac{((2a-2b+\mu)\sqrt{\pi})^2\kappa^2}{2}}e^{-\frac{((2(a+b+\nu)+\mu)\sqrt{\pi})^2\kappa^2}{2}}\right\} \tag{4.105}$$

We can re-write $e^{-\frac{((2a-2b+\mu)\sqrt{\pi})^2\kappa^2}{2}}e^{-\frac{((2(a+b+\nu)+\mu)\sqrt{\pi})^2\kappa^2}{2}} = e^{-\pi\kappa^2(2a+\nu+\mu)^2}e^{-\pi\kappa^2(2b+\nu)^2}$ by expanding and re-collecting terms, substituting this back into equation 4.105 implies:

$$\Rightarrow W\left(q,p\middle|\left|\psi_\mu^{\vec{\Delta}}\right\rangle\right) = \frac{2}{\pi}\frac{\kappa}{\Delta}\sum_{\nu=0}^{1}\sum_{a\in\mathbb{Z}^2}e^{-\frac{(q-(2a+\nu+\mu)\sqrt{\pi})^2}{\Delta^2}}e^{-\pi\kappa^2(2a+\nu+\mu)^2}\frac{\underbrace{\mathcal{F}_{z\to\sqrt{2}p}\left\{\sum_{b\in\mathbb{Z}^2}e^{-\frac{(z+(2b+\nu)\sqrt{2\pi})^2}{2\Delta^2}}e^{-\pi\kappa^2(2b+\nu)^2}\right\}}}{\sum_m e^{-(\frac{\sqrt{\pi}m}{2})^2\frac{\Delta^2}{1+\kappa^2\Delta^2}}e^{-\left(p-\frac{\sqrt{\pi}m}{2(1+\kappa^2\Delta^2)}\right)^2\frac{(1+\kappa^2\Delta^2)}{\kappa^2}}(-1)^{m\nu}} \tag{4.106}$$

$$\Rightarrow W\left(q,p\middle|\left|\psi_\mu^{\vec{\Delta}}\right\rangle\right) = \frac{1}{\pi}\sum_{\nu=0}^{1}\sum_{n,m}e^{-(\frac{\sqrt{\pi}m}{2})^2\frac{\Delta^2}{1+\kappa^2\Delta^2}}e^{-\left(p-\frac{\sqrt{\pi}m}{2(1+\kappa^2\Delta^2)}\right)^2\frac{(1+\kappa^2\Delta^2)}{\kappa^2}}\times\left\{(-1)^{m\nu}e^{-\kappa^2(2n+\nu+\mu)^2\pi}e^{-\frac{(q-(2n+\nu+\mu)\sqrt{\pi})^2}{\Delta^2}}\right\}. \tag{4.107}$$

WLN of the logical GKP state

We can now use this expression of the GKP to compute the WLN of the logical GKP states. Let's split $W\left(q,p\middle|\left|\psi_\mu^{\vec{\Delta}}\right\rangle\right)$ into W_+ (even $m\nu$) and W_- (odd $m\nu$), the positive part and negative part of $W\left(q,p\middle|\left|\psi_\mu^{\vec{\Delta}}\right\rangle\right)$ respectively. Note that, $W = W_+ + W_-$.

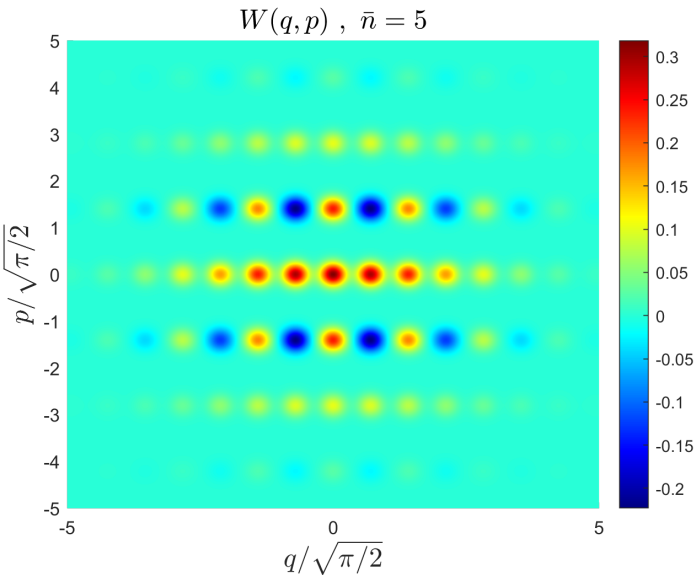

Figure 4.8: GKP ψ_+^Δ Wigner function in phase space with an average photon number of 5.

$$W_+ = \frac{1}{\pi}\sum_{\nu=0}^{1}\sum_{n,m} e^{-(\sqrt{\pi}m)^2\Delta^2} e^{-\frac{(p-\sqrt{\pi}m)^2}{\kappa^2}} e^{-\kappa^2(2n+\nu+\mu)^2\pi} e^{-\frac{(q-(2n+\nu+\mu)\sqrt{\pi})^2}{\Delta^2}}$$
$$+$$
$$\frac{1}{\pi}\sum_{n,m} e^{-(\sqrt{\pi}(2m+1)/2)^2\Delta^2} e^{-\frac{(p-\sqrt{\pi}(2m+1)/2)^2}{\kappa^2}} e^{-\kappa^2(2n+\mu)^2\pi} e^{-\frac{(q-(2n+\mu)\sqrt{\pi})^2}{\Delta^2}} \quad , \tag{4.108}$$

$$W_- = -\frac{1}{\pi}\sum_{n,m} e^{-(\sqrt{\pi}(2m+1)/2)^2\Delta^2} e^{-\frac{(p-\sqrt{\pi}(2m+1)/2)^2}{\kappa^2}} e^{-\kappa^2(2n+1+\mu)^2\pi} e^{-\frac{(q-(2n+1+\mu)\sqrt{\pi})^2}{\Delta^2}} \quad .$$

Now we compute the wigner negativity,

$$\Rightarrow \int dq\ dp\ W_+ = \kappa\Delta\sum_{\nu=0}^{1}\sum_{n,m} e^{-(\sqrt{\pi}m)^2\Delta^2} e^{-\kappa^2(2n+\nu+\mu)^2\pi} + \kappa\Delta\sum_{n,m} e^{-(\sqrt{\pi}(2m+1)/2)^2\Delta^2} e^{-\kappa^2(2n+\mu)^2\pi} \quad ,$$

$$\int dq\ dp\ W_- = -\kappa\Delta\sum_{n,m} e^{-(\sqrt{\pi}(2m+1)/2)^2\Delta^2} e^{-\kappa^2(2n+1+\mu)^2\pi} \quad .$$

(4.109)

Using $\int dq\ dp\ W_+ + \int dq\ dp\ W_- = 1$ and $\int dq\ dp\ W_+ - \int dq\ dp\ W_- = \int dq\ dp\ |W|$,

$$\begin{aligned} \Rightarrow \int dq\ dp\ W_- &= \frac{1 - \int dq\ dp\ |W|}{2} \\ \Rightarrow \int dq\ dp\ |W| &= 1 - 2\int dq\ dp\ W_- \end{aligned} \tag{4.110}$$

$$\Rightarrow \int dq\ dp\ |W| = 1 + 2\kappa\Delta \sum_{n,m} e^{-(\sqrt{\pi}(2m+1)/2)^2\Delta^2} e^{-\kappa^2(2n+1+\mu)^2\pi} \tag{4.111}$$

$$\Rightarrow \int dq\ dp\ |W| = 1 + \Delta\theta_2(0, e^{-\pi\Delta^2})\ \theta_3(\pi(\mu+1)/2, e^{-\pi\kappa^{-2}/4})$$

In the paper [100], the authors calculated the Wigner negativity of the ideal GKP states to be, $\int dq\ dp\ |W| = 2$. In order to check if we recover this result, we take the limit of:

$$\lim_{\Delta,\kappa\to 0} \int dq\ dp\ |W| = \lim_{\Delta,\kappa\to 0} \left(1 + \Delta\theta_2(0, e^{-\pi\Delta^2})\ \theta_3(\pi(\mu+1)/2, e^{-\pi\kappa^{-2}/4})\right) \tag{4.112}$$

Using the $\lim_{\Delta\to 0} \theta_2(0, e^{-\pi\Delta^2}) = \frac{1}{\Delta}$ and $\lim_{\kappa\to 0} \theta_3(\pi(\mu+1)/2, e^{-\pi\kappa^{-2}/4}) = 1$ [104]. We will indeed recover,

$$\lim_{\Delta,\kappa\to 0} \int dq\ dp\ |W| = 2\ . \tag{4.113}$$

We have computed a more general result for non-zero Δ. Numerically, we have plotted both the Wigner negativity and WLN in figure 4.9 and 4.10 respectively.

Notice the WLN of the grid sensor state and GKP logical states are both approximately $\mathcal{W} \approx 0.69$, it's possible to use Gaussian operation and measurements to convert one to another. Using the the inter-conversion ratio from equation 4.93 implies at least 1.38 (in practice 2) single photons is needed to generate a any grid states. Historically, WLN had always been used as a measure for the difficulty of CV state generation [99]. However, unfortunately this bound is not very insightful in this circumstance, but could be useful to check if specific protocols increases/decreases the WLN, an indication of the performance of a particular protocol.

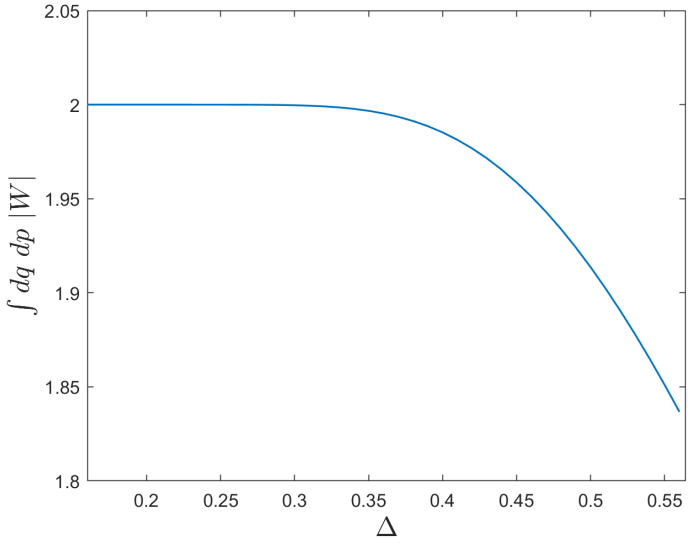

Figure 4.9: $2^{\mathcal{W}}$ of an approximate logical 0 GKP state with $\Delta = \kappa$.

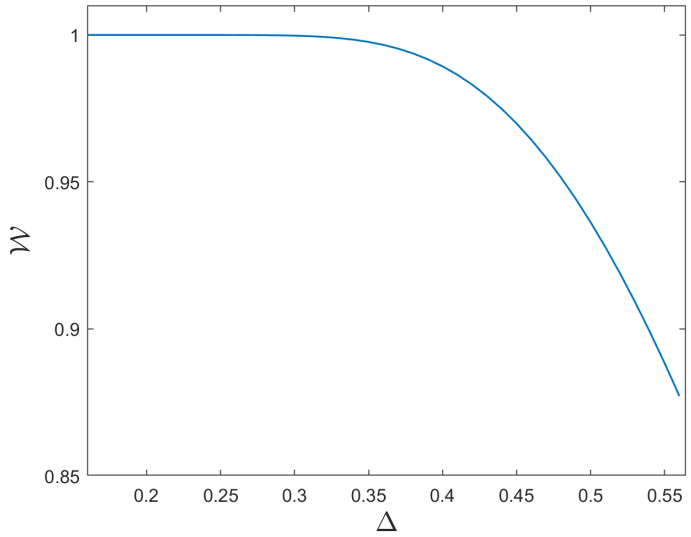

Figure 4.10: WLN of an approximate logical 0 GKP state with $\Delta = \kappa$.

4.7.3 Maximum phase-space variance as a monotone

Subsection 4.7.3 consists of my own work other than the definition of equation 4.114.

The WLN does not give a good bound on the number of single photons needed, the authors from [105] suggested another monotone and resource theory that is operationally relevant for generating states useful for continuous variable quantum information. To simplify the result in [105], one can choose the free states to be Gaussian states and the free operations to be all

probabilistic mixture of passive linear optics along with Gaussian measurements and feedforward. The choice of monotone would be the maximum phase space distance (only for pure states) given by [105]:

$$\mathcal{V}_1(|\Psi\rangle) = \max_\theta \left\{ \mathrm{Var}\big(\hat{B}_\theta |\Psi\rangle\big) \right\} - \frac{1}{2} \,, \tag{4.114}$$

where $\hat{B}_\theta$ is the action of a beamspliter by an arbitrary angle. For the grid sensor state, no matter what the beamsplitter rotation is, the Maximum phase space variance is at least its variance in the q- or the p- quadrature, hence it can be lower bound by the average of these two:

$$\mathcal{V}_1(|S_\Delta\rangle) > \frac{\langle S_\Delta| \hat{q}^2 |S_\Delta\rangle + \langle S_\Delta| \hat{p}^2 |S_\Delta\rangle}{2} - \frac{1}{2} = \langle S_\Delta| \hat{n} |S_\Delta\rangle \approx (\Delta^2 + \Delta^{-2} - 1)/2 \,. \tag{4.115}$$

$$\mathcal{V}_1(|S_\Delta\rangle) > \frac{\Delta^2 + \Delta^{-2} - 1}{2} \,, \tag{4.116}$$

due to its symmetry in the two quadratures. A Fock state $|n\rangle$ have a maximum phase space distance of n, $\mathcal{V}_1(|n\rangle) = n$ [105]. The inter-conversion ratio that gives the minimum number of single photons needed to generate a grid sensor state of a particular quality is given by:

$$\frac{\mathcal{V}_1(|S_\Delta\rangle)}{\mathcal{V}_1(|n=1\rangle)} > \frac{\Delta^2 + \Delta^{-2} - 1}{2} \,. \tag{4.117}$$

This result is computed numerically in figure 4.11. Note that at least 200 single photons is required for a reasonable high quality grid sensor state at $\Delta \approx 0.1$ to be generated on average. With the presence of errors in the state generation optical circuit, it's incredible difficult to have over 200 photons surviving loss over many optical components, making the generation of such states out of reach in our current technologies. However, the grid states could still be potentially useful in other emerging quantum information processing platforms where there had been experimental generation of these states such as [49] (trapped-ions) and [50] (superconducting microwave cavities).

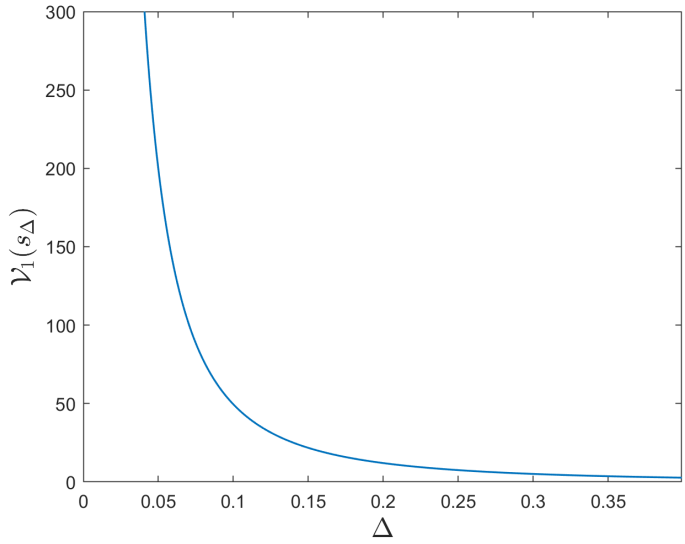

Figure 4.11: Maximum phase space variance of the grid sensor state in terms of Δ.

4.8 Generating a logical GKP Bell states with $|S_\Delta\rangle$ and a 50:50 beam-splitter

Section 4.8 consists of my own work.

Discovered independently by [106, 79], one can transform a pair of grid sensor state to a logical GKP $|00\rangle + |11\rangle$ type Bell state through the application of a 50:50 beamsplitter. Each GKP Gaussian peak is still perfectly circularly symmetric in the 2 mode wavefunction, an advantage to using the convention CNOT gate [77]. The CNOT will introduce additional shearing of the peaks in either directions. We will explicitly calculate how these different Bell states are formed and compare the different states resulting from these two different methods.

Starting with 2 copies of $|S_\Delta\rangle^{\otimes 2}$, we shall work primarily in the two mode q-quadrature basis, where we will manipulate the two-mode wavefunction $S_\Delta(x)S_\Delta(y)$. An application of a beam-splitter transforms $x \to \frac{x+y}{\sqrt{2}}$ and $y \to \frac{-x+y}{\sqrt{2}}$, which is essentially a 45 degree rotation of the 2 mode wavefunction $S_\Delta(x)S_\Delta(y)$ around its origin, in this calculation, we shall use $\lambda(\Delta)$ the normalisation of the grid sensor state to be $(2/\pi)^{1/4}$ for simplicity.

$$S_\Delta(x)S_\Delta(y) \to S_\Delta\Big(\frac{x+y}{\sqrt{2}}\Big)S_\Delta\Big(\frac{-x+y}{\sqrt{2}}\Big) \tag{4.118}$$

$$S_\Delta\Big(\frac{x+y}{\sqrt{2}}\Big)S_\Delta\Big(\frac{-x+y}{\sqrt{2}}\Big) = \sqrt{\frac{2}{\pi}}\sum_{n,m\in\mathbb{Z}^2} e^{-\frac{(n\sqrt{2\pi})^2\Delta^2}{2}} e^{-\frac{\left(\frac{x+y}{\sqrt{2}}-n\sqrt{2\pi}\right)^2}{2\Delta^2}} e^{-\frac{(m\sqrt{2\pi})^2\Delta^2}{2}} e^{-\frac{\left(\frac{x-y}{\sqrt{2}}-m\sqrt{2\pi}\right)^2}{2\Delta^2}} \tag{4.119}$$

Expanding the exponent inside the sum, re-arranging terms and completing the square gives the following result

$$\Rightarrow S_\Delta\Big(\frac{x+y}{\sqrt{2}}\Big)S_\Delta\Big(\frac{-x+y}{\sqrt{2}}\Big) = \sqrt{\frac{2}{\pi}}\sum_{n,m\in\mathbb{Z}^2} e^{-\frac{((n-m)\sqrt{\pi})^2\Delta^2}{2}} e^{-\frac{(x-(n-m)\sqrt{\pi})^2}{2\Delta^2}} e^{-\frac{((n+m)\sqrt{\pi})^2\Delta^2}{2}} e^{-\frac{(y-(n+m)\sqrt{\pi})^2}{2\Delta^2}} \tag{4.120}$$

We can trade the double sum for a triple sum if we make this following sum re-indexing:

$\sum_{n\in\mathbb{Z}}\sum_{n\in\mathbb{Z}} \to \sum_{\mu=0}^{1}\sum_{n'\in\mathbb{Z}}\sum_{m'\in\mathbb{Z}}$, where $n-m=2n'+\mu, n+m=2m'+\mu$:

$$S_\Delta\Big(\frac{x+y}{\sqrt{2}}\Big)S_\Delta\Big(\frac{-x+y}{\sqrt{2}}\Big) = \sqrt{\frac{2}{\pi}}\sum_{\mu=0}^{1}\sum_{n'\in\mathbb{Z}} e^{-\frac{((2n'+\mu)\sqrt{\pi})^2\Delta^2}{2}} e^{-\frac{(x-(2n'+\mu)\sqrt{\pi})^2}{2\Delta^2}} \sum_{m'\in\mathbb{Z}} e^{-\frac{((2m'+\mu)\sqrt{\pi})^2\Delta^2}{2}} e^{-\frac{(y-(2m'+\mu)\sqrt{\pi})^2}{2\Delta^2}}$$
$$= \frac{\psi_0^{\vec{\Delta}}(x)\psi_0^{\vec{\Delta}}(y)+\psi_1^{\vec{\Delta}}(x)\psi_1^{\vec{\Delta}}(y)}{\sqrt{2}}\,. \tag{4.121}$$

Hence we have shown that a 50:50 beamsplitter transforms a 2 copies of the grid sensor state to a GKP Bell state: $|S_\Delta\rangle^{\otimes 2} \to= \frac{1}{\sqrt{2}}\Big(\Big|\psi_0^{\vec{\Delta}}\Big\rangle\Big|\psi_0^{\vec{\Delta}}\Big\rangle+\Big|\psi_1^{\vec{\Delta}}\Big\rangle\Big|\psi_1^{\vec{\Delta}}\Big\rangle\Big)$. Geometrically, it's easier to see. The wavefunction of $|S_\Delta\rangle^{\otimes 2}$ has Gaussian peaks at locations $\big(n\sqrt{2\pi}, m\sqrt{2\pi}\big)^{\mathrm{T}}$ in the x,y plane. If you rotate this grid 45 degrees clockwise/anticlockwise, the Gaussian peaks are located on two overlapping grids at locations $\big(2n\sqrt{2\pi}, 2m\sqrt{2\pi}\big)^{\mathrm{T}}$ and $\big((2n+1)\sqrt{2\pi}, (2m+1)\sqrt{2\pi}\big)^{\mathrm{T}}$, which is exactly what the $|00\rangle+|11\rangle$ logical GKP state is. This is better illustrated with a plot. In

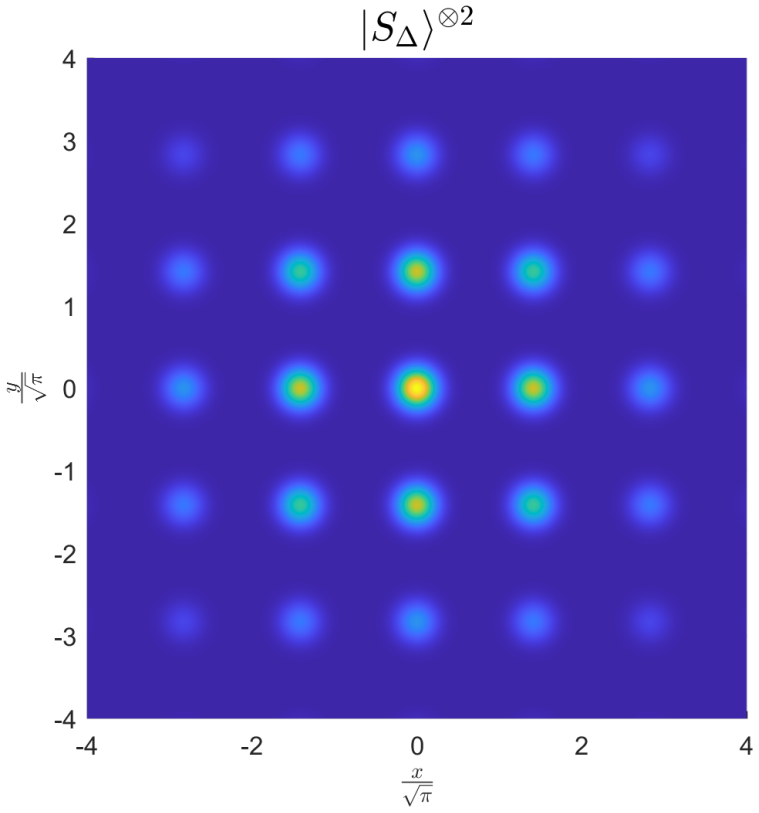

Figure 4.12: Contour plot of the two mode wavefunction of $|S_\Delta\rangle^{\otimes 2}$. The squeezing parameter was arbitrarily chosen to be $\Delta = 0.3$ here.

figure 4.12, we have a contour plot of the q-quadrature wavefunction of $|S_{0.3}\rangle^{\otimes 2}$. An application of a 50:50 beamsplitter rotates the two mode wavefunction by 45 degrees as illustrated by the

top plot in figure 4.14. The middle and bottom plot in figure 4.14, we have the plots $\left|\psi_0^\Delta\right\rangle^{\otimes 2}/\sqrt{2}$ and $\left|\psi_1^\Delta\right\rangle^{\otimes 2}/\sqrt{2}$. One can see that if we superimpose the plots of $\left|\psi_0^\Delta\right\rangle^{\otimes 2}/\sqrt{2}$ and $\left|\psi_1^\Delta\right\rangle^{\otimes 2}/\sqrt{2}$ we have the rotated $\left|S_\Delta\right\rangle^{\otimes 2}$ grid. The other approach to generating Bell states involves using the CNOT gate on $\left|+_{\mathrm{L}}\right\rangle \otimes \left|0_{\mathrm{L}}\right\rangle$. The CV CNOT gates is given by $\hat{C}_X = e^{-i\hat{q}_1 \otimes \hat{p}_2}$ [66]. If we apply $\hat{C}_X$ on $\left|\psi_+^\Delta\right\rangle \otimes \left|\psi_0^\Delta\right\rangle$ we have a wavefunction of:

$$\begin{aligned} e^{-i\hat{q}_1 \otimes \hat{p}_2} \left|\psi_+^\Delta\right\rangle \otimes \left|\psi_0^\Delta\right\rangle &= \int_{x,y} dx\ dy\ \psi_+^\Delta(x)\psi_0^\Delta(y) \left|x, y\right\rangle_q \\ &= \int_{x,y} dx\ dy\ e^{-ix\hat{p}_2}\psi_+^\Delta(x)\psi_0^\Delta(y) \left|x, y\right\rangle_q \end{aligned} \tag{4.122}$$

the operator $e^{-ix\hat{p}_2}$ is just a q-quadrature displacement on the second mode by x:

$$e^{-i\hat{q}_1 \otimes \hat{p}_2} \left|\psi_+^\Delta\right\rangle \otimes \left|\psi_0^\Delta\right\rangle = \int_{x,y} dx\ dy\ \psi_+^\Delta(x)\psi_0^\Delta(y-x) \left|x, y\right\rangle_q \ . \tag{4.123}$$

Hence, the original wavefunction transformed according to $\psi_+^\Delta(x)\psi_0^\Delta(y) \to \psi_+^\Delta(x)\psi_0^\Delta(y-x)$ after the application of $\hat{C}_X$. This makes sense because, the CNOT's purpose is to coupled the two wavefunctions $\psi_+^\Delta(x)$ and $\psi_0^\Delta(y)$.

Now, the function $\psi_+^\Delta(x)\psi_0^\Delta(y-x)$ as shown in figure 4.13 exhibits shearing in each Gaussian peak. Each Gaussian peak is centered at the correct location, but is extremely distorted. This effect is non-negligible in states with non-zero Δ. Which implies

$$\hat{C}_X \left|\psi_+^\Delta\right\rangle \otimes \left|\psi_0^\Delta\right\rangle \neq \frac{\left|\psi_0^\Delta\right\rangle \otimes \left|\psi_0^\Delta\right\rangle + \left|\psi_1^\Delta\right\rangle \otimes \left|\psi_1^\Delta\right\rangle}{\sqrt{2}} \ , \text{ if } \Delta \neq 0 \ . \tag{4.124}$$

The beamsplitter method preserves and creates exact GKP Bell states for all Δ. The beamsplitter method is a better way of generating GKP Bell states, because the continuous variables CNOT gate introduces additional errors.

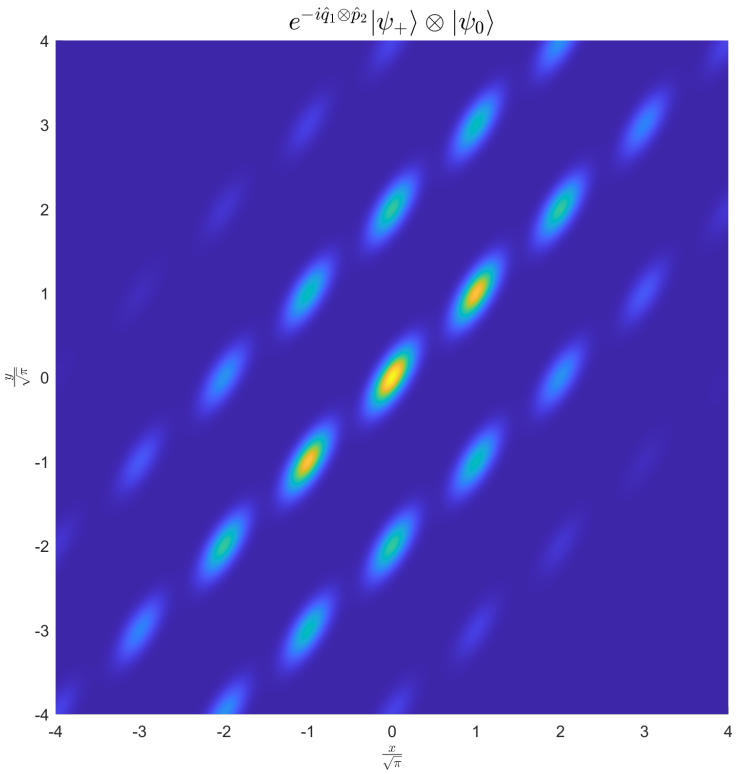

Figure 4.13: The q-quadrature two mode wavefunction of $\hat{C}_X \left|\psi_+^\Delta\right\rangle \otimes \left|\psi_0^\Delta\right\rangle$, with $\Delta = 0.3$.

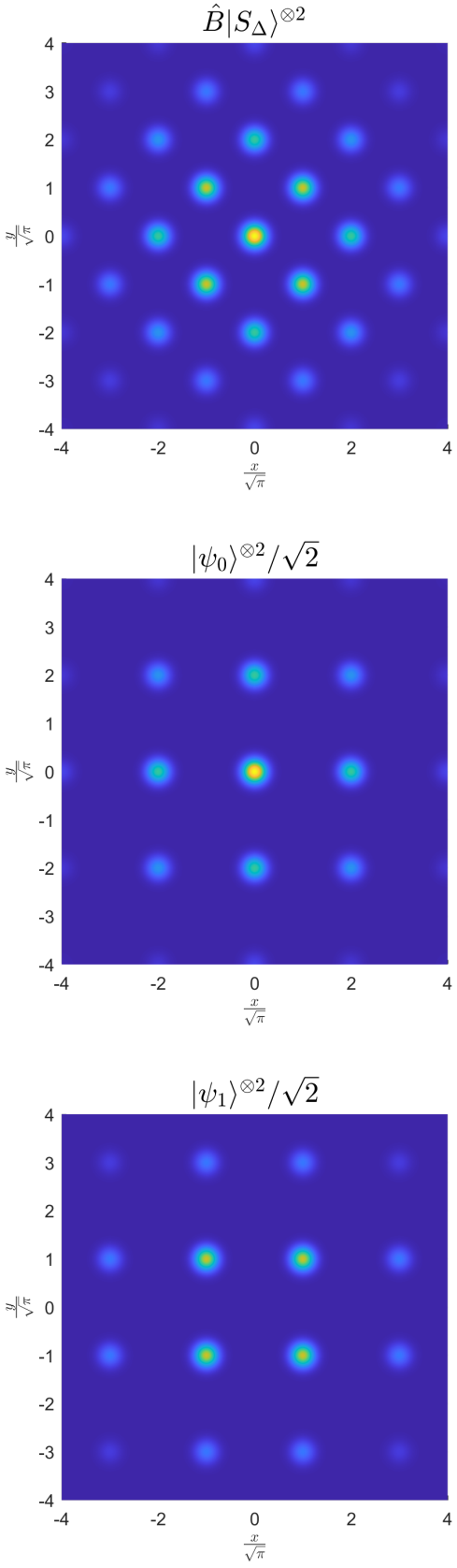

Figure 4.14: Contour plots of and application of a 50:50 beamspliter to $|S_\Delta\rangle^{\otimes 2}$, $\left|\psi_0^\Delta\right\rangle^{\otimes 2}/\sqrt{2}$ and $\left|\psi_1^\Delta\right\rangle^{\otimes 2}/\sqrt{2}$ respectively from top to bottom. The squeezing parameter was arbitrarily chosen to be $\Delta = 0.3$ here.

4.9 Summary

We have studied the grid sensor state, first proposed as a quantum state to infer small displacements in phase space in a bosonic mode. We have showed that grid sensor state has certain level of error resistance to the Gaussian random displacement channel, studied its Fock state amplitudes explicitly, quantitatively bounded the difficulty of state generation, computed the quantum Fisher information matrix explicitly. We also showed that the gird sensor state minimises the trace of the inverse quantum Fisher information matrix for the displacement detection problem in q- and p-quadrature simultaneously, but the Helstrom bound is not attainable. Despite the huge cost of generation experimentally and numerically to study due to its complicated Fock space and phase space state amplitudes structure, it is important to note that because of these qualities, it's a good motivator for the use of grid like states for error correction of errors in phase space because it would often require quite drastically large errors to destroy the grid like structure in phase space entirely.

Chapter 5

Memory assisted Gottesman-Kitaev-Preskill decoder

5.1 Introduction

Gottesman, Kitaev and Preskill published a paper in 2001 [35] using CV quantum mechanics to encode a qubit inside a bosonic mode. The GKP code is a stabilizer code [63], but the codeword wavefunctions are Dirac combs and they are only orthogonal when the energies of the states diverge. GKP also supplied a scheme to regularise the codewords, by replacing the Dirac combs with finite width Gaussians and an overall envelope to suppress the wavefunction at $\pm\infty$. They also supplied an error syndrome extraction scheme based on the CV stabilizer generalisations of the Steane circuits [107] to error correct the GKP states. A few years later, Glancy and Knill (GK) proposed a different optical implementation for error correcting the GKP states based on the geometry of the GKP states [6]. Additionally, Vasconcelos, Sanz, and Glancy proposed an all optical GKP state generation method by using many cat states [108] as inputs. In recent years, Albert et al. [68] showed that the GKP code provides the best performance compared to other bosonic codes if no error occurred during the recovery in light of a Gaussian random displacement error channel. This error channel is the pre-amplified amplitude damping channel. Since the amplitude damping channel is the dominant source

of error in optics in general, this suggests that the GKP code might be a good candidate for optical quantum computing. However, the resource trade-off vs code performance of a GKP code compared to a cat code is not well understood—it is possible that consuming many cat states to generate few GKP states is only beneficial in certain energy and error regimes. Although all the analysis revolves around the Gaussian random displacement channel, this error channel is a pre-amplified amplitude damping channel and the amplification can be interpreted as a step in the error correction. Hence, we can argue that the GKP code is well suited to the amplitude damping channel as well.

In this chapter, we present a new memory [1] decoder for the GKP code undergoing Gaussian random displacement errors, based on the Glancy and Knill error recovery scheme and Bayesian estimation. In particular, we extend the scheme to enable enhanced error estimation using multiple syndrome extractions, enabling improved error supression which we show to be useful in extending the lifetime of states with a mean number of photons as low as ten. We find that many rounds of syndrome extraction without active corrective displacement causes the qubit to drift in phase space by at most approximately $2\sqrt{\pi}$ in each quadrature. Since this bounded drift is finite, a corrective displacement can be used to correct for this drift at the end of the decoding stage. Additionally, we recompile the syndrome extraction circuit in an experimentally friendly way, such that squeezing need only be applied to auxiliary states which can be prepared offline.

5.2 Syndrome Extractions

The GKP syndrome extraction scheme of Glancy and Knill [6] can be broken down into two sequential circuits: q-SE and p-SE, which extract the error syndromes in the q- and p-quadrature respectively (see Fig. 5.1).

We begin our analysis with an arbitrary input qubit wavefunction $Q^{\vec{\Delta}}(x) = \alpha\psi_0^{\vec{\Delta}}(x) + \beta\psi_1^{\vec{\Delta}}(x)$ that has undergone an unknown displacement error (u, v)

[1] The word 'memory' refers to the use of classical memory to store data, which will then be used to assist the decoding of quantum information.

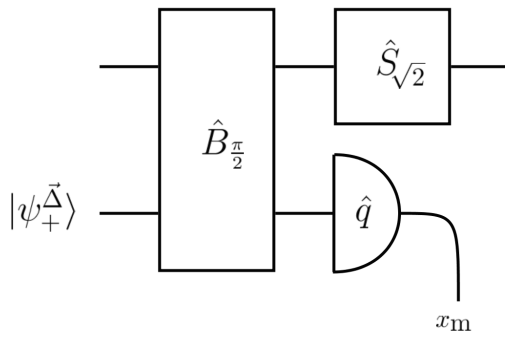

Figure 5.1: The q-quadrature error-syndrome extraction circuit (q-SE), as proposed by Glancy and Knill [6]. The GKP qubit and an auxiliary state are input in the top and bottom modes respectively. Following beamsplitting and squeezing operations, the error syndrome x_{m} is generated by a q-quadrature measurement on the auxiliary mode.

$$Q^{\vec{\Delta}}(x) \xrightarrow[(u,v)]{\text{error}} \mathrm{e}^{ivx} Q^{\vec{\Delta}}(x-u) \ . \tag{5.1}$$

This corrupted qubit is input into the top mode of the q-SE circuit, while an auxiliary GKP state $\left|\psi_+^{\vec{\Delta}}\right\rangle \propto \left|\psi_0^{\vec{\Delta}}\right\rangle + \left|\psi_1^{\vec{\Delta}}\right\rangle$ is input into the bottom mode. The action of the q-SE circuit can be visualised in terms of the two-mode q-quadrature wavefunction. The beamsplitter $\hat{B}_{\frac{\pi}{2}}$ causes an anticlockwise rotation by 45° in the joint quadrature space, and the subsequent squeezer $\hat{S}_{\sqrt{2}}$ scales the top-mode quadrature by $\sqrt{2}$. The error syndrome is then generated by a q-quadrature measurement of the auxiliary mode.

The p-SE circuit proceeds similarly, although there are subtle differences beyond a change of variables $q \to p$, and squeezing in the conjugate direction ($\hat{S}_{\sqrt{2}} \to \hat{S}^\dagger_{\sqrt{2}}$). Indeed, we must also change the auxiliary state $\left|\psi_+^{\vec{\Delta}}\right\rangle \to \left|\psi_0^{\vec{\Delta}'}\right\rangle$ where $\vec{\Delta}' = (\Delta/\sqrt{2}, \kappa\sqrt{2})$—a departure from the proposal of Glancy and Knill, which we found necessary for sequential q-SE and p-SE circuits to be applied to approximate GKP states (see figure 5.2).

5.3 Single-step decoding problem

Section 5.3 to the end of this chapter consists of my own work.

We begin with a graphical illustration with a sydrome extraction step. We define an error shift in the q and p quadrature as (u, v). For example, in the q-SE stage, take an error free $(u, v = 0)$

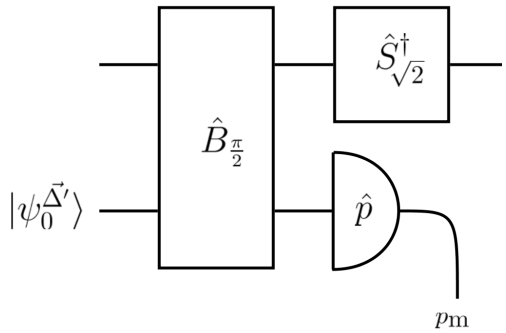

Figure 5.2: The p-quadrature error-syndrome extraction circuit (p-SE), as proposed by Glancy and Knill [6]. The GKP qubit and an auxiliary state are input in the top and bottom modes respectively. Following beamsplitting and anti-squeezing operations, the error syndrome p_{m} is generated by a p-quadrature measurement on the auxiliary mode.

input state of $\psi_{-}^{(\Delta,\kappa)}(x)$ multiplied with its fixed resources state $\psi_{+}^{(\Delta,\kappa)}(y)$ (with $\Delta = 0.14 = \kappa$). The two mode wavefunction is plotted in figure 5.3a. The beam-splitter rotates the two mode wavefunction 45 degrees counter clockwise as shown in figure 5.3b. The squeezing in the top mode will result in a wavefunction as shown in figure 5.3c. Notice that the y-axis in figure 5.3c is rescaled to $\frac{y}{(\sqrt{\frac{\pi}{2}})}$ and x-axis to $\frac{x}{(\frac{\sqrt{\pi}}{2})}$. The peaks will appear at every integer value of $\sqrt{\frac{\pi}{2}}$ in the y-axis and every integer value of $\frac{\sqrt{\pi}}{2}$ in the x-axis in figure 5.3c.

A measurement measurement conditioned displacement should be applied at the end of in the q-SE/p-SE to infer the shift that has occured in order to return the qubit wavefunction into its original position in phase-space before error and syndrome extraction. It can be pictured by taking a line of constant y-values ($y = x_{\mathrm{m}}$) out from plot in figure 5.3c and then asking, how much shift is required such that the peak locations are fixed at $2n\sqrt{\pi}$ for logical 0 and $(2n+1)\sqrt{\pi}$ for logical 1, $\forall n \in \mathbb{Z}$. Glancy and Knill (GK) [6] suggested an adaptive shift function of the form (for errors $|u|, |v| < \sqrt{\pi}/2$):

$$\begin{aligned} f_{\mathrm{GK}}(x_{\mathrm{m}}) = \frac{\sqrt{\pi}}{2}\mathrm{rem}\Big[\mathrm{round}\Big\{\frac{x_{\mathrm{m}}}{\sqrt{\pi/2}}\Big\}\ ,\ 4\Big] \\ - \mathrm{SAW}\Big(x_m, \frac{1}{\sqrt{2}}, \sqrt{\frac{\pi}{2}}\Big)\ , \end{aligned} \tag{5.2}$$

where rem$[z\ ,\ 4]$ is the remainder of z when divided by 4, round$\{z\}$ is the rounding function that includes positive and negative values in its range and domain and SAW is the function

defined in FIG. 5.9 [2]. The SAW part of f_{GK} is to deal with errors. Since we have no external errors we can ignore the sawtooth linear part of f_{GK}. We can define f_{step} as:

$$f_{\mathrm{step}}(x_{\mathrm{m}}) = \frac{\sqrt{\pi}}{2}\mathrm{rem}\Big[\mathrm{round}\Big\{\frac{x_{\mathrm{m}}}{\sqrt{\pi/2}}\Big\}\ ,\ 4\Big]\ . \tag{5.3}$$

We can look at how the peaks shift in figure 5.3d. Figure 5.3d is an enlarged version of figure 5.3c with quiver vectors overlaid on top of the peaks, showing the shift direction and magnitude. The red and blue nodes represents the logical 0 and 1 peaks respectively. The quiver plot shows the effect of shift function $f_{\mathrm{step}}(y)$. We can see that all the red and blue peaks return to even and odd integers of $\sqrt{\pi}$ effectively.

5.3.1 q-SE output wavefunction

Theorem 5.1. *The q-quadrature syndrome extraction circuit transforms the input approximate GKP state with width (Δ, κ) into superpositions of shifted GKP states with width $(\Delta/\sqrt{2}, \kappa\sqrt{2})$.*

Proof. The input state into the q-quadrature syndrome extraction circuit has the wavefunction:

$$\Phi(x,y) = \underbrace{\left(\sum_{\mu=0}^{1} a_\mu \psi_\mu^{(\Delta,\kappa)}(x)\right)}_{\text{qubit}} \cdot \underbrace{\psi_+^{(\Delta,\kappa)}(y)}_{\text{ancilla}}\ . \tag{5.4}$$

$$\begin{aligned}\Phi(x,y) \propto \sum_{\mu=0}^{1}\sum_{n,m\in\mathbb{Z}^2} & a_\mu N_\mu G_{\frac{1}{\kappa}}[(2n+\mu)\sqrt{\pi}] \\ & \cdot G_\Delta[x-(2n+\mu)\sqrt{\pi}] \\ & \cdot G_{\frac{1}{\kappa}}(m\sqrt{\pi})\, G_\Delta(y-m\sqrt{\pi})\end{aligned} \tag{5.5}$$

The beams-plitter transforms the variables $(x,y) \mapsto \left(\frac{x+y}{\sqrt{2}}, \frac{-x+y}{\sqrt{2}}\right)$ and the squeezing transforms this further: $\left(\frac{x+y}{\sqrt{2}}, \frac{-x+y}{\sqrt{2}}\right) \mapsto \left(x+\frac{y}{\sqrt{2}}, -x+\frac{y}{\sqrt{2}}\right)$ and finally the measurement of the sets mode

[2] The SAW function has a Fourier series function of $\mathrm{SAW}(x,a,b) = -\frac{ab}{2\pi}\ln(e^{-i\pi(2x/b-1)})$ defined in its standard form [109]

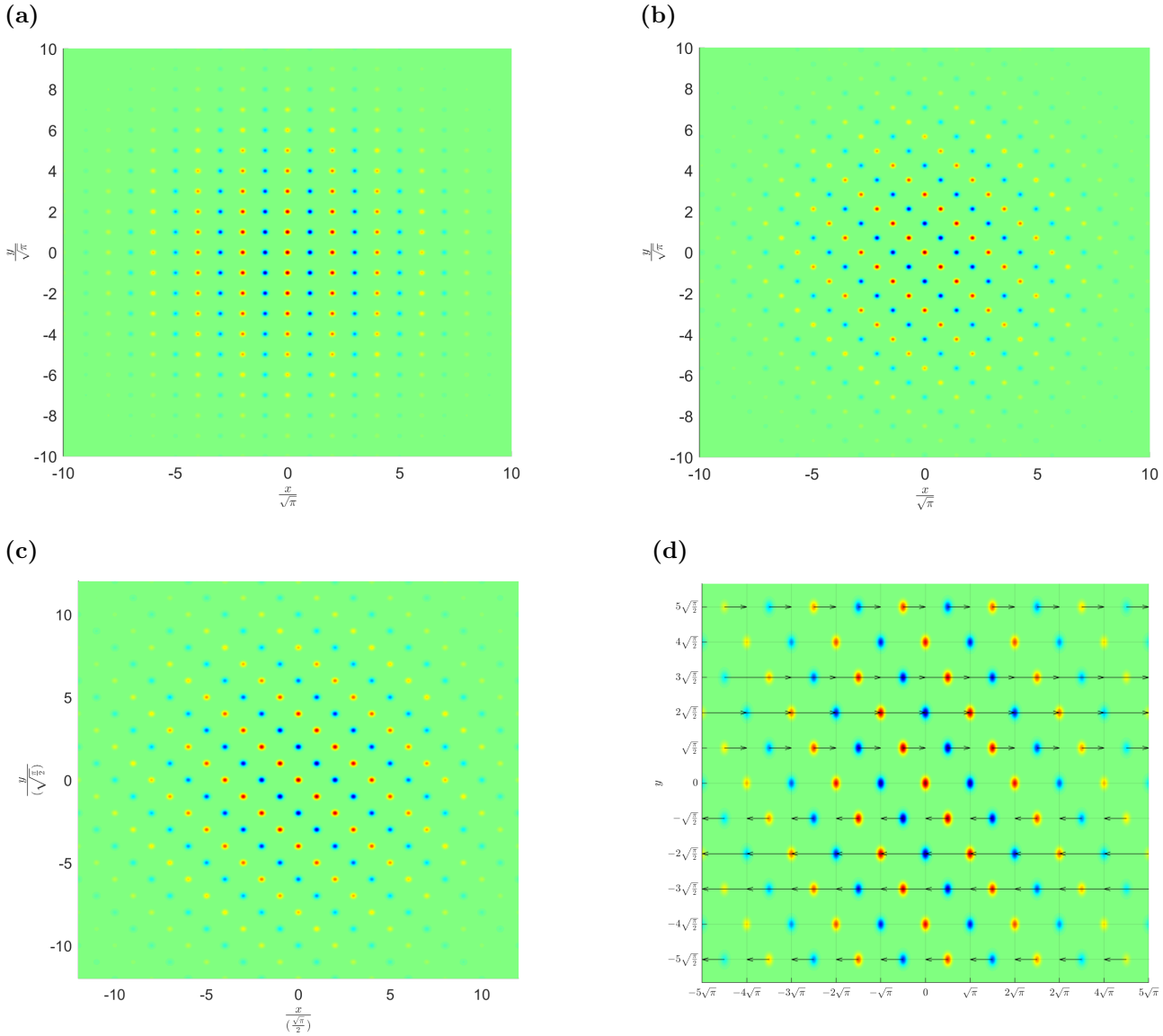

Figure 5.3: a) This is the two mode wavefunction of $\psi_{-}^{(\Delta,\kappa)}(x)\psi_{+}^{(\Delta,\kappa)}(y)$ in the joint qubit-resource q quadrature basis $|x\rangle_q \otimes |y\rangle_q$ with $\Delta = 0.14 = \kappa$. b) This is the two mode wavefunction of $\psi_{-}^{(\Delta,\kappa)}(x)\psi_{+}^{(\Delta,\kappa)}(y)$ rotated 45 degrees counter clockwise after the action of a beam-splitter. c) This is the two mode wavefunction of $\psi_{-}^{(\Delta,\kappa)}(x)\psi_{+}^{(\Delta,\kappa)}(y)$ rotated 45 degrees counter clockwise after the action of a beam-splitter and the squeezing operation in the x mode. d) The black quiver arrow overlay on top shows the effect of an x shift of $x \to x - f_{\text{step}}(y)$ on the two mode wavefunction before shifting.

$y = x_{\text{m}}$, the measurement results. All in all, prior to the conditional shift, the aggregate transformation of the beam-splitter, squeezing and measurement outcome at x_{m} results in the change of variables in the wavefunction from: $(x, y) \to (x + \frac{x_m}{\sqrt{2}}, -x + \frac{x_m}{\sqrt{2}})$.

The resulting wavefunction will now be (up to global normalisation constant):

$$\begin{aligned}\sum_{\mu=0}^{1}\sum_{n,m\in\mathbb{Z}^2} & a_\mu N_\mu G_{\frac{1}{\kappa}}[(2n+\mu)\sqrt{\pi}] \\ & \cdot G_\Delta[x+\frac{x_m}{\sqrt{2}}-(2n+\mu)\sqrt{\pi}] \\ & \cdot G_{\frac{1}{\kappa}}(m\sqrt{\pi})\cdot G_\Delta(-x+\frac{x_m}{\sqrt{2}}-m\sqrt{\pi})\end{aligned} \tag{5.6}$$

Regrouping the Gaussian functions with the same width and then competing the square up in the exponent, i.e. complete the square of the exponents of $G_{\frac{1}{\kappa}}[(2n+\mu)\sqrt{\pi}]\cdot G_{\frac{1}{\kappa}}(m\sqrt{\pi})$ and $G_\Delta(-x+\frac{x_m}{\sqrt{2}}-m\sqrt{\pi})\cdot G_\Delta[x+\frac{x_m}{\sqrt{2}}-(2n+\mu)\sqrt{\pi}]$ separately, this implies,

$$\begin{aligned}\sum_{\mu=0}^{1}\sum_{n,m\in\mathbb{Z}^2} & a_\mu N_\mu G_{\frac{1}{\sqrt{2}\kappa}}\Big(\frac{(2n+m+\mu)\sqrt{\pi}}{2}\Big) \\ & \cdot G_{\frac{\Delta}{\sqrt{2}}}\Big(x-\frac{(2n+m+\mu)\sqrt{\pi}}{2}\Big) \\ & \cdot G_{\frac{1}{\sqrt{2}\kappa}}\Big(\frac{(2n-m+\mu)\sqrt{\pi}}{2}\Big) \\ & \cdot G_{\frac{\Delta}{\sqrt{2}}}\Big(-x_m-\frac{(2n-m+\mu)\sqrt{\pi}}{2}\Big)\end{aligned} \tag{5.7}$$

The natural indices in this sum are $2n+m$ and $2n-m$. We want to decouple the n and m indices so that the double sum factors out into a product of single sums. If we make the following re-indexing, $2n+m=4j+c$ and $2n-m=4l-c$, where $j,l\in\mathbb{Z}^2$ and $c\in\{-1,0,1,2\}$, then we can trade the infinte $(n,m)\in\mathbb{Z}^2$ coupled double sum for a decoupled triple sum over $c,j,l\in\{-1,0,1,2\},\mathbb{Z}^2$, this implies:

$$\begin{aligned}&\sum_{\mu,c} a_\mu N_\mu \\ &\cdot\Big[\sum_{j\in\mathbb{Z}} G_{\frac{1}{\sqrt{2}\kappa}}\Big((2j+\frac{c+\mu}{2})\sqrt{\pi}\Big)G_{\frac{\Delta}{\sqrt{2}}}\Big(x-(2j+\frac{c+\mu}{2})\sqrt{\pi}\Big)\Big] \\ &\cdot\Big[\sum_{l\in\mathbb{Z}} G_{\frac{1}{\sqrt{2}\kappa}}\Big((2l+\frac{\mu-c}{2})\sqrt{\pi}\Big)G_{\frac{\Delta}{\sqrt{2}}}\Big(x_m+(2l+\frac{-c+\mu}{2})\sqrt{\pi}\Big)\Big]\end{aligned} \tag{5.8}$$

Now, we have a product of two separate infinite sums. before we proceed, we need to define the $\pm1/2$ 'logical' wavefunctions. The possible non-Pauli errors of a one step q-SE can be expressed

in terms of two possible wave functions $\psi_{1/2}^{(\Delta,\kappa)}(z)$ and $\psi_{-1/2}^{(\Delta,\kappa)}(z)$:

$$\psi_{\pm 1/2}^{(\Delta,\kappa)}(z) = N_{\pm\frac{1}{2}} \sum_{s\in\mathbb{Z}} e^{-\frac{\kappa^2}{2}((2s\pm 1/2)\sqrt{\pi})^2} e^{\frac{-[z-((2s\pm 1/2)\sqrt{\pi})]^2}{2\Delta^2}}. \tag{5.9}$$

Next, we can expand the wavefunction in c and μ, resulting in 4 terms which are superpositions of $\psi_{\pm 1/2}^{(\frac{\Delta}{\sqrt{2}},\kappa\sqrt{2})}(x), \psi_0^{(\frac{\Delta}{\sqrt{2}},\kappa\sqrt{2})}(x)$ and $\psi_1^{(\frac{\Delta}{\sqrt{2}},\kappa\sqrt{2})}(x)$. Let's name these terms $\{T_i\}$, so that $\Phi_{\text{before shift}}(x) \propto \sum_i T_i$. In the limit where the normalization constants are approximately equal.

$$T_0 = \psi_0^{(\frac{\Delta}{\sqrt{2}},\kappa\sqrt{2})}\Big(\frac{x_{\mathrm{m}}}{\sqrt{2}}\Big) \cdot \Big(a_0\psi_0^{(\frac{\Delta}{\sqrt{2}},\kappa\sqrt{2})}(x) + a_1\psi_1^{(\frac{\Delta}{\sqrt{2}},\kappa\sqrt{2})}(x)\Big) \tag{5.10}$$

$$T_1 = \psi_1^{(\frac{\Delta}{\sqrt{2}},\kappa\sqrt{2})}\Big(\frac{x_{\mathrm{m}}}{\sqrt{2}}\Big) \cdot \Big(a_1\psi_0^{(\frac{\Delta}{\sqrt{2}},\kappa\sqrt{2})}(x) + a_0\psi_1^{(\frac{\Delta}{\sqrt{2}},\kappa\sqrt{2})}(x)\Big) \tag{5.11}$$

$$T_{-1/2} = \psi_{-1/2}^{(\frac{\Delta}{\sqrt{2}},\kappa\sqrt{2})}\Big(\frac{x_{\mathrm{m}}}{\sqrt{2}}\Big) \cdot \Big(a_0\psi_{-1/2}^{(\frac{\Delta}{\sqrt{2}},\kappa\sqrt{2})}(x) + a_1\psi_{1/2}^{(\frac{\Delta}{\sqrt{2}},\kappa\sqrt{2})}(x)\Big) \tag{5.12}$$

$$T_{1/2} = \psi_{1/2}^{(\frac{\Delta}{\sqrt{2}},\kappa\sqrt{2})}\Big(\frac{x_{\mathrm{m}}}{\sqrt{2}}\Big) \cdot \Big(a_0\psi_{1/2}^{(\frac{\Delta}{\sqrt{2}},\kappa\sqrt{2})}(x) + a_1\psi_{-1/2}^{(\frac{\Delta}{\sqrt{2}},\kappa\sqrt{2})}(x)\Big) \tag{5.13}$$

□

Note that the all terms T_i have width change from $(\Delta,\kappa) \to (\Delta/\sqrt{2}, \kappa\sqrt{2})$. Also, T_0 corresponds to the codeword with no logical error and T_1 is a bit flip error of logical 0 to 1 and vice versa, which we refer to as a Pauli error. Finally, $T_{\pm 1/2}$ are shifted codewords of $\mp\sqrt{\pi}/2$ in the envelope and the locations of each individual Gaussian peaks, referred to as non-Pauli errors [3]. Each T_i term has coefficients based on $\psi_i^{(\frac{\Delta}{\sqrt{2}},\kappa\sqrt{2})}(x_{\mathrm{m}}/\sqrt{2})$, and for a likely measurement result x_{m}, one of these terms dominates.

It is useful to see how the q-SE procedure produces Pauli and non-Pauli error terms and also the width change from $(\Delta,\kappa) \to (\Delta/\sqrt{2}, \kappa\sqrt{2})$, no matter what the measurement conditional shift is. If the p-quadrature syndrome extraction procedure is performed on inputs states and

[3] an error that brings the qubits outside of the 2-level qubits logical codeword subspace, also known as a leakage error in [48]

ancilla of (Δ, κ), one could show that the output wavefunction will also consist of Pauli and non-Pauli terms, but the width of the output GKP state would be $(\Delta\sqrt{2}, \kappa/\sqrt{2})$, this looks like the inverse width change compared to the q-SE. This suggests, by performing the q-SE with (Δ, κ) width qubit and ancilla states and then the p-SE with $(\Delta/\sqrt{2}, \kappa/\sqrt{2})$ width ancilla states, one might be able to reverse this width change induced by the syndrome extraction. The effect of width reduction through syndrome extraction cannot be observed in the $\Delta = 0$ unphysical states calculation.

5.3.2 Justification for f_{step}

Looking at the equations T_i, we can see a reason for using the f_{step} terms in the shift function. The relative amplitudes between terms are: $\psi_i^{(\frac{\Delta}{\sqrt{2}}, \kappa\sqrt{2})}\left(\frac{x_{\text{m}}}{\sqrt{2}}\right)$. We can see that if one of the T_i is much bigger than the others, then that term dominates. For example, when $x_{\text{m}} \approx 2n\sqrt{2\pi}, n \in \mathbb{Z}$, then T_0 dominiates.

$x_{\text{m}} \approx$	term	shift
$(2n)\sqrt{2\pi}$	T_0	0
$(2n+\frac{1}{2})\sqrt{2\pi}$	$T_{-\frac{1}{2}}$	$\frac{\sqrt{\pi}}{2}$
$(2n+1)\sqrt{2\pi}$	T_1	$\sqrt{\pi}$
$(2n+\frac{3}{2})\sqrt{2\pi}$	$T_{\frac{1}{2}}$	$\frac{3\sqrt{\pi}}{2}$

Table 5.1: This table shows the dominant T_i term when x_{m} is close certain integers or half-integers of $\sqrt{2\pi}$ and also what amount to shift given a dominant term.

Let's have a look at what does the function $f_{\text{step}}(x_{\text{m}})$ do on the arguement $x_{\text{m}} = (2n+j)\sqrt{2\pi},\ j \in \{0, \frac{1}{2}, 1, \frac{3}{2}\}$.

$$\Rightarrow f_{\text{step}}((2n+j)\sqrt{2\pi}) = \tfrac{\sqrt{\pi}}{2}\text{rem}\Big[\text{round}\Big\{\tfrac{(2n+j)\sqrt{2\pi}}{\sqrt{\pi/2}}\Big\}\ ,\ 4\Big]$$

$$\Rightarrow f_{\text{step}}((4n+j)\sqrt{2\pi}) = \tfrac{\sqrt{\pi}}{2}\text{rem}\Big[\text{round}\Big\{4n+2j\Big\}\ ,\ 4\Big]$$

$$\Rightarrow f_{\text{step}}((4n+j)\sqrt{2\pi}) = \tfrac{\sqrt{\pi}}{2}\text{rem}\Big[2j\ ,\ 4\Big]$$

For $j \in \{0, \frac{1}{2}, 1, \frac{3}{2}\}$, this gives you the exact amount to shift as stated in the table 5.1.

5.3.3 q-SE followed by p-SE with errors

Given an input state of $\psi_\alpha^{\Delta,\kappa}(x)$, undergoing an error shift in phase space by u, v in the q, p quadratures:

$$\psi_\alpha^{\Delta,\kappa}(x) \xrightarrow[(u,v)]{\text{error}} \mathrm{e}^{ivx}\psi_\alpha^{\Delta,\kappa}(x-u) \ , \tag{5.14}$$

by carrying out the syndrome extraction procedures, the output state has an exact decomposition in terms of Pauli/non-Pauli errors and has the same width as the input state (Δ, κ).

Definition 5.1. *The Fourier transform wavefunction of an arbitrarily shifted GKP state* ($\alpha \in \mathbb{R}^+$) *is:*

$$\tilde{\psi}_\alpha^{\Delta,\kappa}(p) = \mathcal{F}_{x\to p}\{\psi_\alpha^{\Delta,\kappa}(x)\} \tag{5.15}$$

The output wavefunction of the combined q-SE and p-SE is:

$$\Psi_{\text{out}}(x,u,v) \propto \mathrm{e}^{i\left(\frac{v}{2}+p_s\right)x} \sum_{\beta\in\{-\frac{1}{2},0,\frac{1}{2},1\}} L_\beta(x,u,v) \tag{5.16}$$

$$\begin{aligned} L_0 = \psi_0^{\vec{\Delta}'}\Big(\frac{x_{\text{m}}}{\sqrt{2}}-\frac{u}{2}\Big)\Big[a_0\tilde{\psi}_0^{\vec{\Delta}}\Big(\frac{p_m}{\sqrt{2}}-\frac{v}{2}\Big)\psi_0^{\vec{\Delta}}\Big(\frac{u}{2}-(x-x_s)\Big) \\ +a_1\tilde{\psi}_1^{\vec{\Delta}}\Big(\frac{p_m}{\sqrt{2}}-\frac{v}{2}\Big)\psi_1^{\vec{\Delta}}\Big(\frac{u}{2}-(x-x_s)\Big)\Big] \end{aligned} \tag{5.17}$$

$$\begin{aligned} L_1 = \psi_1^{\vec{\Delta}'}\Big(\frac{x_{\text{m}}}{\sqrt{2}}-\frac{u}{2}\Big)\Big[a_0\tilde{\psi}_1^{\vec{\Delta}}\Big(\frac{p_m}{\sqrt{2}}-\frac{v}{2}\Big)\psi_1^{\vec{\Delta}}\Big(\frac{u}{2}-(x-x_s)\Big) \\ +a_1\tilde{\psi}_0^{\vec{\Delta}}\Big(\frac{p_m}{\sqrt{2}}-\frac{v}{2}\Big)\psi_0^{\vec{\Delta}}\Big(\frac{u}{2}-(x-x_s)\Big)\Big] \end{aligned} \tag{5.18}$$

$$\begin{aligned} L_{\frac{1}{2}} = \psi_{\frac{1}{2}}^{\vec{\Delta}'}\Big(\frac{x_{\text{m}}}{\sqrt{2}}-\frac{u}{2}\Big)\Big[a_0\tilde{\psi}_{-\frac{1}{2}}^{\vec{\Delta}}\Big(\frac{p_m}{\sqrt{2}}-\frac{v}{2}\Big)\psi_{-\frac{1}{2}}^{\vec{\Delta}}\Big(\frac{u}{2}-(x-x_s)\Big) \\ +a_1\tilde{\psi}_{\frac{1}{2}}^{\vec{\Delta}}\Big(\frac{p_m}{\sqrt{2}}-\frac{v}{2}\Big)\psi_{\frac{1}{2}}^{\vec{\Delta}}\Big(\frac{u}{2}-(x-x_s)\Big)\Big] \end{aligned} \tag{5.19}$$

$$L_{-\frac{1}{2}} = \psi^{\vec{\Delta}'}_{-\frac{1}{2}}\Big(\frac{x_{\mathrm{m}}}{\sqrt{2}} - \frac{u}{2}\Big)\Big[a_0\tilde{\psi}^{\vec{\Delta}}_{\frac{1}{2}}\Big(\frac{p_m}{\sqrt{2}} - \frac{v}{2}\Big)\psi^{\vec{\Delta}}_{\frac{1}{2}}\Big(\frac{u}{2} - (x - x_s)\Big) + a_1\tilde{\psi}^{\vec{\Delta}}_{-\frac{1}{2}}\Big(\frac{p_m}{\sqrt{2}} - \frac{v}{2}\Big)\psi^{\vec{\Delta}}_{-\frac{1}{2}}\Big(\frac{u}{2} - (x - x_s)\Big)\Big] \tag{5.20}$$

$\vec{\Delta}' \equiv (\Delta', \kappa') \equiv (\frac{\Delta}{\sqrt{2}}, \kappa\sqrt{2})$ and $\vec{\Delta} \equiv (\Delta, \kappa)$.

We can see from the forms of the L_β, with errors (u, v) in phase space, it is more difficult to isolate the dominant L_β term. the relative amplitudes of L_β depends on $\frac{x_{\mathrm{m}}}{\sqrt{2}} - \frac{u}{2}$ and $\frac{p_{\mathrm{m}}}{\sqrt{2}} - \frac{v}{2}$. Hence, we need a way to estimate the probability distribution of the errors u, v given $x_{\mathrm{m}}, p_{\mathrm{m}}, \sigma_0$, namely $\mathbb{P}(u|x_{\mathrm{m}})$ and $\mathbb{P}(v|p_{\mathrm{m}})$.

5.3.4 Bayesian estimator for q-SE shift

We now seek an optimized estimator for the total displacement after a q-SE step and then p-SE. In particular by using knowledge of our error model, we derive an improvement upon the GK shift function in equation 5.2.

The probability distribution of measurement outcome x_{m} given error shift u can be approximated by:

$$\mathbb{P}(x_{\mathrm{m}}|u) \propto \psi_+^{(\Delta,\kappa)}(\sqrt{2}x_{\mathrm{m}} - u)\ . \tag{5.21}$$

Note that the probability distribution is proportional to a function that is functionally the same as a GKP wavefunction not the absolute square of it here. This equation is independent of the input qubit to the q-SE. We shall give the proof to equation 5.21 now.

Theorem 5.2. *The probability distribution of the measurement result x_m in the q-SE circuit given an initial arbitary shift u in the q-quadrature is*

$$\mathbb{P}(x_m|u) \propto \psi_+^{(\Delta,\kappa)}(\sqrt{2}x_m - u).$$

Proof. The probability distribution can be computed from $\sum_\alpha T_\alpha$, with T_α from equation 5.10

to 5.13, with $\alpha \in \{0, 1, -\frac{1}{2}, \frac{1}{2}\}$.

$$\mathbb{P}(x_{\mathrm{m}}|u) \propto \int_{x\in\mathbb{R}} \Big|\sum_{\alpha} T_\alpha\Big|^2 \, dx$$

For $\Delta \ll \frac{1}{\sqrt{\pi}}$, the GKP peak don't overlap sufficiently, hence a valid approximation is:

$$\int_{x\in\mathbb{R}} \Big|\sum_{\alpha} T_\alpha\Big|^2 \, dx \approx \int_{x\in\mathbb{R}} \sum_{\alpha} \Big|T_\alpha\Big|^2 \, dx \quad ,$$

ignoring all the cross terms in the sum. Since all the T_α terms can be written as a product of functions in x_{m} and x, i.e. $|T_\alpha|^2 = |A_\alpha(x_{\mathrm{m}})|^2 \cdot |B_\alpha(x)|^2$, the product function of $|B_\alpha(x)|^2$ integrates to 1. Note that, $A_\alpha(x_{\mathrm{m}}) = \psi_\alpha^{\vec{\Delta}'}\Big(\frac{x_{\mathrm{m}}}{\sqrt{2}} - \frac{u}{2}\Big)$.

$$\Rightarrow \mathbb{P}(x_{\mathrm{m}}|u) \propto \sum_{\alpha} \Big|\psi_\alpha^{\vec{\Delta}'}\Big(\frac{x_{\mathrm{m}}}{\sqrt{2}} - \frac{u}{2}\Big)\Big|^2 \underbrace{\int_{x\in\mathbb{R}} \Big|B_\alpha(x)\Big|^2 \, dx}_{=1}$$

With a bit of reindexing,

$$\Big|\psi^{\vec{\Delta}'}_{\alpha=\{0,1\}}\Big(\frac{x_{\mathrm{m}}}{\sqrt{2}} - \frac{u}{2}\Big)\Big|^2 = \psi_+^{\vec{\Delta}}(0)\psi_0^{\vec{\Delta}}\Big(\sqrt{2}x_{\mathrm{m}} - u\Big) \tag{5.22}$$

and

$$\Big|\psi^{\vec{\Delta}'}_{\alpha=\{\pm\frac{1}{2}\}}\Big(\frac{x_{\mathrm{m}}}{\sqrt{2}} - \frac{u}{2}\Big)\Big|^2 = \psi_+^{\vec{\Delta}}(0)\psi_1^{\vec{\Delta}}\Big(\sqrt{2}x_{\mathrm{m}} - u\Big) \; . \tag{5.23}$$

The non-Pauli terms gives the logical 1 component and the Pauli terms returns the logical 0 components.

$$\Rightarrow \mathbb{P}(x_{\mathrm{m}}|u) \propto 2\Big[\psi_0^{\vec{\Delta}}\Big(\sqrt{2}x_{\mathrm{m}} - u\Big) + \psi_1^{\vec{\Delta}}\Big(\sqrt{2}x_{\mathrm{m}} - u\Big)\Big]$$

$$\Rightarrow \mathbb{P}(x_{\mathrm{m}}|u) \propto \psi_+^{\vec{\Delta}}\Big(\sqrt{2}x_{\mathrm{m}} - u\Big)$$

□

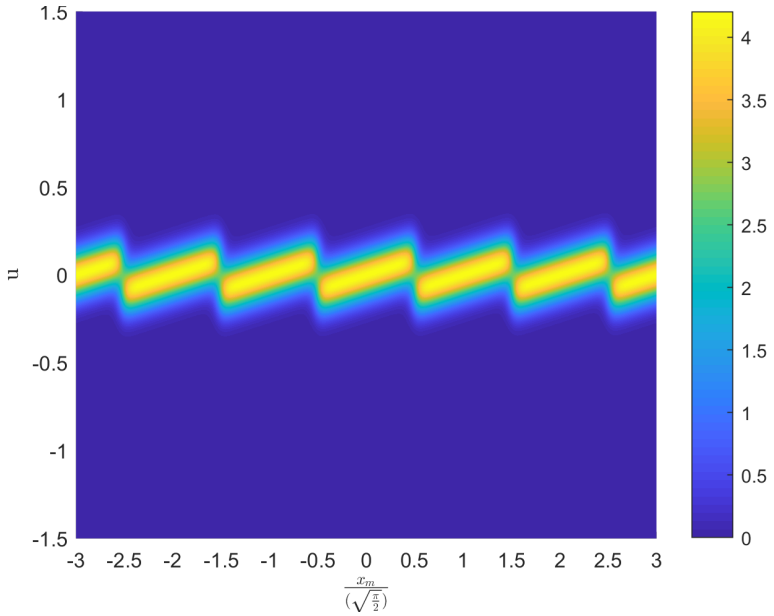

Figure 5.4: The false colour plot (z axis in arbitary units) of the conditional probability distribution $\mathbb{P}(u|x_{\mathrm{m}})$ with $\sigma_0 = 0.1$ and $\Delta = 0.3$. The slope of the repeating rod like structures will steepen as σ_0 increases or Δ decreases.

Using the marginal rule, one can compute

$$\mathbb{P}(x_{\mathrm{m}}) = \int_{u=-\infty}^{\infty} \mathrm{d}u \; \mathbb{P}(x_{\mathrm{m}}|u)\mathbb{P}(u) = \psi_{+}^{(\sqrt{\Delta^2+\sigma_0^2},\kappa)}(\sqrt{2}x_{\mathrm{m}}) \; , \tag{5.24}$$

where $\mathbb{P}(u) \propto \mathrm{e}^{-\frac{(u)^2}{2\sigma_0^2}}$. Using Bayes' theorem,

$$\mathbb{P}(u|x_{\mathrm{m}}) \propto \frac{\psi_{+}^{(\Delta,\kappa)}(\sqrt{2}x_{\mathrm{m}} - u)}{\psi_{+}^{(\sqrt{\Delta^2+\sigma_0^2},\kappa)}(\sqrt{2}x_{\mathrm{m}})} \; \mathrm{e}^{-\frac{u^2}{2\sigma_0^2}} \tag{5.25}$$

From the plot in figure 5.4, one can see why the GK shift has this structure of a sawtooth offset by a step function. The sawtooth part aims to counteract the effects of the shift u and the integer steps bit arise from the rotational structure of the QEC code.

We shall maximise the $\mathbb{P}(u|x_{\mathrm{m}})$ now:

$$\mathbb{P}(u|x_{\mathrm{m}}) \propto \psi_{+}^{(\Delta,\kappa)}(\sqrt{2}x_{\mathrm{m}} - u)G_{\sigma_0}(u) \; . \tag{5.26}$$

For a particular value of x_m and u, given u is small (see section 5.5.3 for error analysis for larger

values of u and its impact on overall qubit recovery fidelity),

$$\begin{aligned} \Rightarrow \max(\mathbb{P}(u|x_{\mathrm{m}})) \propto & G_{\Delta}\Big[\sqrt{2}x_{\mathrm{m}} - u - \sqrt{\pi}\mathrm{round}\Big(\frac{\sqrt{2}x_{\mathrm{m}}}{\sqrt{\pi}}\Big)\Big] \\ & \cdot G_{\sigma_0}(u) \ . \end{aligned} \tag{5.27}$$

Maximising the log of $\max(\mathbb{P}(u|x_{\mathrm{m}}))$ gives an estimator of u, we shall call the estimator: $\tilde{u}$.

$$\tilde{u} = \frac{\sigma_0^2}{\sigma_0^2 + \Delta^2}\Big[\sqrt{2}x_{\mathrm{m}} - \mathrm{round}\Big(\frac{\sqrt{2}x_{\mathrm{m}}}{\sqrt{\pi}}\Big)\Big] \ . \tag{5.28}$$

Now we have the sawtooth structure, shown in figure 5.4, extracted from maximising the conditional probability distribution.

Alternatively, if we expand the sums involved in $\mathbb{P}(u|x_{\mathrm{m}})$ and only concentrate on the central rod, we can extract the mean slope of the diagonal "rods" like figures in figure 5.4, which represents high probability regions of error given measurement result. This can be used to form a new shift function that adaptively changes depending on the parameters σ_0 and Δ to achieve a optimal code for our error model. The mean slope is:

$$S(\Delta, \sigma_0) = \frac{\sqrt{2}\sigma_0^2}{\sigma_0^2 + \Delta^2} \ . \tag{5.29}$$

For unphysical GKP states, $\frac{S(\Delta=0,\sigma_0)}{2} = \frac{1}{\sqrt{2}}$, which saturates the slope value of $\frac{1}{\sqrt{2}}$ provided by the striaght line in the GK shift. Also, the mean square error for the slope estimation is the width of the rods in figure 5.4. This works out to be:

$$\mathrm{MSE}[S(\Delta, \sigma_0)] = \frac{1}{\sqrt{\Delta^{-2} + \sigma_0^{-2}}} \tag{5.30}$$

To optimise the shift function more, when the rounding function outputs 3, take the output -1 instead. This will minimise the overall magnitude of the shift function and hence preserves the overall $1/\kappa$ width of the physical state more. With such a rounding function we shall call it round*. We define the BE shift function f_{BE} as:

$$f_{\mathrm{BE}}(x_{\mathrm{m}},\Delta,\sigma_0)=\overbrace{\frac{\sqrt{\pi}}{2}\mathrm{rem}^{*}\Big[\mathrm{round}\Big\{\frac{x_{\mathrm{m}}}{\sqrt{\pi/2}}\Big\}\ ,\ 4\Big]}^{\text{periodically increasing term}}\underbrace{-\mathrm{SAW}(x_{\mathrm{m}},\frac{S(\Delta,\sigma_0)}{2},\sqrt{\frac{\pi}{2}}\ )}_{\text{sawtooth term}}\ . \tag{5.31}$$

The sawtooth term in equation 5.31 aims to counteract the $\frac{u}{2}-x_s$ term in the argument of the L_β.

5.3.5 q-SE & p-SE combined Bayesian estimator shift

Theorem 5.3. *The probability distribution of the measurement results x_m, p_m after the q-SE followed by p-SE given an initial arbitary shift of u, v in the q,p quadrature is*

$$\mathbb{P}(x_m,p_m|u,v)\propto\psi_{+}^{(\Delta,\kappa)}(\sqrt{2}x_m-u)\cdot\psi_{+}^{(2\Delta,\kappa/2)}(\sqrt{2}p_m-v)\ . \tag{5.32}$$

Proof. Similar to the proof of theorem 5.5. We shall illustrate the sketch of the proof here. The probability distribution can be computed from $\sum_\alpha L_\beta$, with L_β from equation 5.17 to 5.20,

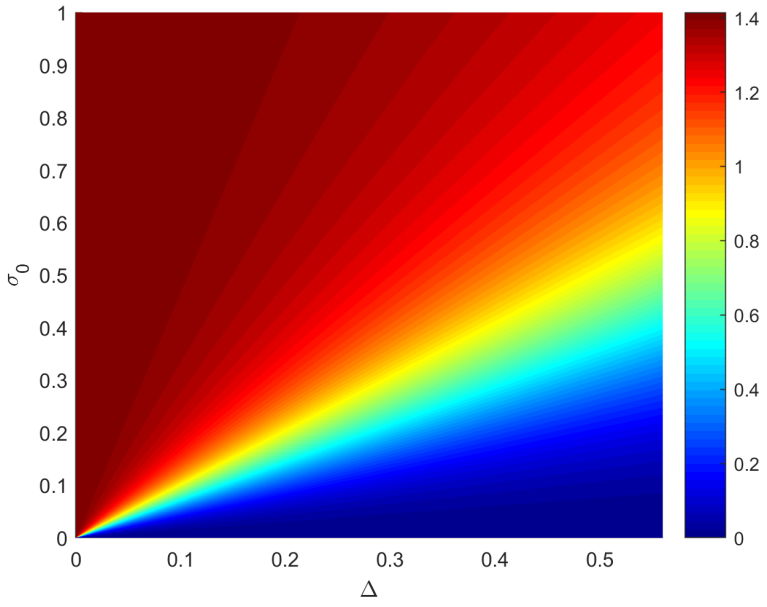

Figure 5.5: This is a false colour plot of $S(\Delta,\sigma_0)$ over all possible $\sigma_0\in[0,1]$ and $\Delta\in[0,\frac{1}{\sqrt{\pi}}\approx 0.56]$. At $\Delta=0$, for all values of σ_0, $S(\Delta,\sigma_0)\to\sqrt{2}\approx 1.414...$.

with $\beta \in \{0, 1, -\frac{1}{2}, \frac{1}{2}\}$.

$$\mathbb{P}(x_{\mathrm{m}}, p_{\mathrm{m}}|u, v) \propto \int_{x\in\mathbb{R}} \Big|\sum_{\beta} L_\beta\Big|^2 \, dx$$

Using the following approximation again for $\Delta \ll \frac{1}{\sqrt{\pi}}$:

$$\int_{x\in\mathbb{R}} \Big|\sum_{\beta} L_\beta\Big|^2 \, dx \approx \int_{x\in\mathbb{R}} \sum_{\beta} \Big|L_\beta\Big|^2 \, dx \quad ,$$

Since $\psi_0^{\vec{\Delta}}(z)$ and $\psi_1^{\vec{\Delta}}(z)$ are approximately orthogonal, we can ignore terms in the expansion of $\Big|L_\beta\Big|^2$ that involves $\psi_0^{\vec{\Delta}}(u/2-(x-x_s)) \cdot \psi_1^{\vec{\Delta}}(u/2-(x-x_s))$ as they integrate to approximated zero. Collecting terms, use the fact that $|a_0|^2 + |a_1|^2 = 1$ and the identities from equation 5.22 and 5.23, we can arrive at:

$$\begin{aligned}
&\mathbb{P}(x_{\mathrm{m}}, p_{\mathrm{m}}|u, v) \propto \\
&\psi_0^{(\Delta,\kappa)}(\sqrt{2}x_{\mathrm{m}} - u)\Big[\Big|\tilde{\psi}_0^{\vec{\Delta}}\Big(\frac{p_m}{\sqrt{2}} - \frac{v}{2}\Big)\Big|^2 + \Big|\tilde{\psi}_1^{\vec{\Delta}}\Big(\frac{p_m}{\sqrt{2}} - \frac{v}{2}\Big)\Big|^2\Big] \\
&+ \\
&\psi_1^{(\Delta,\kappa)}(\sqrt{2}x_{\mathrm{m}} - u)\Big[\Big|\tilde{\psi}_{\frac{1}{2}}^{\vec{\Delta}}\Big(\frac{p_m}{\sqrt{2}} - \frac{v}{2}\Big)\Big|^2 + \Big|\tilde{\psi}_{-\frac{1}{2}}^{\vec{\Delta}}\Big(\frac{p_m}{\sqrt{2}} - \frac{v}{2}\Big)\Big|^2\Big]
\end{aligned} \tag{5.33}$$

Notice that:

$$\begin{aligned}
&\Big|\tilde{\psi}_0^{\vec{\Delta}}\Big(\frac{p_m}{\sqrt{2}} - \frac{v}{2}\Big)\Big|^2 = \Big|\tilde{\psi}_1^{\vec{\Delta}}\Big(\frac{p_m}{\sqrt{2}} - \frac{v}{2}\Big)\Big|^2 \\
&= \Big|\tilde{\psi}_{\frac{1}{2}}^{\vec{\Delta}}\Big(\frac{p_m}{\sqrt{2}} - \frac{v}{2}\Big)\Big|^2 = \Big|\tilde{\psi}_{-\frac{1}{2}}^{\vec{\Delta}}\Big(\frac{p_m}{\sqrt{2}} - \frac{v}{2}\Big)\Big|^2
\end{aligned}$$

$\Rightarrow \mathbb{P}(x_{\mathrm{m}}, p_{\mathrm{m}}|u, v) \propto \psi_+^{(\Delta,\kappa)}(\sqrt{2}x_{\mathrm{m}} - u)\Big|\tilde{\psi}_0^{\vec{\Delta}}\Big(\frac{p_m}{\sqrt{2}} - \frac{v}{2}\Big)\Big|^2$.

With reindexing, $\Big|\tilde{\psi}_0^{\vec{\Delta}}\Big(\frac{p_m}{\sqrt{2}} - \frac{v}{2}\Big)\Big|^2 = \psi_+^{(2\Delta,\kappa/2)}(\sqrt{2}p_{\mathrm{m}} - v)$.

$$\Rightarrow \mathbb{P}(x_{\mathrm{m}}, p_{\mathrm{m}}|u, v) \propto \psi_+^{(\Delta,\kappa)}(\sqrt{2}x_{\mathrm{m}} - u) \cdot \psi_+^{(2\Delta,\kappa/2)}(\sqrt{2}p_{\mathrm{m}} - v)$$

□

Theorem 5.6 implies:

$$\mathbb{P}(x_{\mathrm{m}}, p_{\mathrm{m}}|u, v) = \mathbb{P}(x_{\mathrm{m}}|u) \cdot \mathbb{P}(p_{\mathrm{m}}|v) \ , \tag{5.34}$$

with,

$$\mathbb{P}(p_{\mathrm{m}}|v) = \psi_{+}^{(2\Delta,\kappa/2)}(\sqrt{2}p_{\mathrm{m}} - v) \tag{5.35}$$

$\mathbb{P}(p_{\mathrm{m}}|v)$ differs from $\mathbb{P}(x_{\mathrm{m}}|u)$ by the transformation of $\Delta \to 2\Delta, \kappa \to \kappa/2, x_{\mathrm{m}} \to p_{\mathrm{m}}$ and $u \to v$. Since u, v are both a Gaussian random variable with width σ_0 (because u, v represents the single error realisation of the random shift in light of the Gaussian random displacement channel), hence, we can quickly write down the optimal slope for the p-SE step by using the same shfting function as the q-SE stage but substituting $\Delta \to 2\Delta$.

5.4 Multi-step decoding problem

We aim to derive a Bayesian estimator for multiple steps (M steps) of Gaussian q- and p-quadratures shift errors (width σ_0) followed by GKP syndrome extraction under the assumption: $\sigma_0 \ll \Delta \ll 1$. This translates to looking at the behaviour of our estimator for small Gaussian errors with good GKP states. Our intuition of GKP states tells us that under small errors and SE, at least in the single shot evolution of the wavefunction, we only need to keep track of a reference point of the GKP wavefunction w.r.t the origin in phase space to perform the correction. We present another method of understanding details for a single round of syndrome extraction (SE) and error estimation. This involves tracking the additional terms obtains in the wavefunction via the syndrome extraction as displacements shifts. This will be extremely useful in the understanding of the multi-step syndrome extraction and decoding problem.

5.4.1 Overview of multi-step results [1]

Following sequential q-SE and p-SE circuits, the qubit has transformed according to

$$\mathrm{e}^{ivx}Q^{\vec{\Delta}}(x-u) \xrightarrow[\text{SE}]{\text{q-,p-}} \mathrm{e}^{i\theta(p_\mathrm{m},v)x}Q^{\vec{\Delta}}\big(x-\theta(x_\mathrm{m},u)\big) \tag{5.36}$$

with a high fidelity (see 5.5.3) when the displacement is small. Here, $\theta(x_\mathrm{m},u)$ is given by

$$\theta(x_\mathrm{m},u) = \frac{u}{2} - f^*_{\text{step}}(x_m) \tag{5.37}$$

where $f^*_{\text{step}}(x_m)$ is the modified modular division by 4 function defined in 5.7, and $\theta(p_\mathrm{m},v)$ is defined similarly. These quantities can be interpreted as the total displacement experienced by the qubit: an *unknown*, random part $\frac{u}{2}$ remaining from the error channel and a *known* part $f^*_{\text{step}}(x_m)$ introduced by the measurement.

While an error correcting procedure could involve estimation of the total displacement $\theta(x_m,u)$ and immediately applying a corrective displacement based on this estimate, we note that allowing an uncorrected qubit to undergo a further syndrome extraction process only results in another displaced version of the input qubit. With this in mind, our decoder uses measurement information from multiple rounds of errors and syndrome extraction without intermediate correction to estimate a single corrective displacement to apply. This memory-assisted approach is summarised in Fig. 5.6, alongside a contrasting memoryless approach which applies a correction after each syndrome extraction and then forgets about it.

We now proceed by extending our analysis from one round to multiple rounds of syndrome extraction. Say that after the h^{th} round of syndrome extraction we have histories of q-quadrature syndrome measurements $\vec{x}_\mathrm{m} = (x_\mathrm{m}^{(1)},\ldots,x_\mathrm{m}^{(h)})$ and displacement errors $\vec{u} = (u_1,\ldots,u_h)$, and similarly p-quadrature values $\vec{p}_\mathrm{m} = (p_\mathrm{m}^{(1)},\ldots,p_\mathrm{m}^{(h)})$ and $\vec{v} = (v_1,\ldots,v_h)$ for the p-quadrature. If each displacement error is small, then the input qubit is transformed according to

$$Q^{\vec{\Delta}}(x) \;\to\; \mathrm{e}^{i\theta_h(\vec{p}_\mathrm{m},\vec{v})x}Q^{\vec{\Delta}}\big(x-\theta_h(\vec{x}_\mathrm{m},\vec{u})\big). \tag{5.38}$$

with high fidelity (again, see 5.5.3). Focusing on the q-quadrature: the total shift in q is given by

$$\begin{aligned}\theta_h(\vec{x}_{\mathrm{m}}, \vec{u}) &= \sum_{j=1}^{h} \Big[\frac{u_j}{2^{h-j+1}}\Big] - \sum_{k=1}^{h} \Big[\frac{f^*_{\mathrm{step}}\big(\mathcal{X}^{(k)}_{\mathrm{m}}(\vec{x}_{\mathrm{m}})\big)}{2^{h-k}}\Big] \\ &= \theta^{\mathrm{err}}_h(\vec{u}) - \theta^{\mathrm{step}}_h(\vec{x}_{\mathrm{m}}) \ ,\end{aligned} \tag{5.39}$$

where $\mathcal{X}^{(k)}_{\mathrm{m}}$ can be interpreted as the measurement outcome $x^{(k)}_{\mathrm{m}}$ transformed to account for previous measurement-induced shifts, and is given explicitly by

$$\mathcal{X}^{(h)}_{\mathrm{m}}(\vec{x}_{\mathrm{m}}) = x^{(h)}_{\mathrm{m}} + \frac{1}{\sqrt{2}} \sum_{j=1}^{k-1} \Big[\frac{f^*_{\mathrm{step}}\big(\mathcal{X}^{(j)}_{\mathrm{m}}(\vec{x}_{\mathrm{m}})\big)}{2^{k-j-1}}\Big] \tag{5.40}$$

for $h > 1$, and $\mathcal{X}^{(1)}_{\mathrm{m}} = x^{(1)}_{\mathrm{m}}$. In analogy with the single round case above, we have an unknown contribution to the total displacement $\theta^{\mathrm{err}}_h(\vec{u})$ together with a known, measurement-induced contribution $\theta^{\mathrm{step}}_h(\vec{x}_{\mathrm{m}})$.

Without active corrective shifts at each round, the distance a GKP qubit drifts in phase space after h rounds is bounded above as: $\Big|\theta(\vec{x}_{\mathrm{m}}, \vec{u})\Big| < 2\sqrt{\pi}\ (1-2^{-h}) + |X|$, where $X \sim \mathcal{N}\Big(0, \sigma_0^2 \frac{(1-4^{-h})}{3}\Big)$ is a Gaussian random variable with mean 0 and variance $\sigma_0^2 \frac{(1-4^{-h})}{3}$ (see 5.5 for proof). It follows that the expected value for total displacement error in each quadrature after any number of syndrome extraction rounds is bounded above by approximately $2\sqrt{\pi}$.

In Fig. 5.6a, we identify a practical simplification to the combined q-SE, p-SE circuit that moves all squeezing operations offline onto auxiliary state preparation. To do so, we use a modified p-SE auxiliary state, $\hat{S}^{\dagger}_{\sqrt{2}} \Big|\psi_0^{\vec{\Delta}'}\Big\rangle$, and reinterpret the p-quadrature measurement ($p_{\mathrm{m}} \to \sqrt{2} p_{\mathrm{m}}$) (see 5.5.8 for proof).

5.4.2 Decoder (Bayesian estimation)

We now show how to use the q- and p-SE measurement outcomes to estimate the final displacements when the loss channel is well characterised (i.e. σ_0 is known). For convenience, we set

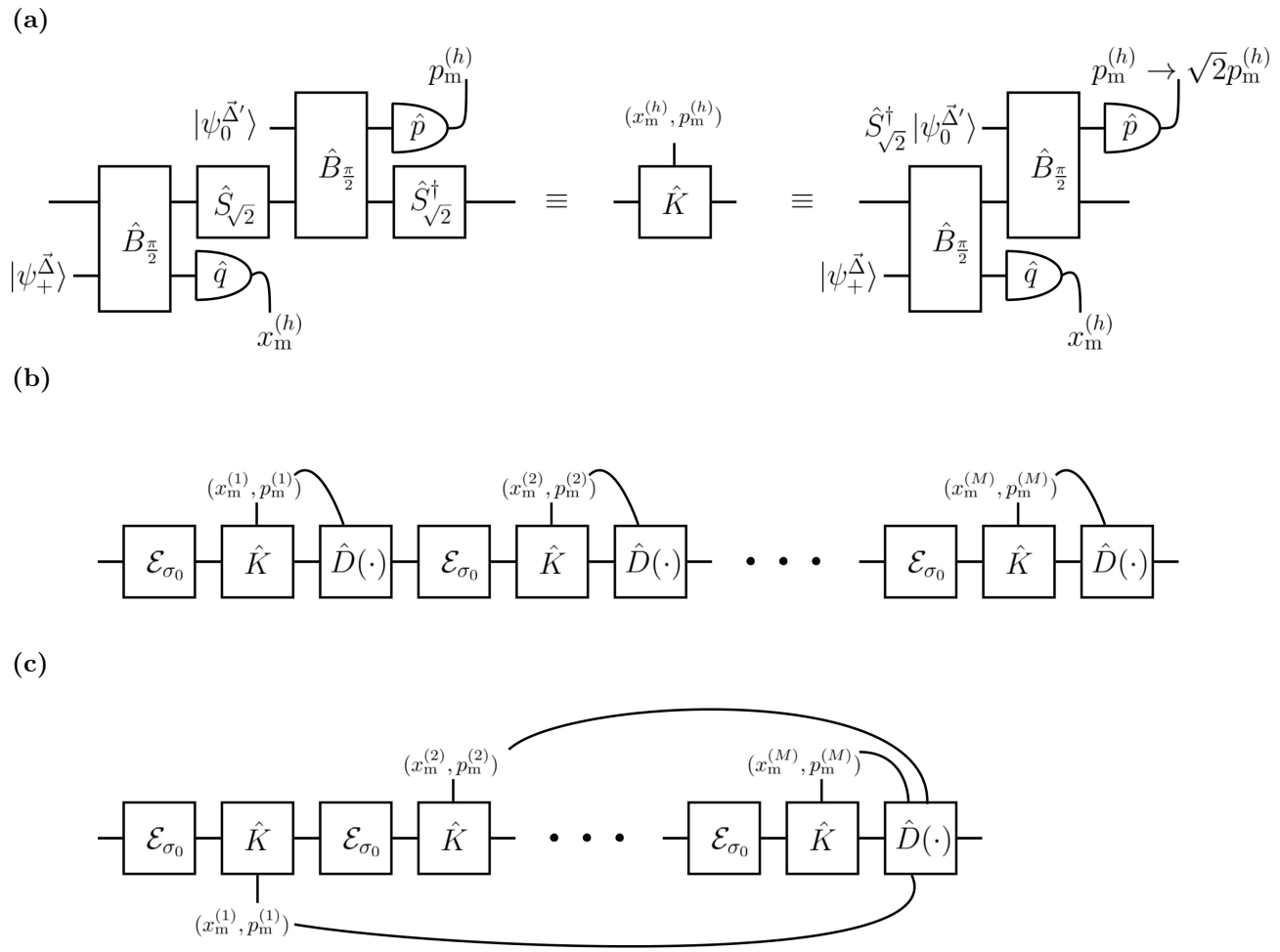

Figure 5.6: a) The standard q- and p-quadrature syndrome extraction circuits (left), which feature squeezing operations on the qubit mode, can be represented by a measurement dependent Kraus operator $\hat{K}$ (centre), and recompiled such that squeezing is applied to the p-auxiliary state, with a reinterpreted p-quadrature measurement (right). b) Memoryless error correction—syndrome measurement results are used to inform a corrective displacement at each round, and no information is carried forward to future rounds. c) Memory-assisted error correction—no active corrective shift is performed after each syndrome measurement. Instead, all the syndrome measurement results are used together to decode and perform a single corrective displacement after M rounds.

$\kappa = \Delta$ in this section, although it is straightforward to extend the results to the more general case.

In the case of a single round of q-SE and p-SE application, the probability of measuring x_{m} given a shift error u can be approximated as $\mathbb{P}(x_{\mathrm{m}}|u) \propto \psi_{+}^{\vec{\Delta}}(\sqrt{2}x_{\mathrm{m}} - u)$, which we note is independent of both v and p_m. By using a prior probability density function (PDF) corresponding to our characterised error channel and applying Bayes' theorem, we obtain a posterior PDF

$$\mathbb{P}(u|x_{\mathrm{m}}) \propto \psi_{+}^{\vec{\Delta}}(\sqrt{2}x_{\mathrm{m}} - u)\mathrm{e}^{-\frac{u^2}{2\sigma_0^2}}. \tag{5.41}$$

Assuming that $\vec{\Delta}$ and σ_0 are both small compared to $\sqrt{\pi}$, this posterior is well approximated by

$$\mathbb{P}(u|x_{\mathrm{m}}) \approx \mathcal{N}\left(\frac{\sqrt{2}\sigma_0^2 x_{\mathrm{m}} - \sqrt{\pi}\sigma_0^2\left\lfloor\frac{\sqrt{2}x_{\mathrm{m}}}{\sqrt{\pi}}\right\rceil}{\Delta^2 + \sigma_0^2}, \frac{\Delta^2\sigma_0^2}{\Delta^2 + \sigma_0^2}\right) \tag{5.42}$$

and we take our estimate $\tilde{u}$ of the shift error u to be the mean of this Gaussian. Explicitly,

$$\tilde{u} = \frac{\sqrt{2}\sigma_0^2 x_{\mathrm{m}} - \sqrt{\pi}\sigma_0^2\left\lfloor\frac{\sqrt{2}x_{\mathrm{m}}}{\sqrt{\pi}}\right\rceil}{\Delta^2 + \sigma_0^2}, \tag{5.43}$$

which is a good approximation of the minimum mean square error (MMSE) estimator for u. The estimate for the displacement required to counteract the acquired error is therefore $\theta(x_{\mathrm{m}}, \tilde{u})$, from combining equations (5.37) and (5.43).

The corresponding p-quadrature conditional probabilities can be obtained by substituting $(u, x_{\mathrm{m}}, \Delta) \to (v, p_{\mathrm{m}}, 2\Delta)$, where the asymmetry between the q- and p-quadrature originates from the differing widths of the auxiliary states.

For multiple rounds, the estimation of the cumulative unknown displacement caused by the vector $\vec{u}$ is achieved in the same spirit as estimating the parameter u in the single round case, except with a messier-looking (although, still efficiently computable) estimator.

The probability of obtaining the q-quadrature measurement outcome $x_{\mathrm{m}}^{(h)}$ in the h^{th} round, given the measurement values obtained in the previous $(h-1)$ rounds and displacement shifts

in all h rounds, is $\mathbb{P}(x_{\mathrm{m}}^{(h)}|u_1,...,u_h,x_{\mathrm{m}}^{(1)},...,x_{\mathrm{m}}^{(h-1)}) \propto \psi_+^{\vec{\Delta}}(\sqrt{2}x_{\mathrm{m}}^{(h)} - \mathcal{U}_h)$. Here, $\mathcal{U}_h$ is the shift contributed in the h^{th} round by the error channel, transformed to account for all previous steps (see 5.7 for an explicit definition). We now apply Bayes' theorem with Gaussian prior PDFs for the error in each of M rounds, resulting in the posterior PDF

$$\mathbb{P}_M^{(\mathrm{q})}\left(\vec{u}\middle|\vec{x}_{\mathrm{m}}\right) \propto \prod_{h=1}^{M} \psi_+^{\vec{\Delta}}\left(\sqrt{2}x_{\mathrm{m}}^{(h)} - \mathcal{U}_h\right) \cdot G_{\sigma_0}\left(u_h\right) \ , \tag{5.44}$$

Assuming, again, that σ_0 and Δ are small compared to $\sqrt{\pi}$, we show that the posterior $\mathbb{P}_M^{(\mathrm{q})}(\vec{u}|\vec{x}_{\mathrm{m}})$ is well approximated by a multivariate Gaussian $\mathcal{N}(\vec{\tilde{u}},\Sigma)$ with mean vector $\vec{\tilde{u}}$ and covariance matrix Σ, in analogy with the single round case. The quantity that we actually wish to estimate is $\theta_M^{\mathrm{err}}(\vec{u})$ from equation (5.39), which is a linear combination of elements from $\vec{u}$. The corresponding PDF is given by

$$\mathbb{P}\left(\theta_M^{\mathrm{err}}(\vec{u})\middle|\vec{x}_{\mathrm{m}}\right) \approx \mathcal{N}\left(\vec{a}\cdot\vec{\tilde{u}}\ ,\ \vec{a}^{\,\mathrm{T}}\cdot\Sigma\cdot\vec{a}\right) \ , \tag{5.45}$$

with $a_k = 2^{-(M+1-k)}$ and

$$\begin{aligned}\tilde{u}_k = \left(\frac{\sigma_0}{\Delta}\right)^2 \Bigg\{ & 2^k \sum_{j=1}^{M} \frac{F_j}{2^j} \\ & - \left(\frac{\sigma_0}{\Delta}\right)^2 \sum_{h=1}^{M} \Big[\Big(\sum_{n=\mathrm{m}_{k,h}}^{M} \frac{2^{k+h}}{4^n} \Big) \Big(\sum_{j=h}^{M} \frac{F_j}{2^j} \Big) \Big] 2^h \Bigg\} \ ,\end{aligned} \tag{5.46}$$

to order $\left(\frac{\sigma_0}{\Delta}\right)^4$, where $\mathrm{m}_{k,h} = \max\{k,h\}$ and $F_h = \sqrt{2}\mathcal{X}_{\mathrm{m}}^{(h)} - \sqrt{\pi}\left\lfloor \sqrt{2}\mathcal{X}_{\mathrm{m}}^{(h)}/\sqrt{\pi} \right\rceil$.

As in the single round case, the posterior mean is used as the MMSE estimator for the displacement error. We see that the posterior is well approximated by a Gaussian with a mean $\vec{a}\cdot\vec{\tilde{u}}$ which can be calculated directly from syndrome measurement results. An explicit approach to this calculation is presented as an algorithm in 5.5.7.

Also of interest is the variance of this Gaussian, $\vec{a}^{\,\mathrm{T}}\cdot\Sigma\cdot\vec{a}$, as it corresponds to the uncertainty in our estimation. In 5.5 we show that, if $\frac{\sigma_0}{\Delta} < \frac{1}{2}$ (which is true for all $M > 1$), the variance

converges to

$$V_{\mathrm{q}}(M) = \frac{\sigma_0^2}{3}\Big[(1-4^{-M}) + \Big(\frac{\sigma_0}{\Delta}\Big)^2 \frac{4}{9}\big(4^{-2M} + 3(1+2M)4^{-M} - 4\big)\Big], \tag{5.47}$$

neglecting terms within the bracket of order $\left(\frac{\sigma_0}{\Delta}\right)^4$ and higher. Note that $V_{\mathrm{q}} \to \frac{\sigma_0^2}{3}$ very quickly as M grows, given that $\frac{\sigma_0}{\Delta} \ll 1$.

5.4.3 Single-Round Error Estimation

Here we present further details for a single round of syndrome extraction (SE) and error estimation.

5.4.4 Wavefunction after the q-SE circuit

First, we show that the state after the q-SE circuit is approximated by simple transformation of its initial wavefunction.

Theorem 5.4. *A q-SE circuit with measurement result x_{m} approximately transforms an input qubit wavefunction according to*

$$Q_\alpha^{\vec{\Delta}}(x-u) \to Q_{s(x_{\mathrm{m}})+\frac{\alpha}{2}}^{\vec{\Delta}'}\big(x - \frac{u}{2}\big).$$

Proof. The two-mode input to the q-SE circuit has the wavefunction

$$\Phi_{\mathrm{in}}(x,y) = Q_\alpha^{\vec{\Delta}}(x-u)\cdot \psi_+^{\vec{\Delta}}(y), \tag{5.48}$$

where the qubit $Q_\alpha^{\vec{\Delta}} = a_0\psi_{0+\alpha}^{\vec{\Delta}} + a_1\psi_{1+\alpha}^{\vec{\Delta}}$ has an error shift u and relative peak shift α.

After the beam-splitter and squeezer of the q-SE circuit, the wavefunction is

$$\Phi(x,y) = Q_{\alpha}^{\vec{\Delta}}(x + \frac{y}{\sqrt{2}} - u) \cdot \psi_{+}^{\vec{\Delta}}(-x + \frac{y}{\sqrt{2}}), \tag{5.49}$$

which may be expanded as

$$\begin{aligned}\Phi(x,y) = \sum_{\mu,n,m} a_\mu N_\mu G_{\frac{1}{\kappa}}[(2n+\mu+\alpha)\sqrt{\pi}] \\ \cdot G_{\Delta}[x - u + \frac{y}{\sqrt{2}} - (2n+\mu+\alpha)\sqrt{\pi}] \\ \cdot G_{\frac{1}{\kappa}}(m\sqrt{\pi}) \cdot G_{\Delta}(-x + \frac{y}{\sqrt{2}} - m\sqrt{\pi}),\end{aligned} \tag{5.50}$$

where the sums are for integer n, m and $\mu \in \{0, 1\}$.

We now identify that this may be written in terms of un-rotated GKP wavefunctions. To do so, we regroup Gaussian functions of the same width by completing the square in the exponent, resulting in

$$\begin{aligned}\Phi(x,y) \propto \sum_{\beta} \psi_{-\beta+\frac{\alpha}{2}}^{\vec{\Delta}'}\Big(\frac{y}{\sqrt{2}} - \frac{u}{2}\Big) \\ \cdot \Big(a_0 \psi_{\beta+\frac{\alpha}{2}}^{\vec{\Delta}'}\big(x - \frac{u}{2}\big) + a_1 \psi_{1+\beta+\frac{\alpha}{2}}^{\vec{\Delta}'}\big(x - \frac{u}{2}\big)\Big)\end{aligned} \tag{5.51}$$

where the sum is over $\beta \in \{-\frac{1}{2}, 0, \frac{1}{2}, 1\}$. This wavefunction is a superposition of two-mode GKP states with relative peaks shifts differing by β. Note also that the initial error u is now shared equally by the modes. To simplify the expression, we have used the approximation that the normalization constants are equal.

For a measurement result x_{m}, the output wavefunction is proportional to $\Phi(x, x_{\mathrm{m}})$. For a particular x_{m}, one term from equation (5.51) is much larger than the others, since the weighting functions are positive-valued and nearly orthogonal if Δ is sufficiently smaller than $\sqrt{\pi}/2$. The dominant term is given by $\beta = s(x_{\mathrm{m}} - \frac{u}{\sqrt{2}} - \alpha\sqrt{\frac{\pi}{2}})$, and therefore we approximate that the output state as that given by the most likely case $u = 0$.

The average fidelity of this approximation is given by the average value of $|\psi_{s(x_{\mathrm{m}})+\frac{\alpha}{2}}^{\vec{\Delta}'}|^2$ taken over the joint probability distribution $\mathbb{P}(x_{\mathrm{m}}, u) = \mathbb{P}(x_{\mathrm{m}}|u)\mathbb{P}(u)$ (these distributions are discussed

below). □

A similar result is obtained for the p-quadrature syndrome extraction. In this case, however, the widths undergo the inverse transformation according to $(\Delta, \kappa) \to (\Delta\sqrt{2}, \kappa/\sqrt{2})$. Appropriately designed q-SE and p-SE steps can therefore be used sequentially to prevent any overall change in the widths. In particular, we begin with a q-SE step using a qubit and auxiliary state of width (Δ, κ). The following p-SE step then uses an auxiliary state of width $(\Delta/\sqrt{2}, \kappa/\sqrt{2})$, and the final state from this has the same width as the initial one. We note that the effect of width reduction through syndrome extraction cannot be observed in the $\Delta = 0$ unphysical states calculation.

5.4.5 Wavefunction after error, q-SE and p-SE

We now extend the above calculation to include a subsequent p-SE step. In particular, we will show the transformation of the input state is well approximated by

$$Q^{\vec{\Delta}}(x-u)\mathrm{e}^{ivx} \to Q^{\vec{\Delta}}\big(x-\theta(x_{\mathrm{m}},u)\big)\mathrm{e}^{i\theta(p_{\mathrm{m}},v)x} \tag{5.52}$$

where the shift function θ is defined as

$$\theta(y,b) = b/2 - f^{*}_{\mathrm{step}}(y). \tag{5.53}$$

The two-mode state after the p-SE beam-splitter and squeezer is given by

$$\begin{aligned}\Phi(x,z) = \mathrm{e}^{i(\frac{x}{2}+\frac{z}{\sqrt{2}})v} \cdot \psi_0^{\vec{\Delta}'}\Big(\frac{x}{2}-\frac{z}{\sqrt{2}}\Big) \\ \cdot Q^{\vec{\Delta}'}\Big(\frac{x}{2}+\frac{z}{\sqrt{2}}-\frac{u}{2}+f^{*}_{\mathrm{step}}(x_{\mathrm{m}}-u/\sqrt{2})\Big)\ ,\end{aligned} \tag{5.54}$$

where the quadrature z corresponds to the mode to be measured. This p-quadrature measure-

ment is achieved using the Fourier transform of the two-mode wavefunction

$$\begin{aligned}\mathcal{F}\big\{\Phi(x,z)\big\} = \; & \mathcal{F}_{y\to p-\frac{p_\mathrm{m}}{\sqrt{2}}}\Big\{\psi_0^{\vec{\Delta}'}(y)\Big\} \\ & \cdot \mathcal{F}_{w\to p+\frac{p_\mathrm{m}}{\sqrt{2}}}\Big\{\mathrm{e}^{iwv}Q^{\vec{\Delta}'}\big(w-\frac{u}{2}+f^*_{\mathrm{step}}(x_\mathrm{m}-u/\sqrt{2})\big)\Big\}.\end{aligned} \tag{5.55}$$

where the transform is taken for variables $(x,z)\to(p,p_\mathrm{m})$, and on the right hand side we use the change of variables $w=\frac{x}{2}+\frac{z}{\sqrt{2}}$ and $y=\frac{x}{2}-\frac{z}{\sqrt{2}}$. The shift property of the transform yields

$$\begin{aligned}\tilde{\Phi}(p,p_\mathrm{m}) =& \tilde{\psi}_0^{\vec{\Delta}'}(p-\frac{p_\mathrm{m}}{\sqrt{2}})\tilde{Q}_0^{\vec{\Delta}'}(p+\frac{p_\mathrm{m}}{\sqrt{2}}-v) \\ & \cdot \mathrm{e}^{-ip(u/2-f^*_{\mathrm{step}}(x_\mathrm{m}-u/\sqrt{2}))}\end{aligned} \tag{5.56}$$

where we denote Fourier transforms as $\tilde{g}=\mathcal{F}\{g\}$.

Since the finite-energy GKP states are approximate eigenstates of the Fourier transform, the first two terms are similar to the product of two rotated GKP states, treated above. Using similar methods, we find the approximate relationship

$$\begin{aligned}\tilde{\psi}_0^{\vec{\Delta}'}\Big(p-\frac{p_\mathrm{m}}{\sqrt{2}}\Big)\cdot\tilde{Q}^{\vec{\Delta}'}\Big(p+\frac{p_\mathrm{m}}{\sqrt{2}}-v\Big) & \\ \propto \tilde{Q}^{\vec{\Delta}}\Big(p-\frac{v}{2}+f^*_{\mathrm{step}}(p_\mathrm{m}-v/\sqrt{2})\Big).&\end{aligned} \tag{5.57}$$

We now simplify the step function by noting that $f^*_{\mathrm{step}}(p_\mathrm{m}-v/\sqrt{2})\approx f^*_{\mathrm{step}}(p_\mathrm{m})$. The success probability of this approximation will be discussed later. Finally, we take the inverse Fourier transform to find the desired result given by equation (5.52).

5.4.6 Bayesian estimation of the q-quadrature error

In order to estimate the unknown shift error, we wish to determine its posterior probability distribution. To do so, we use the prior probability distribution, specified by the error model, and a likelihood function $\mathbb{P}(x_\mathrm{m}|u)$ that we now calculate from the wavefunction.

Theorem 5.5. *The probability of measurement result x_m from a q-SE circuit with initial state*

$\psi_\alpha^{\vec{\Delta}}(x-u)$ *is*

$$\mathbb{P}(x_{\mathrm{m}}|u) \propto \psi_+^{\vec{\Delta}}(\sqrt{2}x_{\mathrm{m}} - u).$$

Proof. We start with the two-mode wavefunction given in equation (5.51). The probability for measurement result x_{m} is

$$\begin{aligned}\mathbb{P}(x_{\mathrm{m}}|u) &= \int_{x\in\mathbb{R}} \left|\Phi(x, x_{\mathrm{m}})\right|^2 dx \\ &\approx \sum_\beta \left|\psi_\beta^{\vec{\Delta}'}\Big(\frac{x_{\mathrm{m}}}{\sqrt{2}} - \frac{u}{2}\Big)\right|^2,\end{aligned} \tag{5.58}$$

where in the second step we neglect overlap of the GKP wavefunctions to approximate $|\sum \psi_\beta|^2 \approx \sum |\psi_\beta|^2$.

An alternate expression is obtained from the relationships

$$\begin{aligned}\sum_{\beta\in\{0,1\}} \left|\psi_\beta^{\vec{\Delta}'}\Big(\frac{x_{\mathrm{m}}}{\sqrt{2}} - \frac{u}{2}\Big)\right|^2 &\propto \psi_0^{\vec{\Delta}}(0)\psi_0^{\vec{\Delta}}\Big(\sqrt{2}x_{\mathrm{m}} - u\Big) \\ \sum_{\beta\in\{\pm\frac{1}{2}\}} \left|\psi_\beta^{\vec{\Delta}'}\Big(\frac{x_{\mathrm{m}}}{\sqrt{2}} - \frac{u}{2}\Big)\right|^2 &\propto \psi_0^{\vec{\Delta}}(0)\psi_1^{\vec{\Delta}}\Big(\sqrt{2}x_{\mathrm{m}} - u\Big),\end{aligned} \tag{5.59}$$

which may be shown by re-indexing akin to the derivation of equation (5.57). Addition of these two equations yields the desired result. □

Using Bayes' theorem, the posterior probability distribution is

$$\begin{aligned}\mathbb{P}(u|x_{\mathrm{m}}) &\propto \mathbb{P}(x_{\mathrm{m}}|u)\mathbb{P}(u) \\ &\propto \psi_+^{\vec{\Delta}}(\sqrt{2}x_{\mathrm{m}} - u)\mathrm{e}^{-\frac{u^2}{2\sigma_0^2}},\end{aligned} \tag{5.60}$$

where in the last step we have explicitly written the Gaussian error model. The unknown shift can now be estimated from equation (5.60) using an appropriate estimator, such as the mean of $\mathbb{P}(u|x_{\mathrm{m}})$. For a given x_{m}, along with $\Delta \ll \sqrt{\pi}$ and $u \ll 1$, $\mathbb{P}(u|x_{\mathrm{m}})$ can be well approximated

by a normal distribution

$$\mathbb{P}(u|x_{\mathrm{m}}) \approx \mathcal{N}\left(\frac{\sqrt{2}\sigma_0^2 x_{\mathrm{m}} - \sqrt{\pi}\sigma_0^2\left\lfloor\frac{\sqrt{2}x_{\mathrm{m}}}{\sqrt{\pi}}\right\rceil}{\Delta^2+\sigma_0^2}, \frac{\Delta^2\sigma_0^2}{\Delta^2+\sigma_0^2}\right) . \tag{5.61}$$

The approximation of the posterior as a normal distribution given reasonable parameter choices is an important step used below in multi-round calculations.

5.4.7 Bayesian estimation of q- and p-quadrature error

We now expand on the previous section to estimate an unknown shift in both quadratures.

Theorem 5.6. *The probability of measurement results x_m and p_m from sequential q-SE and p-SE circuits with an initial state $\mathrm{e}^{ivx}\psi_\alpha^{\vec{\Delta}}(x-u)$ is*

$$\mathbb{P}(x_{\mathrm{m}}, p_{\mathrm{m}}|u,v) \propto \psi_+^{\vec{\Delta}}(\sqrt{2}x_m - u)\cdot\psi_+^{(2\Delta,\kappa/2)}(\sqrt{2}p_m - v) .$$

Proof. Starting from the wavefunction in equation (5.51), the probability of p_{m} is

$$\begin{aligned}\mathbb{P}(p_{\mathrm{m}}|u,v,x_{\mathrm{m}}) &= \int_{p\in\mathbb{R}} \left|\tilde{\Phi}(p,p_{\mathrm{m}})\right|^2 dp \\ &\propto \psi_+^{(2\Delta,\kappa/2)}(\sqrt{2}p_{\mathrm{m}} - v),\end{aligned} \tag{5.62}$$

where the second step follows by analogy to equations (5.49-5.51) and (5.62-5.59). The desired result follows from the relationship of conditional probabilities $\mathbb{P}(x_{\mathrm{m}},p_{\mathrm{m}}|u,v) = \mathbb{P}(x_{\mathrm{m}}|u,v)\mathbb{P}(p_{\mathrm{m}}|u,v,x_{\mathrm{m}})$.

□

Note that $\mathbb{P}(p_{\mathrm{m}}|u,v,x_{\mathrm{m}})$ is independent of x_{m} and u. We can therefore write $\mathbb{P}(x_{\mathrm{m}},p_{\mathrm{m}}|u,v) = \mathbb{P}(x_{\mathrm{m}}|u)\mathbb{P}(p_{\mathrm{m}}|v)$ where the $\mathbb{P}(p_{\mathrm{m}}|v)$ differs from $\mathbb{P}(x_{\mathrm{m}}|u)$ according to the transformation $\Delta\to 2\Delta, \kappa\to\kappa/2$.

5.5 Multi-Round Error Estimation

We now consider M rounds of error followed by q-SE and p-SE circuits, with an aim to estimate the shift error on the final state.

Wavefunction after multiple rounds

As shown for the single-round scenario, the wavefunction after each round is a shifted version of the input. An expression for the shift after each round is calculated iteratively. After round h, with a history of measurements $\vec{x}_{\mathrm{m}} = (x_{\mathrm{m}}^{(1)}, \ldots, x_{\mathrm{m}}^{(h)})$ and shift errors $\vec{u} = (u_1, \ldots, u_h)$, the total q-shift is

$$\theta_h\big(\vec{x}_{\mathrm{m}}, \vec{u}\big) = \sum_{k=1}^{h} \frac{1}{2^{h-k}} \theta\big(\mathcal{X}_k(\vec{x}_{\mathrm{m}}), u_k\big), \tag{5.63}$$

where θ is defined in equation (5.53) and

$$\mathcal{X}_{\mathrm{m}}^{(k)}(\vec{x}_{\mathrm{m}}) = x_{\mathrm{m}}^{(k)} + \frac{1}{\sqrt{2}} \sum_{j=1}^{k-1} \Big[\frac{f_{\mathrm{step}}^{*}\big(\mathcal{X}_{\mathrm{m}}^{(j)}(\vec{x}_{\mathrm{m}})\big)}{2^{k-j-1}} \Big] \tag{5.64}$$

for $h > 1$, and $\mathcal{X}_{\mathrm{m}}^{(1)} = x_{\mathrm{m}}^{(1)}$. The parameter $\mathcal{X}_{\mathrm{m}}^{(k)}$ can be interpreted as the measurement outcome $x_{\mathrm{m}}^{(k)}$ transformed to account for previous measurement-induced shifts.

Equation (5.63) can also be expanded as

$$\begin{aligned} \theta_h\big(\vec{x}_{\mathrm{m}}, \vec{u}\big) &= \sum_{j=1}^{h} \Big[\frac{u_k}{2^{h-j+1}} \Big] - \sum_{k=1}^{h} \Big[\frac{f_{\mathrm{step}}^{*}\big(\mathcal{X}_{\mathrm{m}}^{(k)}(\vec{x}_{\mathrm{m}})\big)}{2^{h-k}} \Big] \\ &= \theta_h^{\mathrm{err}}(\vec{u}) - \theta_h^{\mathrm{step}}(\vec{x}_{\mathrm{m}}), \end{aligned} \tag{5.65}$$

which identifies the total shift as comprised of a known measurement-induced shift $\theta_h^{\mathrm{step}}(\vec{x}_{\mathrm{m}})$ and the accumulation of unknown error $\theta_h^{\mathrm{err}}(\vec{u})$. The aim of our error estimation after M rounds is to use $\vec{x}_{\mathrm{m}}$ to estimate $\theta_M^{\mathrm{err}}(\vec{u})$.

An analogous approach to the p-shifts leads to the wavefunction

$$\mathrm{e}^{i\theta_h(\vec{p}_\mathrm{m},\vec{v})x}Q^{\vec{\Delta}}\big(x-\theta_h(\vec{x}_\mathrm{m},\vec{u})\big) \tag{5.66}$$

after h rounds, for an initial qubit state $Q^{\vec{\Delta}}(x)$. This is assuming that f_step is independent of u_k, which is true if $f^*_\mathrm{step}(x_\mathrm{m}) = f^*_\mathrm{step}(x_\mathrm{m} - u/\sqrt{2})$. We shall discuss the error of such an approximation in a later section.

5.5.1 Total qubit drift

Without active corrective shift at each round of QEC, the magnitude of the total drift of the state in phase space can be bounded. Using the fact that $|f^*_\mathrm{step}| \leq \sqrt{\pi}$ and taking the variance of each the error shifts to be σ_0^2, an application of the triangle inequality gives:

$$\begin{aligned}|\theta(x^{(h)}_\mathrm{m},\mathcal{U}_h)|\,,\ |\theta(p^{(h)}_\mathrm{m},\mathcal{V}_h)| \leq 2\sqrt{\pi}(1-2^{-h}) \\ + \left|\mathcal{N}\Big(0,\sigma_0^2\frac{(1-4^{-h})}{3}\Big)\right|\,,\end{aligned} \tag{5.67}$$

where $\mathcal{N}(\mu,V)$ is a Gaussian random variable with mean μ and Variance V. The quantities $1-4^{-h}$ and $1-2^{-h}$ converge very quickly to 1 as h increases, meaning that for multiple rounds we have

$$|\theta(x^{(h)}_\mathrm{m},\mathcal{U}_h)|\,,\ |\theta(p^{(h)}_\mathrm{m},\mathcal{V}_h)| \leq 2\sqrt{\pi} + \left|\mathcal{N}\Big(0,\frac{\sigma_0^2}{3}\Big)\right|\,. \tag{5.68}$$

This means that even without active error corrective shift after each round of syndrome extraction, the GKP qubit is expected to drift by a maximum of $2\sqrt{\pi}$ in phase space along with some Gaussian random variable with variance $\sigma_0^2/3$ in the worst case scenario. Consequently, the energy of the physical system is not divergent if we extend the QEC for many rounds, if errors are sufficiently small at each round.

5.5.2 Memory-assisted decoder

The probability distributions for the x and p measurement values obtained in the h^{th} round, given all the previous measurement results and displacement shifts, are given by expressions similar in spirit to that in Theorem 5.5:

$$\begin{aligned}\mathbb{P}(x_{\text{m}}^{(h)}|u_1,...,u_h,x_{\text{m}}^{(1)},...,x_{\text{m}}^{(h-1)}) &\propto \psi_+^{(\Delta,\Delta)}(\sqrt{2}x_{\text{m}}^{(h)}-\mathcal{U}_h)\\ \mathbb{P}(p_{\text{m}}^{(h)}|v_1,...,v_h,p_{\text{m}}^{(1)},...,p_{\text{m}}^{(h-1)}) &\propto \psi_+^{(2\Delta,\Delta/2)}(\sqrt{2}p_{\text{m}}^{(h)}-\mathcal{V}_h).\end{aligned} \tag{5.69}$$

Using Bayes' Theorem to flip these distributions, for M rounds we obtain

$$\begin{aligned}\mathbb{P}_M(\vec{u},\vec{v}|\vec{x}_{\text{m}},\vec{p}_{\text{m}}) &= \mathbb{P}_M^{(\text{q})}(\vec{u}|\vec{x}_{\text{m}})\cdot\mathbb{P}_M^{(\text{p})}(\vec{v}|\vec{p}_{\text{m}})\\ \mathbb{P}_M^{(\text{q})}(\vec{u}|\vec{x}_{\text{m}}) &\propto \prod_{h=1}^{M}\psi_+^{\vec{\Delta}}(\sqrt{2}x_{\text{m}}^{(h)}-\mathcal{U}_h)\cdot G_{\sigma_0}(u_h)\\ \mathbb{P}_M^{(\text{p})}(\vec{v}|\vec{p}_{\text{m}}) &\propto \prod_{h=1}^{M}\psi_+^{(2\Delta,\Delta/2)}(\sqrt{2}p_{\text{m}}^{(h)}-\mathcal{V}_h)\cdot G_{\sigma_0}(v_h).\end{aligned} \tag{5.70}$$

We can see that the q- and p-quadratures equations have the similar forms and can be unchangeable ($q \leftrightarrow p$) if $u \leftrightarrow v$, $x_{\text{m}} \leftrightarrow p_{\text{m}}$ and $(\Delta,\kappa) \leftrightarrow (2\Delta,\kappa/2)$, so we will focus on the q-quadature version for now. The PDF for $\vec{u}$ is well approximated by a multivariate Gaussian distribution, a step known as Laplace's approximation in statistics, which we write as

$$\mathbb{P}_M^{(\text{q})}(\vec{u}|\vec{x}_{\text{m}}) \approx \mathcal{N}(\vec{\tilde{u}},\Sigma)\ , \tag{5.71}$$

for mean vector $\vec{\tilde{u}}$ and covariance matrix Σ.

We derive the inverse of the covariance matrix, Σ^{-1}, exactly by completing the square of the exponents of the Gaussians in equation (5.71):

$$\begin{aligned}(\Sigma^{-1})_{\alpha,\beta} &= \Big(\frac{\delta_{\alpha,\beta}}{\sigma_0^2}+\frac{1}{\Delta^2}\sum_{h=m_{\alpha,\beta}}^{M}\frac{1}{4^h 2^{-(\alpha+\beta)}}\Big)\ ,\\ m_{\alpha,\beta} &= \max\{\alpha,\beta\}\ .\end{aligned} \tag{5.72}$$

To derive $\vec{\tilde{u}}$ via completing the square, we need to invert the matrix Σ^{-1}. It's generally hard to invert a $M \times M$ symmetric matrix for an arbitrary M, but we can approximate the covariance matrix via a Neumann series expansion of the matrices, under the assumption of small displacements. We find the covariance matrix has components

$$\Sigma_{\alpha,\beta} \approx \sigma_0^2\,\delta_{\alpha,\beta} - \frac{\sigma_0^4}{\Delta^2}\sum_{h=\mathrm{m}_{\alpha,\beta}}^{M} \frac{1}{4^h 2^{-(\alpha+\beta)}} + \mathcal{O}\Big(\frac{\sigma_0^6}{\Delta^4}\Big)\ , \tag{5.73}$$

and note that this Neumann series converges if $\frac{\sigma_0}{\Delta} < \frac{1}{2}$ (which works for all M). By ignoring from order $\mathcal{O}\Big(\frac{\sigma_0^6}{\Delta^6}\Big)$ upwards in the expansion, we compute

$$\begin{aligned}\tilde{u}_k = \Big(\frac{\sigma_0}{\Delta}\Big)^2 \Bigg\{ & 2^k \sum_{j=1}^{M} \frac{F_j}{2^j} \\ & - \Big(\frac{\sigma_0}{\Delta}\Big)^2 \sum_{h=1}^{M} \Big[\Big(\sum_{n=\mathrm{m}_{k,h}}^{M} \frac{2^{k+h}}{4^n}\Big)\Big(\sum_{j=h}^{M} \frac{F_j}{2^j}\Big)\Big] 2^h \Bigg\}\ ,\end{aligned} \tag{5.74}$$

where $\mathrm{m}_{k,h} = \max\{k,h\}$ and $F_h = \sqrt{2}\mathcal{X}_{\mathrm{m}}^{(h)} - \sqrt{\pi}\Big\lfloor \sqrt{2}\mathcal{X}_{\mathrm{m}}^{(h)}/\sqrt{\pi} \Big\rceil$, which is equation (5.46) in the main text.

Now that we have characterised the multivariate Gaussian noise model (multivariate due to many rounds) by its covariance matrix, we wish to estimate the random part of the total displacement after M rounds, given by $\sum_{k=1}^{M} u_k/2^{M-k+1}$. The corresponding PDF is

$$\mathbb{P}\Big(\sum_{k=1}^{M} \frac{u_k}{2^{M-k+1}}\Big|\vec{x}_{\mathrm{m}}\Big) = \mathcal{N}(\vec{a}\cdot\vec{\tilde{u}}\ ,\ \vec{a}^{\,\mathrm{T}}\cdot\Sigma\cdot\vec{a})\ , \tag{5.75}$$

with $a_k = 2^{-(M+1-k)}$.

We use the mean of this posterior distribution as the MMSE estimator, with uncertainty given by the variance

$$V_{\mathrm{q}} = \mathrm{Var}\Big(\sum_{k=1}^{M} \frac{u_k}{2^{M-k+1}}\Big) = \vec{a}^{\,\mathrm{T}}\cdot\Sigma\cdot\vec{a}. \tag{5.76}$$

Neglecting terms of order $\left(\frac{\sigma_0^6}{\Delta^4}\right)$ and higher, we compute

$$V_{\mathrm{q}}(M) = \frac{\sigma_0^2}{3}\Big[(1-4^{-M}) + \left(\frac{2\sigma_0}{3\Delta}\right)^2 (4^{-2M} + 3(1+2M)4^{-M} - 4)\Big] . \tag{5.77}$$

We can see that $V_{\mathrm{q}} \to \frac{\sigma_0^2}{3}$, very quickly as M grows. Note that using measurement results from all rounds of syndrome measurements allows the error to be estimated more precisely than is achievable otherwise.

5.5.3 Approximations and qubit fidelity

In our calculations, two significant approximations are made in expressing the qubit wavefunction emerging from a syndrome extraction circuit as a displacement of the incoming wavefunction. For the single-round case, these were discussed following equation (5.51). First, in identifying the dominant GKP-like term in the resulting wavefunction, we approximate that $f^*_{\mathrm{step}}(x_{\mathrm{m}} - u/\sqrt{2}) = f^*_{\mathrm{step}}(x_{\mathrm{m}})$. Second, we keep only the dominant term in the sum of equation (5.51). Each of these approximations reduce the fidelity of our description of the final state.

5.5.4 Tracking error

Unlikely measurement outcomes and unusually large displacement errors can cause an incorrect identification of the dominant GKP-like term, which we refer to as a tracking error. In this section, we estimate the probability that our description of the state after one or multiple rounds of syndrome extraction, as given in equation 5.66, does not contain a tracking error.

Single round

For a single round, the joint probability density function of x_m and u is

$$\mathbb{P}(u, x_\mathrm{m}) = C \sum_{n\in\mathbb{Z}} G_{1/\Delta}(n\sqrt{\pi}) G_\Delta(\sqrt{2}x_\mathrm{m} - u - n\sqrt{\pi}) G_{\sigma_0}(u) \ . \tag{5.78}$$

No tracking error occurs if x_m and u are in the region $\mathcal{S}$ for which $|f^*_\mathrm{step}(x_\mathrm{m}) - f^*_\mathrm{step}(x_\mathrm{m} - u/\sqrt{2})| = 0$.

We therefore define the success probability for one round and error width σ_0 to be

$$P^\mathrm{succ}_\mathrm{track}(1, \sigma_0) = \int_S \mathbb{P}(u, x_\mathrm{m}) \mathrm{d}\mathcal{S} \ , \tag{5.79}$$

for which the integration region could be re-written as $x_\mathrm{m} \in \mathbb{R}$ and $u \in \mathcal{T}$, where $\mathcal{T} = [-\sqrt{\pi}, 0] + \sqrt{2}\mathrm{mod}(x - \sqrt{\frac{\pi}{2}}/2, \sqrt{\frac{\pi}{2}})$. The normalisation constant $C = [\sqrt{2}\pi\sigma_0\Delta\Theta_3(0, \mathrm{e}^{-\pi\Delta^2/2})]^{-1}$, where Θ_3 is the Jacobi-Theta function of the third kind.

For our example in the main text where $(\Delta, \sigma_0^2) = (0.2182, 0.0005)$, we calculate $1 - P^\mathrm{succ}_\mathrm{track}(1, \sigma) \approx 1 \times 10^{-5}$.

Multiple rounds

For multiple rounds, the joint probability density function of $\vec{x}_\mathrm{m}$ and $\vec{u}$ is

$$\mathbb{P}(\vec{u}, \vec{x}_\mathrm{m}) = \prod_{h=1}^{M} \psi^{\vec{\Delta}}_+(\sqrt{2}x^{(h)}_\mathrm{m} - \mathcal{U}_h) \cdot G_{\sigma_0}(u_h) \tag{5.80}$$

Similar to the single round case, the probability for M successful rounds is given by

$$P^\mathrm{succ}_\mathrm{track}(M, \sigma_0) = \int_\mathcal{L} \mathbb{P}(\vec{u}, \vec{x}_\mathrm{m}) \mathrm{d}\mathcal{L} \ , \tag{5.81}$$

where $\mathcal{L}$ is the region defined by $f^*_\mathrm{step}(\mathcal{X}^{(j)}_\mathrm{m}) = f^*_\mathrm{step}(x^{(j)}_\mathrm{m} - \mathcal{U}_j/\sqrt{2})$, $\forall 1 < j < M$.

This calculation is simplified by changing variables to $\vec{\mathcal{X}}$ and $\vec{\mathbb{U}}$, where $\mathbb{U}_h = \sum_{k=1} \frac{u_k}{2^{h-k}}$ for $h > 1$ and $\mathbb{U}_1 = u_1$, which leads to

$$\begin{aligned} P^{\text{succ}}_{\text{track}}(M,\sigma_0) > \int_{\mathcal{L}} \prod_{h=2}^{M} \Big[\psi_+^{\vec{\Delta}}(\sqrt{2}\mathcal{X}_{\text{m}}^{(h)} - \mathbb{U}_h) \cdot G_{\frac{2\sigma_0}{\sqrt{5}}}(\mathbb{U}_h)\Big] \\ \cdot \psi_+^{\vec{\Delta}}(\sqrt{2}\mathcal{X}_{\text{m}}^{(1)} - \mathbb{U}_1) \cdot G_{\sigma_0}(\mathbb{U}_h) \cdot \mathrm{d}^M\vec{\mathcal{X}}\,\mathrm{d}^M\vec{\mathbb{U}} \ . \end{aligned} \tag{5.82}$$

Note the multidimensional integral is now separated into a product of single integrals over the integration regions $f^*_{\text{step}}(\mathcal{X}_{\text{m}}^{(j)}) = f^*_{\text{step}}(\mathcal{X}_{\text{m}}^{(j)} - \mathbb{U}_j/\sqrt{2})$ for all $2 < j < M$. A convenient bound lower bound can be written in terms of single-round probabilities

$$P^{\text{succ}}_{\text{track}}(M,\sigma_0) > \Big[P^{\text{succ}}_{\text{track}}\Big(1, \frac{2\sigma_0}{\sqrt{5}}\Big)\Big]^M. \tag{5.83}$$

For $(\Delta, \sigma_0^2) = (0.2182, 0.0005)$ and $M = 200$, we calculate $1 - P^{\text{succ}}_{\text{track}}(M,\sigma_0) \approx 3 \times 10^{-3}$.

5.5.5 Truncation error

The approximation that only the dominant term in the state survives at each round of syndrome extraction leads to a probability that our decoder fails. We use an approximation of this probability to bound the long term fidelity of a state recovered using information from the memory-assisted decoder. In particular, we approximate the state after each round of syndrome extraction by decohering the dominant term with respect to the rest of the state: $p\hat{\rho}_{\text{dom.}} + (1-p)\hat{\rho}_{\text{junk}}$, where p is the phenomenological success probability per round, $\hat{\rho}_{\text{dom.}}$ is the dominant term we keep and $\hat{\rho}_{\text{junk}}$ is the state we throw away in the truncation.

Single round

The wavefunction emerging from single syndrome extraction circuit, described by equation 5.51, can be expressed in ket notation as

$$|\Phi(x|u, x_{\text{m}})\rangle = R(u, x_{\text{m}}) \sum_{\gamma} \psi_{\gamma}^{\vec{\Delta}'}\Big(\frac{x_{\text{m}}}{\sqrt{2}} - \frac{u}{2}\Big) \Big| Q_{\gamma}^{\vec{\Delta}'} \Big\rangle \ , \tag{5.84}$$

where $R(u, x_\mathrm{m})$ is a normalisation constant. We note the dominant term as $\left|Q_\beta^{\vec{\Delta}}\right\rangle$ and calculate its amplitude

$$A(\beta) = R(u, x_\mathrm{m}) \sum_\gamma \psi_\gamma^{\vec{\Delta}'} \Big(\frac{x_\mathrm{m}}{\sqrt{2}} - \frac{u}{2} \Big) \left\langle Q_\beta^{\vec{\Delta}} | Q_\gamma^{\vec{\Delta}'} \middle| Q_\beta^{\vec{\Delta}} | Q_\gamma^{\vec{\Delta}'} \right\rangle \ . \tag{5.85}$$

The average success of the truncated description is given by

$$P_\mathrm{trunc}^\mathrm{succ}(1, \sigma_0) = \int_\text{all space} |A(\beta)|^2 \mathbb{P}(u, x_\mathrm{m}) \ \mathrm{d}u \, \mathrm{d}x_\mathrm{m}. \tag{5.86}$$

For the example $(\Delta, \sigma_0^2) = (0.2182, 0.0005)$, we calculate $1 - P_\mathrm{trunc}^\mathrm{succ}(1, \sigma_0) \approx 5 \times 10^{-5}$.

Multiple rounds

Similarly, we estimate a success probability after M rounds as

$$\begin{aligned} P_\mathrm{trunc}^\mathrm{succ}(M, \sigma_0) = & \prod_{h=1}^{M} \int \sum_{\beta_h} |A(\beta_h)|^2 G_{\sigma_0}(u_h) \\ & \cdot \psi_+^{\vec{\Delta}}(\sqrt{2} x_\mathrm{m}^{(h)} - \mathcal{U}_h) \ \mathrm{d}\vec{u} \, \mathrm{d}\vec{x}_\mathrm{m} \ . \end{aligned} \tag{5.87}$$

As in equation 5.83, we bound the multi-round probability in terms of the single-round expression

$$P_\mathrm{trunc}^\mathrm{succ}(M, \sigma_0) > (P_\mathrm{trunc}^\mathrm{succ}(1, 2\sigma_0/\sqrt{5}))^M \ . \tag{5.88}$$

For $(\Delta, \sigma_0^2) = (0.2182, 0.0005)$ and $M = 200$ we calculate $1 - P_\mathrm{trunc}^\mathrm{succ}(M, \sigma_0) \approx 1 \times 10^{-2}$.

5.5.6 Total error and state fidelity

To estimate a final qubit fidelity, as in the example shown in Fig. 5.8, we first calculate the fidelity F_ρ from the output state described by our Bayesian estimation procedure, following the approach of Pantaleoni et al. [110]. We then assume that a tracking, truncation or syndrome

error results in a complete depolarized qubit with probability upper-bounded by $1 - P_{\text{total}}^{\text{succ}}$. A lower bound on the final qubit fidelity is therefore given by $F = (F_\rho - \frac{1}{2})P^{\text{succ}} + \frac{1}{2}$.

5.5.7 Pseudocode for Error Estimation

After M rounds of syndrome extraction, as depicted in Fig. 5.6c, our results can be used to estimated the random contribution of the total displacement error from measurement results $\vec{x}_{\text{m}}$ and $\vec{p}_{\text{m}}$. Algorithm 1 gives an explicit description of this calculation for the q-quadrature.

5.5.8 Offline Squeezing Derivation

A diagrammatic derivation of the offline squeezing circuit is shown in FIG. 5.7. Starting with the Glancy-Knill syndrome extraction circuits, we recompile and re-interpret measurement results to obtain a circuit in which the qubit state interacts only with 50:50 beamsplitters.

Algorithm 1 Estimation of the q-quadrature error

Initialise empty vectors $\vec{\mathcal{X}}_{\text{m}}, \vec{F}, \vec{\tilde{u}}$

for h = 1 to M **do**

Receive data $x_{\text{m}}^{(h)}$

Compute $\mathcal{X}_{\text{m}}^{(h)} = x_{\text{m}}^{(h)} + \dfrac{1}{\sqrt{2}} \displaystyle\sum_{k=1}^{h-1} \frac{f_{\text{step}}^{*}(\mathcal{X}_{\text{m}}^{(k)})}{2^{h-k-1}}$

Compute $F_h = \sqrt{2}\mathcal{X}_{\text{m}}^{(h)} - \sqrt{\pi}\left\lfloor \dfrac{\sqrt{2}\mathcal{X}_{\text{m}}^{(h)}}{\sqrt{\pi}} \right\rceil$

Append $\mathcal{X}_{\text{m}}^{(h)}$ to $\vec{\mathcal{X}}_{\text{m}}$ and F_h to $\vec{F}$

end for

Compute total displacement $\displaystyle\sum_{k=1}^{M} \frac{\tilde{u}_k}{2^{M-k+1}}$ where

$$\tilde{u}_k = \Big(\frac{\sigma_0}{\Delta}\Big)^2 \Bigg\{ 2^k \sum_{j=1}^{M} \frac{F_j}{2^j} - \Big(\frac{\sigma_0}{\Delta}\Big)^2 \sum_{h=1}^{M} \Big[\Big(\sum_{n=\text{m}_{k,h}}^{M} \frac{2^{k+h}}{4^n} \Big) \Big(\sum_{j=h}^{M} \frac{F_j}{2^j} \Big) \Big] 2^h \Bigg\}$$

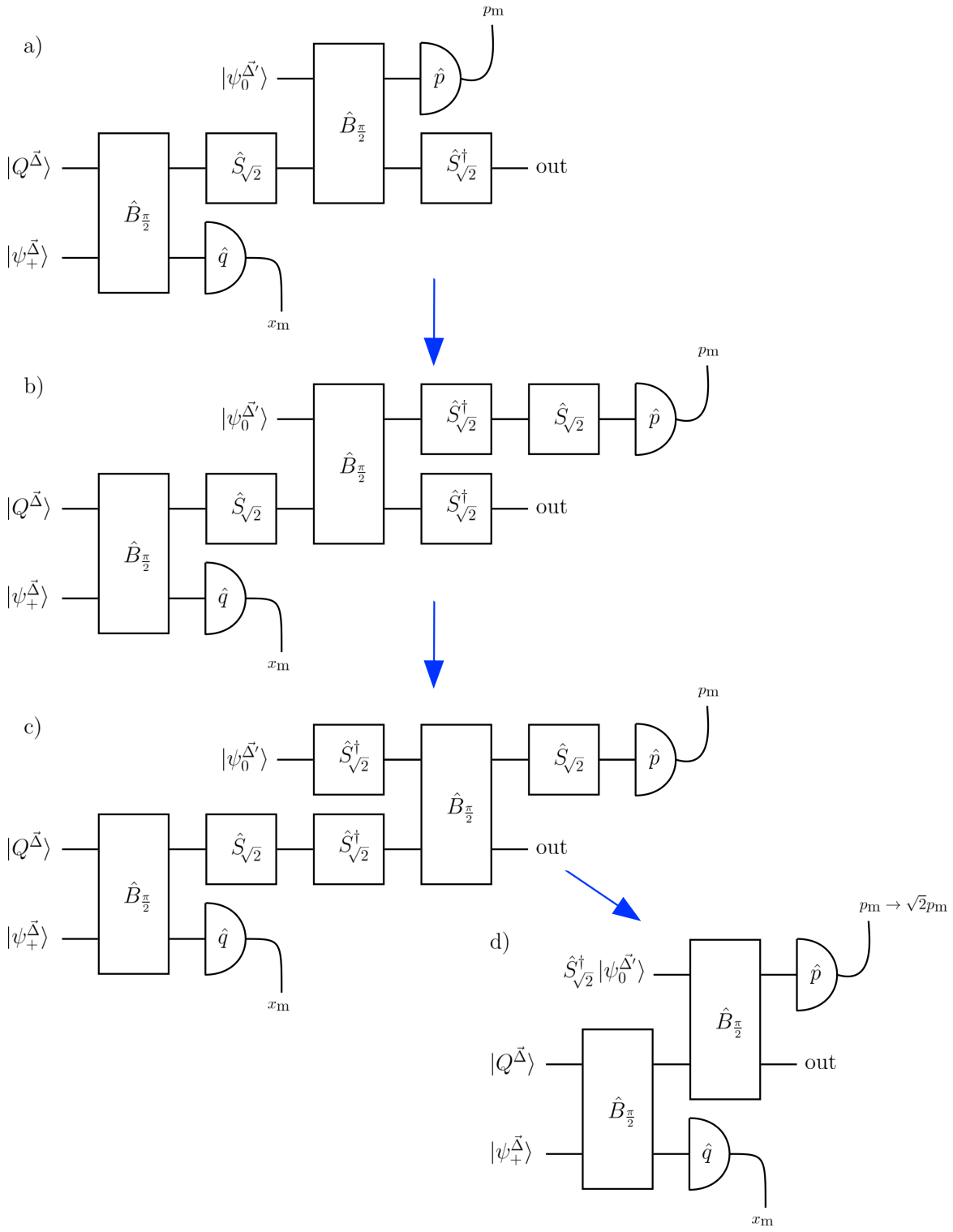

Figure 5.7: Diagrammatic derivation of the offline squeezing circuit. In a), we start with the GK syndrome-extraction circuit with the corrective displacement removed. In b), we insert an identity operator before the momentum measurement. In c), we rearrange the 50:50 beamsplitter and squeezers in both modes. Finally in d), we achieve a simplified circuit in which all squeezing is effectively moved to the momentum resource state and interpretation of the momentum measurement result.

5.5.9 Numerical results

The aim of a quantum error correction (QEC) procedure is to protect logical quantum information. Pantaleoni et al. recently reported a method to extract logical information from approximate GKP states [110]. In essence, this reduces a density matrix function describing a CV state to a qubit density matrix ($\hat{\rho}^{\mathrm{CV}} \to \hat{\rho}^{\mathrm{qubit}}$). Using this, fidelities between qubit density matrices at the input and output of an error correction procedure can be computed in order to benchmark its performance.

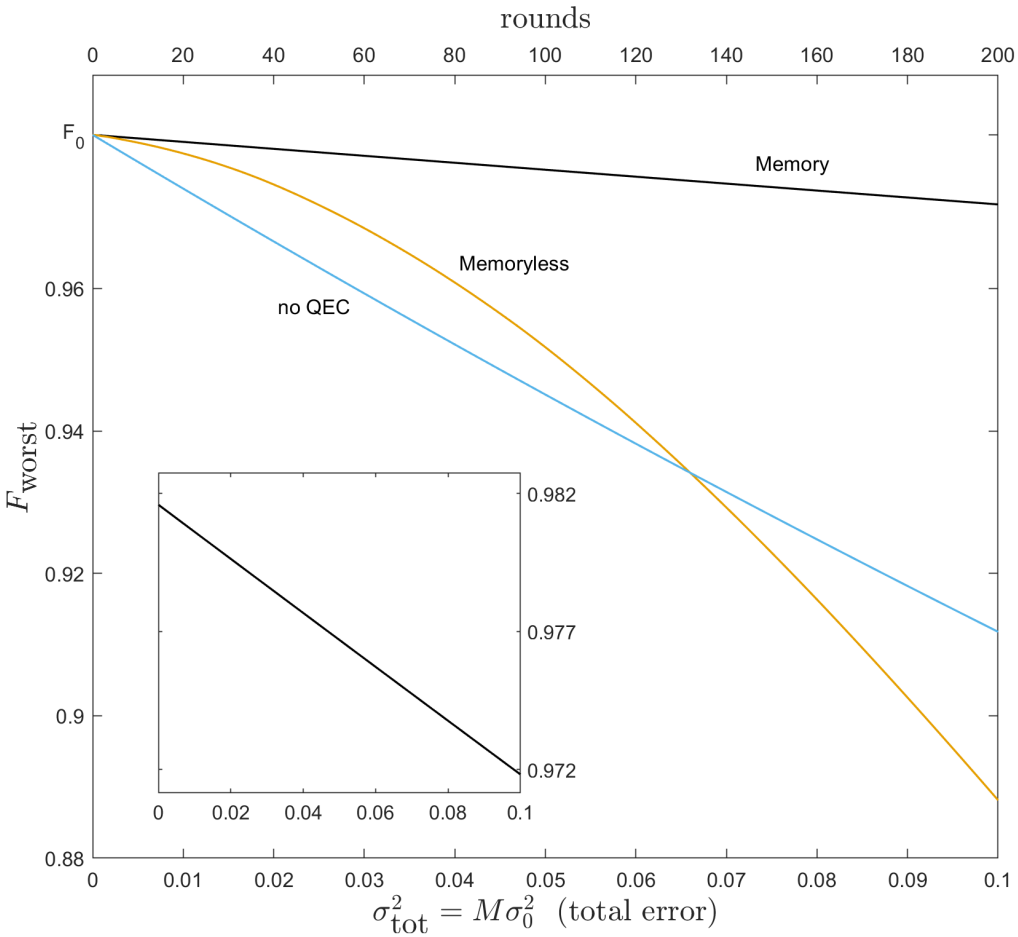

Figure 5.8: Qubit fidelity achieved by the memory-assisted decoder (black), memoryless decoder (yellow) and no QEC (aqua). A Gaussian error channel of width $\sigma_0^2 = 0.0005$ is applied in each of the M rounds of syndrome extraction to a GKP-state with width $\Delta = \kappa = 0.22$. The initial fidelity $F_0 = 0.981$, and the inset plot shows how the black curve decreases over a smaller range.

In Fig. 5.8 we present the results of numerical simulations for the specific case of a GKP code with $\Delta \approx 0.22$ (corresponding to an average number of bosons $\bar{n} \approx 10$). For varying numbers

of rounds of error channel application followed by syndrome extraction, we benchmark error correction with our memory-assisted decoder against density matrix function simulations of the memoryless decoder and no error correction at all.

We observe that error correction is improved by using our memory-assisted decoder instead of the memoryless decoder — a finding similar to that of Vuillot et al. [111] and Noh et al. [48] for Steane-based GKP syndrome extraction. Note that Δ is large enough that the memoryless decoder performs worse than no QEC once a few hundred rounds are considered. We also see that the quality of the memory-assisted error corrected state is higher than the uncorrected state, despite the state containing a low average number of bosons. Furthermore, the fidelity of the input state is approximately preserved through application of the memory-assisted error correction scheme.

5.6 Summary

We have described an explicit protocol for GKP quantum error correction that provides improved protection from Gaussian displacement errors with reduced experimental requirements. Notably, we have shown that GKP states undergo a total displacement (and therefore require a correction) that is approximately bounded by $2\sqrt{\pi}$ in each quadrature, after multiple rounds of error syndrome extraction. A memory-assisted decoder based on Bayesian estimation was developed to specify the near-optimal corrective displacement, and numerical simulations have shown that this results in significantly improved error correction compared to a memoryless decoder when applied to an approximate GKP state with a small average number of bosons.

Recent experiments have demonstrated GKP states encoded in oscillations of trapped ions [49] and microwave fields of superconducting resonators [50]. In the latter case, states are shown with widths of $(\Delta, \kappa) = (0.16, 0.32)$. As these values are similar to those we have studied here, this suggests that our decoder can be exploited by near-term experiments as part of an error correction procedure. Additionally, the Glancy-Knill syndrome extraction circuit at the core of our method may be better suited to realistic devices than the more studied SUM gate syndrome

extraction, since the latter requires more gates, and therefore more physical components, to implement [112].

The error model that we have considered in this work also pertains to errors that arise in teleporting a GKP state along a CV cluster state with finite squeezing [113]. In this situation, the finite squeezing of the cluster state induces a displacement error. We anticipate that it will therefore be possible to apply our error correction scheme between nodes on a CV cluster state graph, and thereby lower the squeezing threshold for universal fault tolerant quantum computation using CV cluster states and GKP state injection.

5.7 Useful formulae

Throughout our text, we use the following notations and conventions:

- Plank's constant $\hbar = 1$.
- Displacement operator $\hat{D}(\alpha) = \mathrm{e}^{\frac{\alpha\hat{a}^\dagger - \alpha^*\hat{a}}{\sqrt{2}}}$.
- Beamsplitter operator $\hat{B}_\phi = \mathrm{e}^{-\frac{\phi}{2}(\hat{a}^\dagger\hat{b} - \hat{a}\hat{b}^\dagger)}$.
- Squeezing operator $\hat{S}_a = \mathrm{e}^{\frac{\ln(a)}{2}(\hat{a}^2 - (\hat{a}^\dagger)^2)}$.
- Gaussian function $G_\sigma(x) = \exp\left(-\frac{x^2}{2\sigma^2}\right)$.
- $\mathcal{N}(\mu, V)$ is a Gaussian random vector with mean μ and covariance V.
- Rounding function $\lfloor x \rceil$ gives the nearest integer to x.
- Remainder function $\mathrm{rem}(n, 4)$ gives the remainder from dividing integer n by 4.

Additionally, we define:

- GKP wavefunctions widths $\vec{\Delta} = (\Delta, \kappa)$ and $\vec{\Delta}' = (\Delta/\sqrt{2}, \kappa\sqrt{2})$.

- Normalized GKP wavefunctions

$$\psi_{\mu}^{\vec{\Delta}}(x) = N_{\mu} \sum_{s\in\mathbb{Z}} G_{\frac{1}{\kappa}}[(2s+\mu)\sqrt{\pi}]\, G_{\Delta}[x-(2s+\mu)\sqrt{\pi}]. \tag{5.89}$$

- Step functions

$$\begin{aligned} s(x) &= \frac{1}{2}\mathrm{rem}\Big(\Big\lfloor x/\sqrt{\pi/2}\Big\rceil\ ,\ 4\Big)\ , \\ f^{*}_{\mathrm{step}}(x) &= \frac{\sqrt{\pi}}{2}\mathrm{rem}^{*}\Big(\Big\lfloor x/\sqrt{\pi/2}\Big\rceil\ ,\ 4\Big)\ . \end{aligned} \tag{5.90}$$

- The effective measurement results $\mathcal{X}_{\mathrm{m}}^{(h)}$ and effective errors $\mathcal{U}_h$ if passive error correction is carried out:

$$\begin{aligned} \mathcal{X}_{\mathrm{m}}^{(h)} &= x_{\mathrm{m}}^{(h)} + \frac{1}{\sqrt{2}} \sum_{k=1}^{h-1} \Big[\frac{f^{*}_{\mathrm{step}}(\mathcal{X}_{\mathrm{m}}^{(k)})}{2^{h-k-1}}\Big]\ ,\ \forall\ h>1 \\ \mathcal{X}_{\mathrm{m}}^{(1)} &= x_{\mathrm{m}}^{(1)} \\ \mathcal{U}_h &= u_h + \sum_{k=1}^{h-1} \Big[\frac{u_k}{2^{h-k}} - \frac{f^{*}_{\mathrm{step}}(\mathcal{X}_{\mathrm{m}}^{(k)})}{2^{h-k-1}}\Big]\ ,\ \forall\ h>1 \\ \mathcal{U}_1 &= u_1\ . \end{aligned} \tag{5.91}$$

-

$$\sum_{n,m\in\mathbb{Z}^2} f(n+m)g(n-m) = \sum_{l=0}^{1} \sum_{n,m\in\mathbb{Z}^2} f(2n+l)g(2m+l)\ , \tag{5.92}$$

- $\mathrm{SAW}(x,a,b)$ is the sawtooth function with slope a and period b as shown in figure 5.9.

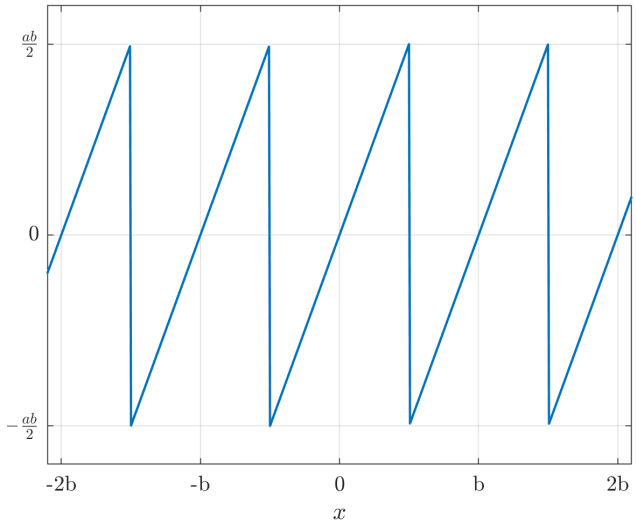

Figure 5.9: This is a sawtooth function with a positive slope a and period b.

Chapter 6

Summary and outlook

This thesis consisted of two related pieces of work. Chapter 4 introduces and investigates several different properties of the grid sensor and GKP state, providing motivations for the GKP state as a suitable quantum state for optical quantum error detection. The main project in this thesis covered the theoretical studies of an improved decoder for the GKP code in chapter 5, expanding on the work done by Glancy and Knill. We introduced new methods to calculate the Fock state, investigate the resource count of state generation and finally introduced a detailed analysis of a memory decoder biased under the Gaussian random displacement error channel.

In chapter 4, we briefly assessed and showed that both the GKP and grid sensor states require high number of single photons to generate. Coupled with their complicated Fock state amplitude structure and the need to retain up to a 100 basis states to simulate in the Fock basis, they are difficult to study both theoretically and experimentally. In general, a highly localised state in one quadrature provides good inference of displacement errors in that particular quadrature. However, this means the sensing state is highly de-localised in the conjugate quadrature, and so inference is poor in this quadrature. On the other hand, de-localisation of the sensing state in phase makes it resilient to errors. The grid sensor state combines both features, while being roughly identical in both the q- and p-quadrature and is localised in packets periodically spread out over phase space. This gives the grid sensor state error resilience and good performance in sensing displacement errors in perpendicular directions in phase space. These ideas then moti-

vated the investigation of the quantum Fisher information matrix of the displacement problem using the grid sensor state - which was shown to be a diagonal matrix. This showed that this state satisfies the Helstrom bound and is therefore optimal for estimating errors in both directions in phase space. Further analysis is required to studying how this compares with the squeezed state and which measurement POVMs are required to potentially achieve this.

In chapter 5, a memory-assisted decoder based on Bayesian estimation was developed to enhance the corrective displacement needed for state recovery. Numerical simulations have shown that this result significantly improved error correction compared to a memoryless decoder when applied to an approximate GKP state with a small average number of bosons. The results showed that multiple rounds of error-syndrome extraction with Bayesian estimation offer enhanced protection of GKP-encoded qubits over comparable single-round approaches. Furthermore the expected total displacement error after multiple rounds of error followed by syndrome extraction is bounded by $2\sqrt{\pi}$ in phase space. It was demonstrated that the syndrome extraction circuits could be recompiled in a way such that all squeezing operations are pushed into auxiliary state preparation offline. This reduced the circuit to beamsplitter transformations and quadrature measurements, providing a realistic picture of a bosonic GKP qubit undergoing a physical error channel in quantum optics.

We hope this work motivates further study into the relatively unexplored Glancy-Knill approach to quantum error correction with the GKP code. We want to highlight that offline squeezing of auxiliary states have been generalised to arbitrary n-mode GKP codes [114] using techniques from the Heisenberg representation of quantum mechanics. Independently, authors from [115] are actively trying to generalise the Glancy-Knill approach as a teleportation error correcting scheme for the GKP code. Interestingly, the grid sensor state have been used as resource state in a separate scheme of quantum error correcting [79]. Combining and comparing different schemes of GKP error correcting biased for realistic noise models in a larger architecture of optical quantum computing could lead to a fully error corrected fault tolerant quantum computer.

Bibliography

[1] K. H. Wan, A. Neville, and S. Kolthammer, "Memory-assisted decoder for approximate gottesman-kitaev-preskill codes," *Phys. Rev. Research*, vol. 2, p. 043280, Nov 2020.

[2] G. Chiribella and H. Kristjánsson, "Quantum Shannon theory with superpositions of trajectories," *Proc. R. Soc. A*, vol. 475, no. 2225, p. 20180903, 2019.

[3] F. Milthaler, "Thesis-latex-template." `https://github.com/fmilthaler/Thesis-LaTeX-Template`, 2021.

[4] A. Kay, "Quantikz," 2019.

[5] E. T. Jaynes, *Probability theory: The logic of science*. Cambridge: Cambridge University Press, 2003.

[6] S. Glancy and E. Knill, "Error analysis for encoding a qubit in an oscillator," *Phys. Rev. A*, vol. 73, p. 012325, Jan 2006.

[7] R. P. Feynman, "Simulating physics with computers," *International journal of theoretical physics*, vol. 21, no. 6/7, pp. 467–488, 1982.

[8] S. Wolfram, "Statistical mechanics of cellular automata," *Rev. Mod. Phys.*, vol. 55, pp. 601–644, Jul 1983.

[9] J. L. Park, "The concept of transition in quantum mechanics," *Foundations of Physics*, vol. 1, pp. 23–33, Mar. 1970.

[10] A. S. Holevo, "Bounds for the quantity of information transmitted by a quantum communication channel," *Problemy Peredachi Informatsii*, vol. 9, no. 3, pp. 3–11, 1973.

[11] R. S. Ingarden, "Quantum information theory," *Reports on Mathematical Physics*, vol. 10, no. 1, pp. 43–72, 1976.

[12] D. Deutsch, "Quantum theory, the church–turing principle and the universal quantum computer," *Proceedings of the Royal Society of London. A. Mathematical and Physical Sciences*, vol. 400, no. 1818, pp. 97–117, 1985.

[13] B. Schumacher, "Quantum coding," *Phys. Rev. A*, vol. 51, pp. 2738–2747, Apr 1995.

[14] D. Deutsch and R. Jozsa, "Rapid solution of problems by quantum computation," *Proceedings of the Royal Society of London. Series A: Mathematical and Physical Sciences*, vol. 439, no. 1907, pp. 553–558, 1992.

[15] N. Johansson and J.-Å. Larsson, "Efficient classical simulation of the deutsch–jozsa and simon's algorithms," *Quantum Information Processing*, vol. 16, aug 2017.

[16] D. R. Simon, "On the power of quantum computation," *SIAM journal on computing*, vol. 26, no. 5, pp. 1474–1483, 1997.

[17] P. W. Shor, "Polynomial-time algorithms for prime factorization and discrete logarithms on a quantum computer," *SIAM review*, vol. 41, no. 2, pp. 303–332, 1999.

[18] R. Crandall and C. Pomerance, *Prime Numbers: A Computational Perspective*. Lecture notes in statistics, Springer New York, 2006.

[19] D. Bernstein, J. Buchmann, and E. Dahmen, *Post-Quantum Cryptography*. Springer Berlin Heidelberg, 2009.

[20] L. K. Grover, "A fast quantum mechanical algorithm for database search," in *Proceedings of the twenty-eighth annual ACM symposium on Theory of computing*, pp. 212–219, 1996.

[21] C. H. Bennett, E. Bernstein, G. Brassard, and U. Vazirani, "Strengths and weaknesses of quantum computing," *SIAM Journal on Computing*, vol. 26, pp. 1510–1523, oct 1997.

[22] A. W. Harrow, A. Hassidim, and S. Lloyd, "Quantum algorithm for linear systems of equations," *Phys. Rev. Lett.*, vol. 103, p. 150502, Oct 2009.

[23] A. Montanaro, "Quantum algorithms: an overview," *npj Quantum Information*, vol. 2, jan 2016.

[24] C. Gardiner and P. Zoller, *Quantum Noise: A Handbook of Markovian and Non-Markovian Quantum Stochastic Methods with Applications to Quantum Optics*. Springer series in synergetics, Springer, 2000.

[25] *Quantum Error Correction*. Cambridge University Press, 2013.

[26] M. Nielsen and I. Chuang, *Quantum Computation and Quantum Information*. Cambridge Series on Information and the Natural Sciences, Cambridge University Press, 2000.

[27] A. Peres, "Reversible logic and quantum computers," *Phys. Rev. A*, vol. 32, pp. 3266–3276, Dec 1985.

[28] P. W. Shor, "Scheme for reducing decoherence in quantum computer memory," *Phys. Rev. A*, vol. 52, pp. R2493–R2496, Oct 1995.

[29] A. M. Steane, "Error correcting codes in quantum theory," *Phys. Rev. Lett.*, vol. 77, pp. 793–797, Jul 1996.

[30] E. Chitambar and G. Gour, "Quantum resource theories," *Rev. Mod. Phys.*, vol. 91, p. 025001, Apr 2019.

[31] E. Knill, R. Laflamme, and W. H. Zurek, "Resilient quantum computation," *Science*, vol. 279, no. 5349, pp. 342–345, 1998.

[32] D. Aharonov and M. Ben-Or, "Fault-tolerant quantum computation with constant error rate," *SIAM Journal on Computing*, 2008.

[33] A. Y. Kitaev, "Fault-tolerant quantum computation by anyons," *Annals of Physics*, vol. 303, no. 1, pp. 2–30, 2003.

[34] P. F. Victor V. Albert and many contributors., "Error correction zoo, quantum domain," 1999.

[35] D. Gottesman, A. Kitaev, and J. Preskill, "Encoding a qubit in an oscillator," *Phys. Rev. A*, vol. 64, p. 012310, Jun 2001.

[36] S. L. Braunstein and P. van Loock, "Quantum information with continuous variables," *Reviews of Modern Physics*, vol. 77, pp. 513–577, jun 2005.

[37] S. Barnett and P. Radmore, *Methods in Theoretical Quantum Optics*. Oxford Series in Optical and Imaging Sciences, Clarendon Press, 2002.

[38] M. O. Scully and M. S. Zubairy, *Quantum Optics*. Cambridge University Press, 1997.

[39] C. Gerry and P. Knight, *Introductory Quantum Optics*. Cambridge University Press, 2004.

[40] S. Lloyd and S. L. Braunstein, "Quantum computation over continuous variables," *Phys. Rev. Lett.*, vol. 82, pp. 1784–1787, Feb 1999.

[41] S. L. Braunstein and P. van Loock, "Quantum information with continuous variables," *Rev. Mod. Phys.*, vol. 77, pp. 513–577, Jun 2005.

[42] C. Weedbrook, S. Pirandola, R. García-Patrón, N. J. Cerf, T. C. Ralph, J. H. Shapiro, and S. Lloyd, "Gaussian quantum information," *Reviews of Modern Physics*, vol. 84, no. 2, p. 621, 2012.

[43] J.-i. Yoshikawa, S. Yokoyama, T. Kaji, C. Sornphiphatphong, Y. Shiozawa, K. Makino, and A. Furusawa, "Invited Article: Generation of one-million-mode continuous-variable cluster state by unlimited time-domain multiplexing," *APL Photonics*, vol. 1, p. 060801, Sep 2016.

[44] A. Furusawa and P. van Loock, *Quantum Teleportation and Entanglement, A Hybrid Approach to Optical Quantum Information Processing*. Wiley, 2011.

[45] N. C. Menicucci, "Fault-tolerant measurement-based quantum computing with continuous-variable cluster states," *Phys. Rev. Lett.*, vol. 112, p. 120504, Mar 2014.

[46] B. Q. Baragiola, G. Pantaleoni, R. N. Alexand er, A. Karanjai, and N. C. Menicucci, "All-Gaussian universality and fault tolerance with the Gottesman-Kitaev-Preskill code," *arXiv e-prints*, p. arXiv:1903.00012, Feb 2019.

[47] K. Fukui, A. Tomita, A. Okamoto, and K. Fujii, "High-threshold fault-tolerant quantum computation with analog quantum error correction," *Phys. Rev. X*, vol. 8, p. 021054, May 2018.

[48] K. Noh and C. Chamberland, "Fault-tolerant bosonic quantum error correction with the surface-GKP code," *arXiv e-prints*, p. arXiv:1908.03579, Aug 2019.

[49] C. Flühmann, T. L. Nguyen, M. Marinelli, V. Negnevitsky, K. Mehta, and J. P. Home, "Encoding a qubit in a trapped-ion mechanical oscillator," *Nature*, vol. 566, no. 7745, pp. 513–517, 2019.

[50] P. Campagne-Ibarcq, A. Eickbusch, S. Touzard, E. Zalys-Geller, N. E. Frattini, V. V. Sivak, P. Reinhold, S. Puri, S. Shankar, R. J. Schoelkopf, L. Frunzio, M. Mirrahimi, and M. H. Devoret, "A stabilized logical quantum bit encoded in grid states of a superconducting cavity," *arXiv e-prints*, p. arXiv:1907.12487, Jul 2019.

[51] S. Pirandola, S. Mancini, S. L. Braunstein, and D. Vitali, "Minimal qudit code for a qubit in the phase-damping channel," *Physical Review A*, vol. 77, mar 2008.

[52] P. T. Cochrane, G. J. Milburn, and W. J. Munro, "Macroscopically distinct quantum-superposition states as a bosonic code for amplitude damping," *Physical Review A*, vol. 59, pp. 2631–2634, apr 1999.

[53] M. H. Michael, M. Silveri, R. T. Brierley, V. V. Albert, J. Salmilehto, L. Jiang, and S. M. Girvin, "New class of quantum error-correcting codes for a bosonic mode," *Phys. Rev. X*, vol. 6, p. 031006, Jul 2016.

[54] V. V. Albert, K. Noh, K. Duivenvoorden, D. J. Young, R. T. Brierley, P. Reinhold, C. Vuillot, L. Li, C. Shen, S. M. Girvin, B. M. Terhal, and L. Jiang, "Performance and structure of single-mode bosonic codes," *Physical Review A*, vol. 97, mar 2018.

[55] K. Duivenvoorden, B. M. Terhal, and D. Weigand, "Single-mode displacement sensor," *Phys. Rev. A*, vol. 95, p. 012305, Jan 2017.

[56] P. Kok, W. J. Munro, K. Nemoto, T. C. Ralph, J. P. Dowling, and G. J. Milburn, "Linear optical quantum computing with photonic qubits," *Reviews of Modern Physics*, vol. 79, pp. 135–174, jan 2007.

[57] R. W. Hamming, "Error detecting and error correcting codes," *The Bell System Technical Journal*, vol. 29, no. 2, pp. 147–160, 1950.

[58] J. Massey, "Review of 'theory and practice of error control codes' (blahut, r.e.; 1983)," *IEEE Transactions on Information Theory*, vol. 31, no. 4, pp. 553–554, 1985.

[59] M. Schlosshauer, *Decoherence: And the Quantum-To-Classical Transition*. The Frontiers Collection, Springer, 2007.

[60] D. P. Divincenzo, "The Physical Implementation of Quantum Computation," *Fortschritte der Physik*, vol. 48, pp. 771–783, Jan. 2000.

[61] A. Y. Kitaev, "Quantum computations: algorithms and error correction," *Russian Mathematical Surveys*, vol. 52, no. 6, p. 1191, 1997.

[62] D. Litinski, "A game of surface codes: Large-scale quantum computing with lattice surgery," *Quantum*, vol. 3, p. 128, mar 2019.

[63] D. Gottesman, "The heisenberg representation of quantum computers," 1998.

[64] J. ichi Yoshikawa, S. Yokoyama, T. Kaji, C. Sornphiphatphong, Y. Shiozawa, K. Makino, and A. Furusawa, "Invited article: Generation of one-million-mode continuous-variable cluster state by unlimited time-domain multiplexing," *APL Photonics*, vol. 1, p. 060801, sep 2016.

[65] R. Jozsa, "An introduction to measurement based quantum computation," 2005.

[66] A. L. Grimsmo and S. Puri, "Quantum error correction with the gottesman-kitaev-preskill code," *PRX Quantum*, vol. 2, p. 020101, Jun 2021.

[67] E. Wigner, "On the quantum correction for thermodynamic equilibrium," *Phys. Rev.*, vol. 40, pp. 749–759, Jun 1932.

[68] V. V. Albert, K. Noh, K. Duivenvoorden, D. J. Young, R. T. Brierley, P. Reinhold, C. Vuillot, L. Li, C. Shen, S. M. Girvin, B. M. Terhal, and L. Jiang, "Performance and structure of single-mode bosonic codes," *ArXiv e-prints*, Aug. 2017.

[69] K. Noh, S. Pirandola, and L. Jiang, "Enhanced energy-constrained quantum communication over bosonic gaussian channels," *Nature Communications*, vol. 11, jan 2020.

[70] K. Noh, V. V. Albert, and L. Jiang, "Quantum capacity bounds of gaussian thermal loss channels and achievable rates with gottesman-kitaev-preskill codes," *IEEE Transactions on Information Theory*, vol. 65, pp. 2563–2582, April 2019.

[71] T. Matsuura, H. Yamasaki, and M. Koashi, "Equivalence of approximate gottesman-kitaev-preskill codes," *Phys. Rev. A*, vol. 102, p. 032408, Sep 2020.

[72] C. Saltzer, "The theory of distributions," vol. 5 of *Advances in Applied Mechanics*, pp. 91–110, Elsevier, 1958.

[73] K. Duivenvoorden, B. M. Terhal, and D. Weigand, "Single-mode displacement sensor," *Physical Review A*, vol. 95, Jan 2017.

[74] D. Gottesman, "Stabilizer codes and quantum error correction," 1997.

[75] "Square-lattice gkp code," in *The Error Correction Zoo* (V. V. Albert and P. Faist, eds.), 2022.

[76] M. P. Stafford and N. C. Menicucci, "Biased gottesman-kitaev-preskill repetition code," 2022.

[77] D. Gottesman, A. Kitaev, and J. Preskill, "Encoding a qubit in an oscillator," *Physical Review A*, vol. 64, Jun 2001.

[78] A. J. Brady, C. Gao, R. Harnik, Z. Liu, Z. Zhang, and Q. Zhuang, "Entangled sensor-networks for dark-matter searches," *arXiv e-prints*, p. arXiv:2203.05375, Mar. 2022.

[79] B. W. Walshe, B. Q. Baragiola, R. N. Alexander, and N. C. Menicucci, "Continuous-variable gate teleportation and bosonic-code error correction," *Physical Review A*, vol. 102, dec 2020.

[80] Q. Zhuang, J. Preskill, and L. Jiang, "Distributed quantum sensing enhanced by continuous-variable error correction," *New Journal of Physics*, vol. 22, p. 022001, feb 2020.

[81] D. Braun, G. Adesso, F. Benatti, R. Floreanini, U. Marzolino, M. W. Mitchell, and S. Pirandola, "Quantum-enhanced measurements without entanglement," *Rev. Mod. Phys.*, vol. 90, p. 035006, Sep 2018.

[82] C. Weedbrook, S. Pirandola, R. García-Patrón, N. J. Cerf, T. C. Ralph, J. H. Shapiro, and S. Lloyd, "Gaussian quantum information," *Reviews of Modern Physics*, vol. 84, p. 621–669, May 2012.

[83] "Bosonic code," in *The Error Correction Zoo* (V. V. Albert and P. Faist, eds.), 2022.

[84] F. Olver, N. I. of Standards, T. (U.S.), D. Lozier, R. Boisvert, and C. Clark, *NIST Handbook of Mathematical Functions Hardback and CD-ROM*. Cambridge University Press, 2010.

[85] J. Liu, H. Yuan, X.-M. Lu, and X. Wang, "Quantum Fisher information matrix and multiparameter estimation," *Journal of Physics A Mathematical General*, vol. 53, p. 023001, Jan. 2020.

[86] K. Matsumoto, "A new approach to the Cramér-Rao-type bound of the pure-state model," *Journal of Physics A Mathematical General*, vol. 35, pp. 3111–3123, Apr. 2002.

[87] R. N. Bracewell and R. N. Bracewell, *The Fourier transform and its applications*, vol. 31999. McGraw-Hill New York, 1986.

[88] D. A. Brannan, M. F. Esplen, and J. J. Gray, *Geometry*. Cambridge University Press, 1999.

[89] G. PANTALEONI, *Subsystem methods for continuous-variable quantum computing with the Gottesman-Kitaev-Preskill code*. PhD thesis, RMIT University.

[90] M. Gu, C. Weedbrook, N. C. Menicucci, T. C. Ralph, and P. van Loock, "Quantum computing with continuous-variable clusters," *Phys. Rev. A*, vol. 79, p. 062318, Jun 2009.

[91] V. Fock, "Konfigurationsraum und zweite quantelung," *Zeitschrift für Physik*, vol. 75, pp. 622–647, Sep 1932.

[92] K. N. BOYADZHIEV and A. D. DIL, "Series with hermite polynomials and applications," *Publicationes Mathematicae Debrecen*, vol. 80, p. 385–404, Apr 2012.

[93] G. Andrews, R. Askey, and R. Roy, *Special Functions*. Encyclopedia of Mathematics and its Applications, Cambridge University Press, 1999.

[94] M. S. Kim, F. A. M. de Oliveira, and P. L. Knight, "Properties of squeezed number states and squeezed thermal states," *Phys. Rev. A*, vol. 40, pp. 2494–2503, Sep 1989.

[95] F. A. M. de Oliveira, M. S. Kim, P. L. Knight, and V. Buek, "Properties of displaced number states," *Phys. Rev. A*, vol. 41, pp. 2645–2652, Mar 1990.

[96] L. Albano, D. F. Mundarain, and J. Stephany, "On the squeezed number states and their phase space representations," *Journal of Optics B: Quantum and Semiclassical Optics*, vol. 4, p. 352–357, Sep 2002.

[97] B. M. Terhal, J. Conrad, and C. Vuillot, "Towards scalable bosonic quantum error correction," *Quantum Science and Technology*, vol. 5, p. 043001, Jul 2020.

[98] F. Arute, K. Arya, R. Babbush, D. Bacon, J. Bardin, R. Barends, R. Biswas, S. Boixo, F. Brandao, D. Buell, B. Burkett, Y. Chen, J. Chen, B. Chiaro, R. Collins, W. Courtney, A. Dunsworth, E. Farhi, B. Foxen, A. Fowler, C. M. Gidney, M. Giustina, R. Graff, K. Guerin, S. Habegger, M. Harrigan, M. Hartmann, A. Ho, M. R. Hoffmann, T. Huang, T. Humble, S. Isakov, E. Jeffrey, Z. Jiang, D. Kafri, K. Kechedzhi, J. Kelly, P. Klimov, S. Knysh, A. Korotkov, F. Kostritsa, D. Landhuis, M. Lindmark, E. Lucero, D. Lyakh, S. Mandrà, J. R. McClean, M. McEwen, A. Megrant, X. Mi, K. Michielsen, M. Mohseni,

J. Mutus, O. Naaman, M. Neeley, C. Neill, M. Y. Niu, E. Ostby, A. Petukhov, J. Platt, C. Quintana, E. G. Rieffel, P. Roushan, N. Rubin, D. Sank, K. J. Satzinger, V. Smelyanskiy, K. J. Sung, M. Trevithick, A. Vainsencher, B. Villalonga, T. White, Z. J. Yao, P. Yeh, A. Zalcman, H. Neven, and J. Martinis, "Quantum supremacy using a programmable superconducting processor," *Nature*, vol. 574, p. 505–510, 2019.

[99] F. Albarelli, M. G. Genoni, M. G. A. Paris, and A. Ferraro, "Resource theory of quantum non-gaussianity and wigner negativity," *Phys. Rev. A*, vol. 98, p. 052350, Nov 2018.

[100] L. Garcí a-Álvarez, C. Calcluth, A. Ferraro, and G. Ferrini, "Efficient simulatability of continuous-variable circuits with large wigner negativity," *Physical Review Research*, vol. 2, dec 2020.

[101] U. Chabaud, P.-E. Emeriau, and F. Grosshans, "Witnessing wigner negativity," *Quantum*, vol. 5, p. 471, jun 2021.

[102] W. P. Schleich, *Quantum Optics in Phase Space*. Berlin: Wiley-VCH, 2001.

[103] A. Kenfack and K. yczkowski, "Negativity of the wigner function as an indicator of non-classicality," *Journal of Optics B: Quantum and Semiclassical Optics*, vol. 6, pp. 396–404, aug 2004.

[104] R. Bellman, *A Brief Introduction to Theta Functions*. Dover Books on Mathematics, Dover Publications, Incorporated, 2013.

[105] B. Yadin, F. C. Binder, J. Thompson, V. Narasimhachar, M. Gu, and M. S. Kim, "Operational resource theory of continuous-variable nonclassicality," *Phys. Rev. X*, vol. 8, p. 041038, Dec 2018.

[106] K. Noh, C. Chamberland, and F. G. S. L. Brandão, "Low-Overhead Fault-Tolerant Quantum Error Correction with the Surface-GKP Code," *PRX Quantum*, vol. 3, p. 010315, Jan. 2022.

[107] A. M. Steane, "Active stabilization, quantum computation, and quantum state synthesis," *Phys. Rev. Lett.*, vol. 78, pp. 2252–2255, Mar 1997.

[108] H. M. Vasconcelos, L. Sanz, and S. Glancy, "All-optical generation of states for "encoding a qubit in an oscillator"," *Opt. Lett.*, vol. 35, pp. 3261–3263, Oct 2010.

[109] E. W. Weisstein, "Fourier series–sawtooth wave. From MathWorld—A Wolfram Web Resource." Last visited on 05/08/2023.

[110] G. Pantaleoni, B. Q. Baragiola, and N. C. Menicucci, "Modular Bosonic Subsystem Codes," *arXiv e-prints*, p. arXiv:1907.08210, Jul 2019.

[111] C. Vuillot, H. Asasi, Y. Wang, L. P. Pryadko, and B. M. Terhal, "Quantum error correction with the toric gottesman-kitaev-preskill code," *Phys. Rev. A*, vol. 99, p. 032344, Mar 2019.

[112] I. Tzitrin, J. E. Bourassa, N. C. Menicucci, and K. K. Sabapathy, "Towards practical qubit computation using approximate error-correcting grid states," *arXiv e-prints*, p. arXiv:1910.03673, Oct 2019.

[113] M. Gu, C. Weedbrook, N. C. Menicucci, T. C. Ralph, and P. van Loock, "Quantum computing with continuous-variable clusters," *Phys. Rev. A*, vol. 79, p. 062318, Jun 2009.

[114] F. Schmidt and P. van Loock, "Quantum error correction with higher gottesman-kitaev-preskill codes: Minimal measurements and linear optics," *Phys. Rev. A*, vol. 105, p. 042427, Apr 2022.

[115] B. Royer, S. Singh, and S. Girvin, "Encoding qubits in multimode grid states," *PRX Quantum*, vol. 3, p. 010335, Mar 2022.